Instituto Universitario de Investigación
en Ingeniería de Aragón
Universidad Zaragoza

PhD Thesis

Multilead analysis of T-wave alternans in the electrocardiogram

Análisis multiderivacional de alternancias de onda T en la señal electrocardiográfica

Violeta Monasterio Bazán

Supervisor:
Juan Pablo Martínez Cortés

June 2011

ACKNOWLEDGMENTS

What a journey this has been! I would not have made it here without the help, guidance, and support of many people. To all of them, I extend my most sincere and heartfelt thanks.

To Juan Pablo Martínez, my PhD advisor. I am profoundly grateful for his constant support, his patient guidance, and his brilliant ideas. Working with him has been a great opportunity to grow scientifically and personally, and it has also been a lot of fun thanks to his cheerful disposition. Looking back at the last five years, I can say I've been very fortunate to have him as supervisor.

To Pablo Laguna, head of our research group. Pablo has always provided me with detailed feedback on my work, and has offered me sound advice on multiple occasions. His contagious energy and enthusiasm for research have been great help along the way.

To Gari Clifford, from the Laboratory for Computational Physiology (MIT, Cambridge MA). He made me feel part of his group during my stay at MIT, and opened the door for new exciting opportunities.

To all the members of our research group, I am indebted for their help and support. It has been a pleasure to collaborate with them and to learn from them. The more I travel around, the more convinced I am that it is a privilege to be part of such a collaborative and supportive group.

To my friends inside and outside university: Clara, Dani, Zurdo, Chuso, Chúster, Alberto... thanks for putting up with me and my thesis! Having your support along the way has made it so much easier. In particular, I want to thank Michele and Ana for being the most fun labmates to share the final sprint with.

Por último, me gustaría dedicar este trabajo a mis padres Maite y Manolo, a mi hermana Maite, y a mi compañero Viorreta. Ellos son siempre mi mejor apoyo y mi ejemplo a seguir. Familia, ¡lo hemos conseguido!

Contents

ABSTRACT

T-wave alternans (TWA) is a cardiac phenomenon related to the mechanisms leading to ventricular arrhythmias and sudden cardiac death (SCD). It appears in the surface electrocardiogram (ECG) as a beat-to-beat alternation in the morphology of the repolarization, and its amplitude can be so low that it is imperceptible to the naked eye. Several signal processing methods have been proposed to detect TWA in the ECG and to quantify its amplitude. Most of them analyze each lead (channel) of the ECG independently, and only basic multilead strategies are adopted in commercial TWA systems. However, the joint analysis of various ECG channels provides additional information about the spatial and temporal distribution of cardiac phenomena, which can be exploited to improve the detection and quantification of TWA in the ECG.

The objective of this thesis is to develop multilead schemes for TWA analysis that improve the detection and quantification of TWA in the ECG, and that increase the clinical value of TWA as a risk index. The work carried out to achieve this goal is divided in three parts: design of novel multilead schemes for TWA analysis, methodological validation of the proposed techniques, and clinical validation of the multilead scheme that presents the best performance.

The first part of the thesis introduces a general scheme for multilead analysis of TWA. The proposed scheme is an extended version of a usual single-lead scheme with two additional stages, signal transformation and signal reconstruction, which are included to increase the detectability of TWA and to improve the estimation of TWA amplitude and waveform. Various techniques are proposed for the transformation stage: principal component analysis (PCA), periodic component analysis (πCA), independent component analysis (ICA) and spectral ratio maximization (SRM). Techniques πCA and ICA have been applied to TWA analysis for the first time in this work. SRM is a new technique developed in this work which exploits the periodicity of TWA to increase its detectability in the transformed signal.

The general multilead scheme can be combined with any single-lead method which detects and estimates TWA in separate stages. Along the thesis, it is combined with the Laplacian Likelihood Ratio Method for TWA analysis, and also with the Spectral Method for comparison. Several modifications of the general scheme are also proposed for its adaptation to different clinical settings.

The second part of the thesis presents the methodological evaluation of the multilead scheme based on the different transformation techniques. The alternatives are compared in various simulation studies, in which synthetic, semi-synthetic and real signals with known TWA are analyzed. Differences between schemes are quantified using common performance metrics such as probability of detection and probability of false alarm, and also using new global measures of the bias and variance of the TWA estimation. The improvements in the detection performance and in the accuracy of TWA estimation over a single-lead scheme are quantified for all the multilead alternatives. Results show that using the periodicity as a criterion to separate TWA from noise is the best multilead strategy among the compared options. Among the periodicity-based schemes, the one with the best performance is the πCA-based multilead scheme.

The last part of the thesis demonstrates that the improvements in TWA analysis obtained with the πCA-based scheme, together with a new strategy for computing global TWA indices, make it possible to stratify cardiac risk in Holter recordings without the need for visual validation. The method presented here allows a multilead, fully-automated computation of TWA markers of cardiac risk in ambulatory ECGs. Results from a clinical study show that the average TWA activity over a 24-hour period provides important prognostic information in patients with chronic heart failure. Two novel indices, AAI and AAI_{90}, are proposed to quantify the average TWA activity, and are found to independently predict the risk of cardiac death and SCD.

RESUMEN Y CONCLUSIONES

Las alternancias de onda T (TWA) se definen como una alteración en la morfología de la repolarización que se repite cada dos latidos. Este fenómeno cardíaco está relacionado con el riesgo de sufrir arritmias ventriculares malignas que pueden conducir a la muerte súbita cardíaca. Actualmente, el análisis de TWA en el electrocardiograma (ECG) se utiliza para estratificar el riesgo de sufrir arritmias ventriculares, y decidir si un paciente puede beneficiarse de la implantación de un desfibrilador automático implantable.

La amplitud de las TWA puede ser muy baja, del orden de los microvoltios, resultando indetectables a simple vista en el ECG, lo que dificulta en gran medida su detección. Existen diferentes métodos de procesado de la señal para detectar las TWA y estimar sus parámetros (amplitud, forma de onda). El principal inconveniente de los métodos existentes es o bien una alta sensibilidad a la presencia de componentes no alternantes de gran amplitud, o bien una baja sensibilidad a las TWA de baja amplitud. Habitualmente, estos métodos se aplican a cada derivación (canal) del ECG de manera independiente, es decir, siguiendo un esquema de análisis monoderivacional. Sin embargo, el análisis conjunto de varios canales del ECG proporciona información adicional sobre la distribución espacial y temporal de los fenómenos cardiacos, que se podría aprovechar para mejorar la detección y la cuantificación de TWA.

El objetivo de esta tesis es desarrollar estrategias de análisis multiderivacional que mejoren la detección y la cuantificación de TWA en el ECG, y que aumenten el valor clínico de las TWA como índice de riesgo. El trabajo desarrollado para conseguir este objetivo se divide en tres partes: propuesta de nuevas estrategias de análisis multiderivacional para detectar y cuantificar TWA, validación metodológica de las estrategias propuestas, y validación clínica de la alternativa multiderivacional con mejores prestaciones.

En la primera parte de la tesis se propone un esquema general para el análisis multiderivacional de TWA. El esquema propuesto se ha diseñado como una versión extendida de un esquema monoderivacional habitual, al que se le han añadido dos etapas de procesado adicionales: transformación de la señal y reconstrucción de la señal. Con estas etapas se consigue incrementar la detectabilidad de las TWA y mejorar la estimación de su amplitud y de su forma de onda. Se proponen diferentes técnicas para la transformación de la señal: análisis de componentes principales (PCA), análisis de componentes periódicos (πCA), análisis de componentes independientes

(ICA) y maximización del ratio espectral (SRM). Las técnicas πCA e ICA se han aplicado al análisis de TWA por primera vez en este trabajo. La técnica SRM es una nueva propuesta de esta tesis que aprovecha la periodicidad de las TWA para incrementar su detectabilidad en la señal transformada.

El esquema multiderivacional propuesto se puede combinar con cualquier método de análisis monoderivacional que detecte y cuantifique las TWA en etapas separadas. A lo largo de la tesis, el esquema se combina con el método del cociente de verosimilitudes para ruido Laplaciano (LLRM), y también con el método espectral (SM) como comparación. Además, se proponen modificaciones del esquema multiderivacional general para adaptarlo a los diferentes escenarios clínicos en los que se realiza análisis de TWA.

En la segunda parte de la tesis se evalúan las prestaciones del esquema multiderivacional, comparando los resultados que se obtienen con las diferentes técnicas de transformación de la señal, y cuantificando la mejora obtenida respecto a un esquema monoderivacional habitual. Para ello se diseñan varios estudios de simulación, en los que se analizan señales sintéticas, semi-sintéticas y reales donde los parámetros de las TWA (presencia, amplitud, forma de onda) se conocen de antemano. Las diferencias entre esquemas se cuantifican utilizando métricas habituales como la probabilidad de detección y la probabilidad de falsa alarma, y también nuevas métricas globales de sesgo y varianza de la estimación. Los resultados de la evaluación metodológica muestran que la mejor estrategia multiderivacional entre las alternativas comparadas es usar la periodicidad de la señal como criterio para separar las TWA del ruido y resto de componentes no deseadas del ECG. De las estrategias basadas en la periodicidad, la que ofrece mejores prestaciones es la basada en πCA.

En la última parte de la tesis se comprueba que las mejoras en el análisis de TWA que se obtienen con el esquema multiderivacional basado en πCA, junto con una nueva estrategia para calcular índices de TWA globales, hacen posible la estratificación del riesgo cardiaco en registros ambulatorios (*Holter*). El método multiderivacional propuesto en esta tesis permite calcular de manera totalmente automática nuevos marcadores de riesgo cardiaco en registros ambulatorios. Los resultados de un estudio clínico muestran que la actividad media de las TWA en un periodo de 24 horas proporciona información pronóstica en pacientes con insuficiencia cardiaca crónica. En concreto, se ha encontrado que dos de los índices propuestos en esta tesis para cuantificar la actividad media de las TWA, AAI y AAI_{90}, son predictores independientes del riesgo de muerte cardiaca y muerte súbita cardiaca.

List of Figures

List of Tables

Chapter 1

Introduction

1.1 Motivation of the thesis

Cardiovascular diseases (CVD) are the major cause of death in adults and the elderly in the majority of the developed countries and in many developing countries. According to the last report of the American Heart Association [Roger et al., 2011], more than 82 million people (>1 in 3) have a cardiovascular disease in the United States (US). Mortality data show that CVD as the underlying cause of death accounted for 33.6% of all deaths in 2007, or 1 of every 3 deaths in the US. According to the Spanish National Statistics Institute (www.ine.es), 36.6% of all deaths in 2008 were caused by CVD in the European Union, and 31.7% in Spain (4273 deaths in Aragón), being the major cause of death in both cases.

A great part of these deaths occur suddenly, shortly after the onset of the first symptoms, and are related to malignant ventricular arrhythmias that lead to a heart attack. This kind of outcome is known as sudden cardiac death (SCD). According to the World Health Organization, the incidence of SCD in developed areas varies from 20 to 160 cases per 100,000 inhabitants each year among men aged 35 to 64 years. In the US, the annual incidence varies between 300,000 and 400,000 cases. In Spain, the incidence is 40 cases per 100,000 inhabitants each year, which represents 10 - 30% from all deaths by natural causes [Marrugat et al., 1999]. These statistics justify any effort in reducing the incidence of CVD by improving the prevention, diagnosis and treatment of these diseases.

Implantable cardioverter defibrillators (ICD) are the most effective way of preventing SCD. However, the implantation of an ICD is an invasive pro-

cedure with associated risks and a high cost—according to the clinical study MADIT-II [Bloomfield et al., 2004, Armoundas et al., 2005], it is necessary to implant an ICD to 18 patients to save one life—so it is only applied to patients at high risk of suffering ventricular arrhythmias. A reliable way of assessing this risk is to perform an electrophysiologic (EP) study, which evaluates if arrhythmias can be induced in the heart by stimulating the myocardium in a controlled manner with an electrode placed inside a catheter. The EP study is also an invasive procedure, so it cannot be used as a general screening test. Therefore, it is necessary to determine non-invasive risk markers that identify patients at a higher risk of suffering malignant arrhythmias, so that invasive diagnostic tests and treatments can be selectively applied only to those patients who will benefit the most, saving risks for the patients and also health-care costs.

Various non-invasive indices have been proposed to predict the risk of arrhythmias. Most of them are based either on the analysis of echocardiographic images (for example, ejection fraction), or on the analysis of electrocardiographic signals (presence of ectopic beats in ambulatory records, QRS duration, QT dispersion, heart rate variability, etc.) [Kusmirek and Gold, 2007, Kreuz et al., 2008]. The main limitation of existing indices is their low specificity and predictive value [Priori et al., 2003]. One of the most promising non-invasive indices is T-wave alternans (TWA) [Rosenbaum et al., 1994, Narayan, 2006]. Its prognostic value is being intensively studied, and significant evidence of the relation between TWA and the susceptibility to ventricular fibrillation has been found in recent years [Costantini et al., 2009, Chow et al., 2007, Armoundas et al., 2002]. This thesis presents new advances in the analysis of TWA in the electrocardiogram with the objective to increase the clinical value of TWA tests.

1.2 Background

The material and figures in this section are taken from [Zaret et al., 1992, Guyton and Hall, 2006, Sörnmo and Laguna, 2005, Clifford et al., 2006], to which the reader is referred for a more detailed overview of the topics covered here.

1.2.1 The electrocardiogram

An electrocardiogram (ECG) describes the electrical activity of the heart. The heart is comprised of muscle (myocardium) that contracts rhythmically and drives the circulation of blood throughout the body. Before every normal heart beat, or systole, a wave of electrical current passes through the entire heart, which triggers myocardial contraction. The electrical current spreads over the structure of the heart in a coordinated pattern which leads to an effective, coordinated systole. This results in a measurable change in potential difference on the body surface of the subject. The resultant amplified signal is known as an electrocardiogram.

The anatomy of the heart is divided into two "mirrored" sides, left and right, which support different circulatory systems but which pump in a synchronized, rhythmic manner. Each side of the heart consists of two chambers: the *atrium*, were the blood enters, and the *ventricle*, where the blood is forced into further circulation. The direction of blood flow is controlled by four different valves which are located between the atria and the ventricles (atrio-ventricular valves) and between the ventricles and the arteries (pulmonary and aortic valves). The structure of the heart, and the course of blood flow through the heart chambers and heart valves is depicted in figure 1.1.

Each cardiac cycle is composed of two phases, activation and recovery, which are referred to in electrical terms as *depolarization* and *repolarization*, and in mechanical terms as contraction and relaxation. The initialization of a cardiac cycle occurs in the *sinoatrial* (SA) *node*, a mass of pacemaker cells with the ability to spontaneously fire an electrical impulse. The electrical impulse then propagates through the different parts of the electrical conductive system of the heart: the internodal pathways that conduct the impulse from the sinus node to the atrio-ventricular (A-V) node; the A-V node, in which the impulse from the atria is delayed before passing into the ventricles; the A-V bundle, which conducts the impulse from the atria into the ventricles; and the left and right bundle branches of Purkinje fibers, which conduct the cardiac impulse to all parts of the ventricles (see figure 1.2). While the ventricles are being electrically activated, the atria recover their initial state (*atrial repolarization*). Finally, the cardiac cycle ends when the ventricles recover their resting electrical state (*ventricular repolarization*).

The normal electrocardiogram (see figure 1.3) is composed of a P wave, a QRS complex, and a T wave. The QRS complex is often, but not always,

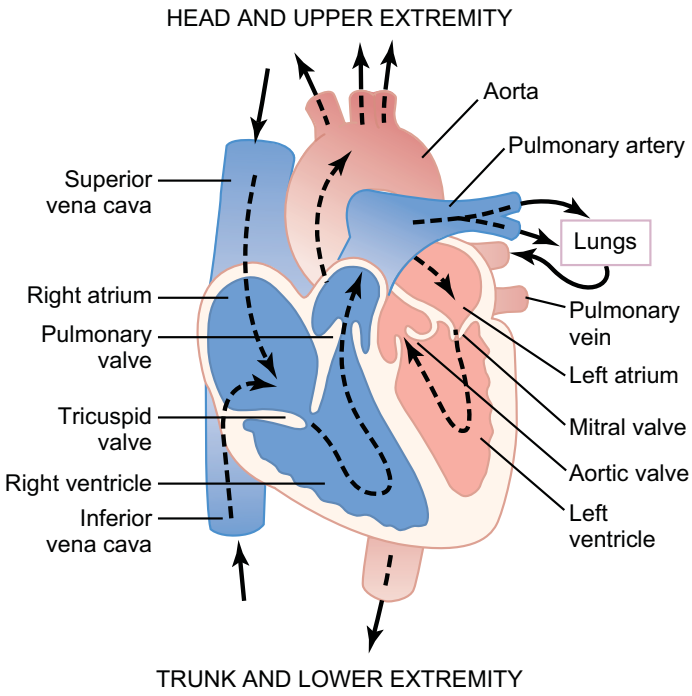

Figure 1.1: Structure of the heart, and course of blood flow through the heart chambers and heart valves. Reproduced from [Guyton and Hall, 2006].

three separate waves: the Q wave, the R wave, and the S wave. The P wave is caused by electrical potentials generated when the atria depolarize before atrial contraction begins. The QRS complex is caused by potentials generated when the ventricles depolarize before contraction, that is, as the depolarization wave spreads through the ventricles. The T wave is caused by potentials generated as the ventricles recover from the state of depolarization. This process normally occurs in the ventricular muscle from 0.25 to 0.35 seconds after depolarization, and the T wave is known as a repolarization wave. The interval between the end of the QRS complex (known as the J point) and the end of the T wave is known as ST-T complex, and reflects the repolarization activity of the ventricles. The phenomenon studied in this thesis, TWA, occurs in this last part of the cycle.

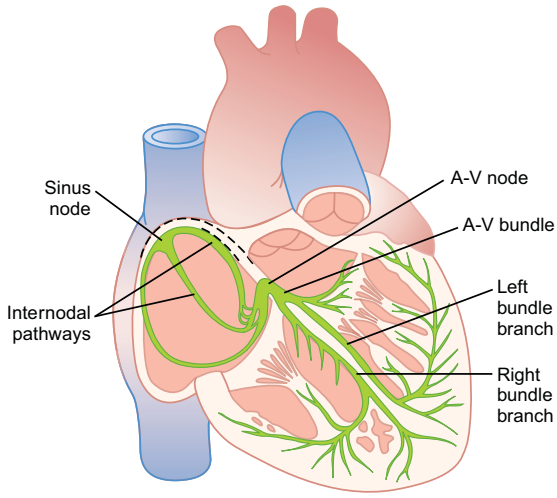

Figure 1.2: Sinus node, and the Purkinje system of the heart, showing also the A-V node, atrial internodal pathways, and ventricular bundle branches. Reproduced from [Guyton and Hall, 2006].

Lead systems

The electrical activity of the heart is measured on the body surface by attaching a set of electrodes to the skin. For an ECG recording, the difference in voltage between a pair of electrodes is referred to as a *lead*. The ECG is typically recorded with a multiple lead configuration which includes unipolar or bipolar leads, or both. A so-called *unipolar lead* reflects the voltage variation of a single electrode and is measured in relation to a reference electrode (commonly called the *central terminal*) whose voltage remains almost constant throughout the cardiac cycle. A *bipolar lead* reflects the voltage difference between two electrodes.

Each lead represents a different electrical axis onto which the electrical activity of the heart is projected. Therefore, each lead can be considered to represent a different spatial perspective of the heart's electrical activity. If leads are appropriately placed in a multilead ECG, the ensemble of the different waveforms provides a robust understanding of the electrical activity throughout the heart, allowing the clinician to determine pathologies through spatial correlation of events on specific leads.

A variety of lead configurations are used in clinical practice, from a standard 12-lead setup to a simple hospital two or 3-lead configuration, or just a single lead. The choice of a particular lead system is guided

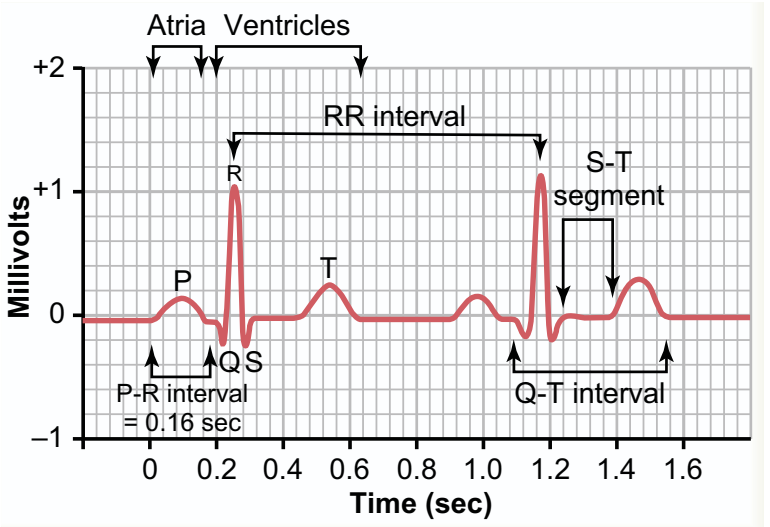

Figure 1.3: Normal electrocardiogram. Reproduced from [Guyton and Hall, 2006].

by the type of clinical information desired and by various clinical issues and practical considerations. The two lead systems that receive the most attention are the standard 12-lead ECG and the orthogonal lead system.

The standard 12-lead ECG is the most widely used lead system in clinical routine and is defined by a combination of three different lead configurations: the bipolar limb leads, the augmented unipolar limb leads, and the unipolar precordial leads. The three *bipolar limb leads* are denoted *I*, *II* and *III* and are obtained by measuring the voltage difference between the left arm, right arm, and left leg. These three electrode positions can be viewed as the corners of a triangle ("Einthoven's triangle") with the heart at its center (see figure 1.4). The *augmented unipolar leads* (*aVF, aVL* and *aVR*) use the same electrodes as the bipolar limb leads but are defined as the voltage differences between one corner of the triangle and the average of the remaining two corners. The six *precordial leads*, by convention labeled *V1,..., V6*, are unipolar leads positioned on the front and the left side of the chest, and related to a central terminal which is defined as the average of the voltages measured on the right and left arms and the left leg (figure 1.5).

An orthogonal lead system reflects the electrical activity in three perpendicular directions, *X*, *Y* and *Z*. The most widely used orthogonal lead system, known as the *Frank lead system* after its inventor [Frank, 1956], is

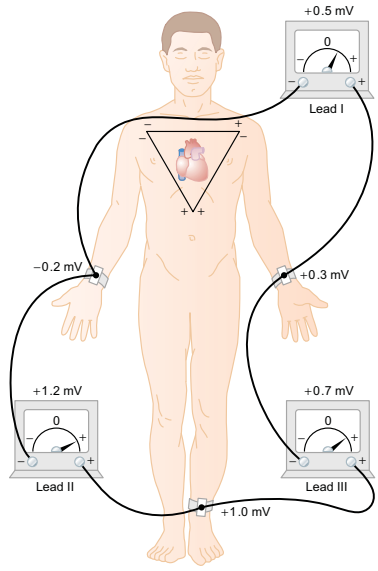

Figure 1.4: Conventional arrangement of electrodes for recording the standard electrocardiographic leads. Einthoven's triangle is superimposed on the chest. Reproduced from [Guyton and Hall, 2006].

obtained as linear combinations of seven electrodes positioned on the chest, back, neck, and left foot. The resulting leads X, Y and Z view the heart from the left side, from below, and from the front.

It is important to realize that the polarity and morphology of individual ECG waves are strongly dependent on where the electrodes are placed on the body. For some positions, a wave may actually be completely absent because the electrical wavefront in the heart is propagating perpendicularly to the vector defined by the lead. Furthermore, the amplitude of the wave depends on the distance between the heart and the electrode.

ECG monitoring

Since its invention, the usage of the ECG as a clinical tool has become greatly diversified. Two common ways of monitoring the ECG for TWA studies are the stress test and the ambulatory recording.

A *stress test*, or exercise test, is a method of investigating the ability of the heart to cope with physical work, and is usually performed with a bicycle or a running treadmill. Exercise starts at a low workload, and the load is increased progressively. During the exercise, the standard 12-lead ECG is

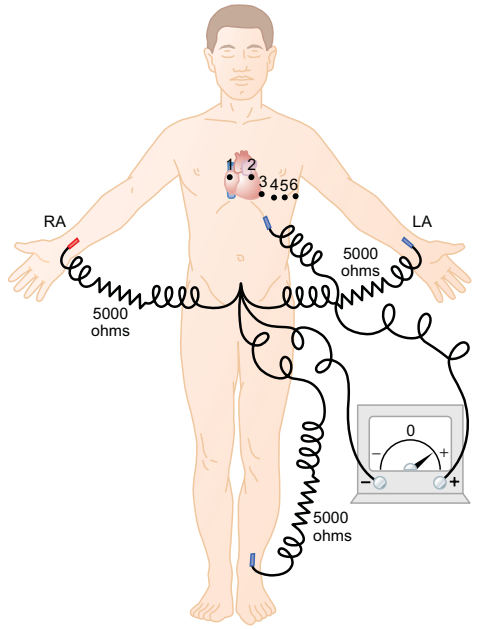

Figure 1.5: Connections of the body for recording precordial leads. LA, left arm; RA, right arm. Reproduced from [Guyton and Hall, 2006].

recorded an monitored on a screen. The stress test is terminated when the patient reaches a predefined maximum heart rate, experiences fatigue or symptoms like chest pain and shortness of breath, or when abnormal ECG changes appear. The overall response to exercise is assessed in terms of maximum workload, maximum heart rate, ECG changes, blood pressure and respiratory rate.

Ambulatory ECG monitoring, also called *Holter monitoring*, is used to identify patients with transient symptoms that are indicative of arrhythmias, or patients at high risk of sudden death after infarction. Also, it is used to assess the reaction of patients to treatment with antiarrhythmic drugs. During 24 hours or more of normal daily activities, the patient carries a recording device that stores the ECG. A 3-lead configuration is often used because the 12-lead configuration is less practical in these recording conditions. Once the patient has returned the device to the hospital, the recorded ECG is analyzed by a physician.

1.2.2 Cardiovascular diseases

Three major cardiovascular diseases associated to SCD are coronary artery disease, cardiac arrhythmias, and heart failure.

Coronary artery disease

Coronary artery disease (CAD), coronary heart disease, and ischemic heart disease are various names given to a condition in which the coronary arteries—those that feed the heart muscle itself—are narrowed. As a result, the supply of blood to the heart muscle is decreased. This deficiency in oxygen is called ischemia. The narrowing is almost invariably due to atherosclerosis, the buildup of fatty plaques on the inner walls of the arteries.

In the absence of symptoms, CAD may be diagnosed as a result of positive findings during an exercise stress test (possibly including a nuclear imaging study), or it may be documented by a coronary angiogram. The most common and serious complications of CAD are myocardial infarction (MI) and SCD. A MI occurs when there is a marked decrease in the oxygen supply to an area of the heart muscle, and the damaged tissue dies. Other complications of CAD may include various heart rhythm disturbances and heart failure.

Cardiac arrhythmias

Cardiac arrhythmias occur when the heart's electrical system does not function properly. An arrhythmia can be anything from an extra beat in the atria to dangerous ventricular tachycardias.

A tachycardia is an abnormally fast rate, which can be originated in the atria (supraventricular tachycardia) of in the ventricles (ventricular tachycardia). In both instances, an extra or early beat may trigger the rapid rhythms. Although the sinus node develops as the specialized site of impulse production, all cardiac muscle cells retain the capacity to become pacemaker cells. Normally, the pacemaking activity of the sinus node suppresses impulse production by other cells, but if conductance to some part of the heart muscle is blocked, or if the heart is overstimulated, islands of cells may express their latent impulse-production ability. This may lead to the division of the cardiac impulse along multiple pathways, resulting in a chaos of uncoordinated electrical impulses. Such situation is called fibrilla-

tion. Ventricular fibrillation is potentially fatal, because the heart ceases to pump blood effectively, and death can occur within few minutes.

Heart failure

Heart failure occurs when the heart is not pumping effectively enough to meet the body's needs for oxygen-rich blood, either during exercise or at rest. The term congestive heart failure is often synonymous with heart failure but also refers to the state in which decreased heart function is accompanied by a buildup of body fluid in the lungs and elsewhere. When the condition develops over long periods, it is also called chronic heart failure (CHF). A number of different problems can cause heart failure: ischemic heart disease, a heart attack resulting in acute damage and then scarring of heart muscle tissue, chronic high blood pressure, major cardiac arrhythmias, diseased heart valves, and congenital heart diseases (which are faults in the anatomy of the heart that are present at birth).

1.2.3 T-wave alternans

T-wave alternans (TWA) is a beat-to-beat alternation in the morphology of the ST segment and the T wave (the ST-T complex, see figure 1.6). TWA has been recognized and linked to arrhythmogenesis for more than a century, dating from the pioneering observations of Hering in 1909 [Hering, 1909]. It was considered as a rare finding until nonvisible (microvolt level) TWA were discovered and first described by Adam in 1981 [Adam et al., 1981]. TWA has been reported under diverse clinical conditions in association with the risk of suffering life-threatening arrhythmias, including acute myocardial ischemia and infarction, heart failure, Printzmetal's angina, and congenital diseases including Brugada syndrome and long QT syndrome (LQTS) [Narayan, 2006].

TWA is considered to reflect temporal [Pastore et al., 1999] or spatial [Chinushi et al., 1998] heterogeneity of ventricular repolarization. The clinical utility of TWA as an index of SCD risk has been evaluated in numerous studies [Gehi et al., 2005], including patients with dilated cardiomyopathy [Ferrari and Sanzo, 2008], long QT syndrome [Hassan and Kaufman, 2005], ischemic cardiopathy [Bloomfield et al., 2004, Costantini et al., 2009], previous myocardium infarction [Ikeda et al., 2002, Stein et al., 2008], other cardiopathies [Salerno-Uriarte et al., 2007, Grimm et al., 2003], general population [Nieminen et al., 2007] and healthy subjects [Gibelli et al., 2008].

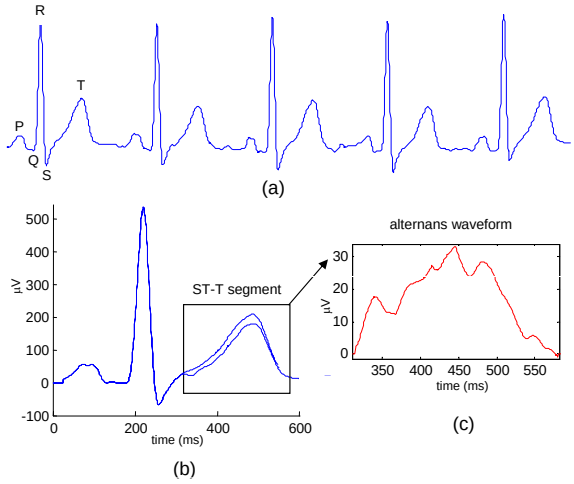

Figure 1.6: (a) ECG signal with TWA. (b) Superposition of two consecutive beats. (c) Alternans waveform: difference between odd and even beats.

Since TWA is usually non-visible to the naked eye, a number of signal processing techniques have been proposed to detect and quantify TWA in the ECG [Martínez and Olmos, 2005]. The application of the two commercially available techniques, namely the Spectral and the Modified Moving Average Methods, to different patient populations has generated an extensive literature of clinical studies, involving more than 12,000 patients [Gehi et al., 2005]. A review of the literature on TWA analysis methods is presented in chapter 2.

1.3 Objectives and outline of the thesis

Existing TWA analysis methods are usually applied to each lead of the ECG independently, that is, they follow a *single-lead* analysis scheme. However, ECG signals with multiple leads, or *multilead* signals, present some spatial and temporal redundancy, as well as complementary information. All this information can be exploited to find the combination of leads that allows for the best possible TWA analysis in a particular recording setting. This is the **main objective of the thesis**: to develop a *multilead analysis scheme* that improves the detection and quantification of TWA in the ECG, and that increases the clinical value of TWA as a risk index.

To achieve this goal, several multilead schemes are proposed. The improvement in the detection and estimation of TWA that can be achieved

with these schemes is fully evaluated by means of simulation studies and application to real ECG datasets. After selecting the multilead approach that presents the best performance, new TWA indices are proposed to quantify TWA in ambulatory records. Finally, the prognostic utility of the new indices is evaluated with a clinical study.

The content of the thesis is organized as follows:

- **Chapter 2**: this chapter contains a review of the literature on TWA analysis methods. The problem of detecting and quantifying TWA in the ECG is presented, and the main methods that have been proposed to solve it are described. Different ways of evaluating TWA methods are then discussed, establishing the main differences between methodological and clinical validation.

- **Chapter 3**: this chapter contains the common materials and methods that are used throughout the rest of the thesis. It begins with a description of the single-lead scheme that represents the starting point of this thesis. Then, a general multilead scheme is proposed as a reference framework for the different techniques developed in the thesis, and each alternative is presented. The proposed alternatives for multilead analysis are based on principal component analysis (PCA), periodic component analysis (πCA), and other blind source separation (BSS) techniques. The chapter ends with a brief description of the ECG datasets that are used for the evaluation of the methods.

- **Chapter 4**: this chapter describes the methodological evaluation of the multilead scheme based on PCA. The performance of this scheme is compared to the usual single-lead approach in terms of TWA detection rate and accuracy of TWA estimation. The clinical utility of the proposed PCA scheme is demonstrated with its application to a stress test ECGs dataset. The content of this chapter has been published in:

  - V. Monasterio, P. Laguna, J. P. Martínez. "Multilead Analysis of T Wave Alternans in the ECG using Principal Component Analysis". IEEE Transactions on Biomedical Engineering, vol.56, no.7, pp.1880-1890; 2009.
  - V. Monasterio, P. Laguna, J. P. Martínez. "Multilead estimation of T-wave alternans in the ECG using principal component anal-

ysis". 16^{th} European Signal Processing Conference (EUSIPCO 2008). Lausanne (Switzerland). CD. August 2008.

- V. Monasterio, J. P. Martínez. "Multilead T-Wave Alternans Quantification Based on Spatial Filtering and the Laplacian Likelihood Ratio Method." Computers in Cardiology 2008, pp. 601-604. Bologna (Italy). September 2008.
- V. Monasterio, J. P. Martínez. "A multilead approach to T-wave alternans detection combining principal component analysis and the Laplacian likelihood ratio method". Computers in Cardiology 2007, pp. 5-8. Durham (NC, USA). September 2007.

- **Chapter 5**: this chapter describes the methodological evaluation of the multilead scheme based on πCA. The πCA scheme is compared to the single-lead scheme, the PCA scheme, and to other BSS techniques in terms of TWA detection rate and accuracy of TWA estimation. Like in chapter 4, the clinical utility of the scheme is demonstrated with its application to a stress test ECGs dataset. The content of this chapter has been published in:

  - V. Monasterio, G. D. Clifford, P. Laguna, J. P. Martínez. "A Multilead Scheme based on Periodic Component Analysis for T Wave Alternans Analysis in the ECG". Annals of Biomedical Engineering, Vol. 38, No. 8, pp. 2532-2541; 2010.
  - V. Monasterio, J. P. Martínez. "Analysis of T-wave Alternans in Stress Tests with Periodic Component Analysis". Proceedings of the 37^{th} International Congress on Electrocardiology, pp.12. Lund (Sweden). June 2010.
  - V. Monasterio, G. D. Clifford, J. P. Martínez. "Comparison of Source Separation Techniques for Multilead T-Wave Alternans Detection in the ECG". Proceedings of the 32^{nd} Annual International Conference of the IEEE EMBS, pp. 5367-5370. Buenos Aires (Argentina). August 2010.
  - V. Monasterio, J. P. Martínez. "Comparison of two eigenvalue decomposition techniques to detect T Wave Alternans in the ECG". World Congress on Medical Physics and Biomedical Engineering, IFMBE Proceedings 25/IV, pp.631-634. Munich (Germany). September 2009.

- **Chapter 6**: this chapter describes the adaptation of the πCA scheme for the analysis of ambulatory ECGs, and presents new indices to quantify TWA in long-term ECG recordings. A clinical study demonstrates that these indices are independent predictors of sudden cardiac death in patients with chronic heart failure. A manuscript with the content of this chapter has been submitted and is currently under review:
  - V. Monasterio, I. Cygankiewicz, P. Laguna, J. P. Martínez. "Average T-wave alternans activity in ambulatory records predicts cardiac death in patients with chronic heart failure". Under review.
- **Chapter 7**: the final chapter contains the conclusions and possible extensions of the thesis.

Chapter 2

Review of TWA analysis methods

2.1 Introduction

Over the last decades, evaluation of TWA has evolved from visual inspection of the ECG to the use of computerized methods for detection and quantification of nonvisible TWA in the microvolt range. This chapter offers an overview of the most widely used methods for TWA analysis, as well as several recently proposed techniques.

Measuring TWA embedded in noise is a difficult task because the amplitude of TWA can be lower than the noise level, specially in noisy signals such as stress test ECGs. Existing methods for TWA analysis perform two basic procedures: deciding about the presence or absence of TWA in the signal (*detection*), and quantifying TWA parameters such as its magnitude (*estimation*). Not every method performs both procedures; some techniques detect TWA without estimating its magnitude, while other techniques consider TWA as a continuously present phenomenon whose magnitude can be estimated at every point of an ECG. Such differences are further discussed in section 2.2, where TWA techniques of both types are described.

After measuring TWA parameters in the ECG, clinical indices are computed to identify patients with "abnormal" TWA activity. In addition to TWA presence and/or magnitude, other variables are evaluated in clinical TWA tests, such as the heart rate at which TWA appears, the duration of TWA episodes, the number of leads in which TWA amplitude surpasses a predefined threshold, and others. Therefore, a clear distinction can be

made between the performance of a given TWA analysis method (in terms of detection power and accuracy of TWA estimation), and the utility of the obtained TWA measurements for clinical testing (for example, in terms of risk predictive power of the clinical TWA test). We will refer to the performance evaluation of TWA techniques as *methodological evaluation*, and to the evaluation of the clinical utility of TWA measurements as *clinical evaluation*. The distinction between methodological and clinical evaluation is further discussed in section 2.3.

2.2 Methods for TWA analysis

Since Adam and coworkers discovered microvolt TWA in the ECG [Adam et al., 1981], numerous techniques have been proposed to automatically analyze TWA in ECG signals. In 2005, Martínez and Olmos published a review of more than ten TWA analysis methods [Martínez and Olmos, 2005], and proposed a common framework to describe the methodological principles of TWA analysis. They proposed a general analysis structure including three main processes: signal preprocessing, TWA detection, and estimation of the TWA waveform and/or amplitude.

The preprocessing stage prepares the ECG signal for posterior stages, and includes operations such as baseline cancellation, beats detection, noise filtering, or data reduction to accelerate further processing. In the detection stage, it is decided whether there is TWA in the signal or not, and in the estimation stage the amplitude and/or the waveform of TWA is estimated. Depending on the specific method, detection and estimation can be performed simultaneously or consecutively, or one of them may be omitted. From here on, we will use the term *analysis* to denote both detection and estimation as a whole.

The rest of the section is devoted to describe the methods which are most widely used either in clinical practice or in research studies, as well as several new methods proposed in recent years. The two methods which are commercially available are the Spectral Method (SM) and the Modified Moving Average Method (MMAM).

2.2.1 Spectral Method

The spectral method (SM) was proposed in 1988 by Smith and coworkers [Smith et al., 1988]. The SM first aligns the ECG beats, and then generates

beat-to-beat series with the amplitudes of corresponding points in consecutive ST-T complexes. After that, the beat-to-beat series of amplitude fluctuations are subjected to spectral analysis using the Fast Fourier Transform. Because the resulting spectrum is based on measurements taken once per beat, its frequencies are in units of cycles per beat (cpb). The frequency that corresponds to an oscillation occurring on every other beat is 0.5 cpb, and is referred to as the alternans frequency. The alternans power (in μV) is defined as the difference between the power at the alternans frequency and the power at an adjacent frequency band, which is taken as a reference for noise measurement. Detection is performed by means of a significance measure called the TWA Ratio (TWAR), which is calculated as the ratio of alternans power divided by the standard deviation of the noise in the reference frequency band. TWA is considered to be present if TWAR ≥ 3.

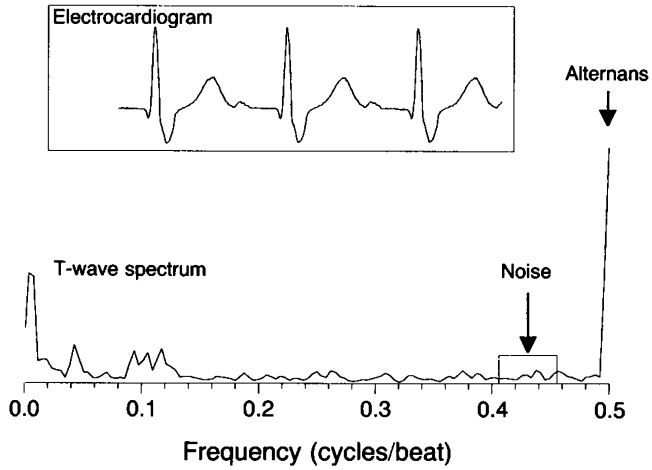

Figure 2.1: Example of spectral analysis of an ECG with TWA, performed with 128 consecutive beats. Reproduced from [Rosenbaum et al., 1994].

In 1994, the same group presented the adaptation of the original SM to the analysis of human ECGs [Rosenbaum et al., 1994], which was later included in commercial equipments such as CH2000© and Heartwave© (Cambridge Heart Inc, Bedford, MA). The SM is the most widely used method for analyzing exercise-induced TWA in clinical stress tests [Gehi et al., 2005].

2.2.2 Modified Moving Average Method

The Modified Moving Average Method (MMAM) was proposed by Nearing and Verrier in 2002 [Nearing and Verrier, 2002]. The analysis is performed in

the temporal domain. A stream of beats is divided into odd and even bins, and the morphology of the beats in each bin is averaged over a few beats successively to create a moving average complex. A limiting nonlinearity is applied to the innovation of every new beat in the running average to avoid the effect of impulsive artifacts. TWA magnitude is computed as the maximum difference in amplitude between the odd-beat and even-beat average ST-T complexes. The MMAM does not include a detection stage, but analyzes TWA as a continuous variable along the complete ECG.

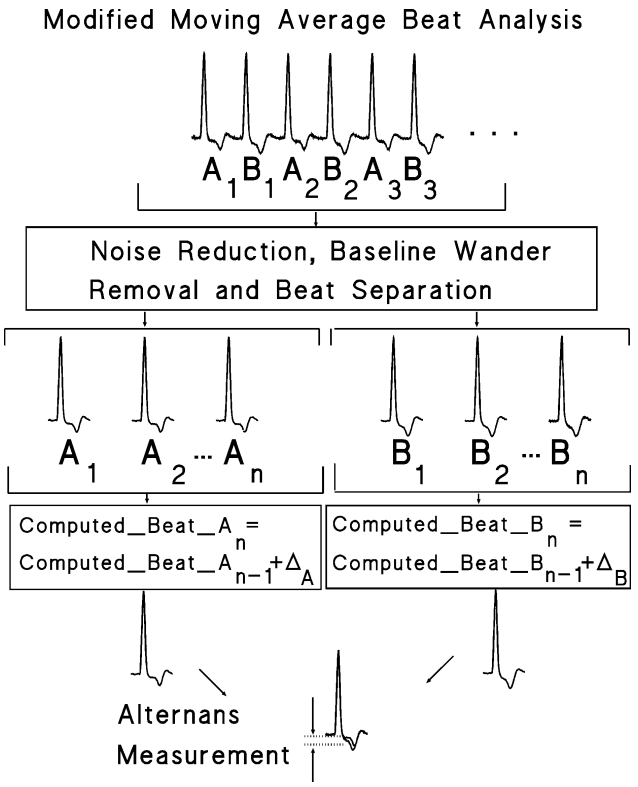

Figure 2.2: Flowchart of the major components of the MMA method. Reproduced from [Nearing and Verrier, 2002].

The MMAM is mostly used for TWA analysis in ambulatory records [Verrier et al., 2005a, Stein et al., 2008]. Also, it has recently been applied to stress test ECGs, although evidence of the prognostic value of MMAM results in such settings is still weaker than in the SM case [de Vilhena Garcia, 2008]. The MMAM is included in commercial equipments such as CASE-8000© (GE Marquette Inc., Milwaukee, Wisconsin).

Besides SM and MMAM, several methods proposed in the late 1990's and early 2000's continue to be used in research. Among them we can find the Correlation Method (CM), the Intrabeat Average Method (IBAM), and the Laplacian Likelihood Ratio Method (LLRM).

2.2.3 Correlation Method

The Correlation Method (CM) is a time-domain approach proposed by Burattini and coworkers in 1997 [Burattini et al., 1997, 1999]. With this method, consecutive T waves are aligned with a cross-correlation technique, and the median T wave is computed for its use as a template. An alternans correlation index (ACI) is then computed for each T wave by computing its cross-correlation with the template. TWA is detected by looking for an alternating pattern of ACI values (see figure 2.3). A fixed threshold must be exceeded by the alternating ACI series for TWA to be considered significant.

The CM has been used to study TWA in CAD and LQTS patients [Burattini et al., 1998], and has been included in comparative studies of TWA methodologies [Janusek et al., 2007, Burattini et al., 2010a].

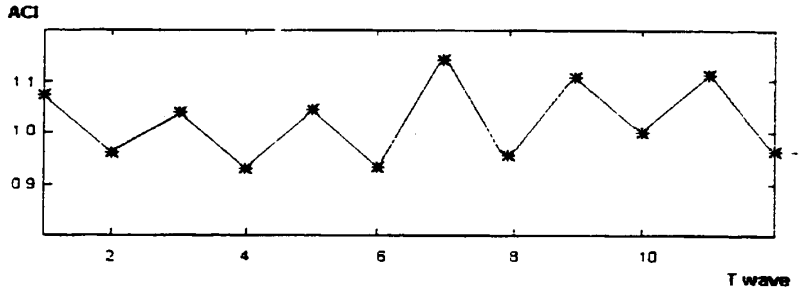

Figure 2.3: Oscillations in the alternans correlation index (ACI) computed by the CM in the presence of TWA. Reproduced from [Burattini et al., 1999].

2.2.4 Intrabeat Average Method

The Intrabeat Average Method (IBAM) [Shusterman and Goldberg, 2004] applies intra-beat averaging to compute the mean T wave amplitude in each beat. TWA is then calculated by serial subtraction of these mean T-wave amplitudes for all consecutive cardiac complexes in a 5-minute ECG segment. The IBAM has been used to study the temporal relation between

TWA and the spontaneous initiation of ventricular tachyarrhythmias [Shusterman et al., 2006] and the association of ICD shocks with increases of repolarization instability [Lampert et al., 2007].

2.2.5 Laplacian Likelihood Ratio Method

In 2002, Martínez and Olmos presented a new approach to TWA detection [Martínez and Olmos, 2002], the Laplacian Likelihood Ratio Method (LLRM), based on the signal processing theory for estimation and detection [Kay, 1993, 1998]. Given a signal model including alternans and noise terms, the maximum likelihood estimator (MLE) and the generalized likelihood ratio test (GLRT) can be derived for TWA estimation and detection, respectively. This method assumes a Laplacian distribution for physiological noise, since extreme noise values are likely to appear in real ECGs, and therefore a normal distribution would not describe the noise in a realistic manner. In this way, the LLRM computes the MLE and the GLRT for a Laplacian noise model to perform both estimation and detection of TWA. In [Martínez and Olmos, 2003], the model was extended to account for non-stationary noise. The LLRM has been used to quantify and characterize TWA in patients undergoing coronary angioplasty [Martínez et al., 2006].

2.2.6 Recent Methods

Research on TWA techniques has experimented noticeable advances in the last years, and several techniques have been published in parallel to the development of this thesis. This section describes the most relevant recent techniques, distinguishing between TWA analysis methods (those who perform both detection and estimation), TWA detection methods, TWA estimation methods, and improvements over existing methods.

Among the recent TWA analysis methods, we can find different approaches. Some methods follow the approach of the LLRM, assuming a model for the signal and deriving the GLRT and the MLE for TWA detection and estimation, respectively. In 2007, Meste and coworkers [Meste et al., 2007] proposed a signal model that assumed Laplacian noise (like the LLRM), but also included the factors of amplitude modulation and baseline wander. In 2009, Helfenbein and coworkers presented a method which computed the GLRT after projecting the input signal onto a set of basis functions [Helfenbein et al., 2009].

A different approach is adopted by a second group of methods. The assumption of a particular statistical distribution for noise has been considered a limitation by some authors, and alternative non-parametric methods have been proposed. In 2008, Rojo-Álvarez and coworkers developed a nonparametric method which first used PCA to obtain a set of orthogonal leads, then created odd and even T wave templates with an amplitude matched filter, and finally applied a nonparametric paired bootstrap test to obtain the relative magnitude of TWA and its significance difference with respect to the noise level [Rojo-Álvarez et al., 2008]. Another example is the work by Nemati and coworkers [Nemati et al., 2010], who proposed a nonparametric significance test based on surrogate data analysis to perform TWA detection, in combination with an estimation stage based on simple averaging of even and odd beats. This approach was tested on clinical data [Nemati et al., 2011] and was shown to improve the differentiation of patient groups.

Various methods have been proposed to only detect or estimate TWA. Bortolan and Christov presented a detection method based on single-lead PCA transformation and significance testing with a nonparametric rank test [Bortolan and Christov, 2008]. This method was tested on ambulatory recordings from Brugada syndrome patients, but no significant differences were found in TWA results between patient populations [Bortolan et al., 2009]. Two recent estimation methods are the adaptive-match-filter method (AMFM) [Burattini and Burattini, 2008], which has been tested on patients with CAD [Burattini et al., 2009b, 2010b], and a technique based on the dominant T-wave paradigm [Mainardi and Sassi, 2011].

The last group of recent advances comprises new techniques proposed to improve existing TWA methods. In 2007, Cuesta-Frau and coworkers proposed a preprocessing stage for the MMAM which used a dynamic time warping technique to improve the alignment of T waves [Cuesta-Frau et al., 2007]. Another example is the work by Blanco-Velasco and coworkers [Blanco-Velasco et al., 2010], in which the technique of empirical mode decomposition was applied to remove noise and artifacts from the ECG signal before using the SM for TWA analysis.

Most of the methods cited in this section analyze each lead of the ECG independently from the others. The few methods which do not follow a purely single-lead scheme perform TWA analysis on a set of combined leads, computed either by using a fixed transformation [Bortolan and Christov, 2008], or by applying PCA [Rojo-Álvarez et al., 2008], or singular value decomposition (SVD) [Mainardi and Sassi, 2011]. In those cases, the multilead

transformation is either chosen to diagonalize the initial leads set (thus allowing a vectorcardiographic interpretation of the results), or chosen so that the energy of the T wave is mostly projected in a subset of leads. However, none of these multilead transformations are specifically designed to improve the detectability of TWA in the ECG.

2.3 Validation of methods

When referring to evaluation of TWA methods, we can distinguish between methodological evaluation (that is, the quantification of the detection power and the estimation accuracy of the method) and clinical evaluation (which quantifies the utility of TWA measurements as clinical indices to identify patients with different pathologies, or as cardiac risk markers). It is desirable to evaluate the method's performance before using it to extract clinical conclusions, so, ideally, clinical studies with a new TWA method should be preceded by a methodological evaluation study.

2.3.1 Methodological evaluation

The main problem of methodological evaluation is the absence of a gold standard for TWA analysis. The existence of TWA evaluation databases annotated by human experts would be desirable, but a big difficulty resides in the fact that TWA is often not visible due to its low amplitude. As there are is a lack of evaluation databases, a usual approach for validating TWA methods is the use of simulated signals, where TWA parameters (presence, amplitude, waveform, etc.) are known *a priori*. A review of simulation studies published before 2005 can be found in [Martínez and Olmos, 2005].

In simulation studies, evaluation datasets are created by adding known TWA to ECG signals. In most cases, ECG signals are synthetically generated. To generate synthetic signals, the background ECG can be built as the repetition of a single noiseless beat, usually extracted from a real ECG [Burattini et al., 2009a, Blanco-Velasco et al., 2010], or can be created using a mathematical model that may include effects such as variations in heart rate, or respiration effects [Cuesta-Frau et al., 2007, 2009, Clifford et al., 2010]. Noise is then added to the background ECG. This noise can be computer-generated with a given statistical distribution (such as Gaussian or Laplacian [Janusek et al., 2007]) or can be physiological noise recorded in real ECGs [Blanco-Velasco et al., 2010, Nemati et al., 2010].

A drawback of synthetic ECGs is their lack of physiological variability. Using real ECG recordings as background ECGs, with their own noise and physiological variability, is a more realistic alternative [Boix et al., 2009, Blanco-Velasco et al., 2010, Ghoraani et al., 2011], but the difficulty in this case is to find real ECGs where the absence of TWA can be assured.

TWA is usually simulated using a mathematical model, such as a Gaussian curve [Meste et al., 2007], a sinusoidal wave [Boix et al., 2009], or a Hamming window [Cuesta-Frau et al., 2009]. The TWA waveform, that is, the distribution of the TWA amplitude along the ST-T complex, can be symmetric with respect to the maximum of the T wave, or can be asymmetrically distributed [Burattini et al., 2009a]. Various nonstationary effects can also be simulated, such as TWA phase reversals, or spikes in the amplitude of the T wave simulating motion artifacts [Shusterman and Goldberg, 2004].

Simulation studies are the most common way of assessing the performance of TWA methods. A different alternative is to use a comparative approach, in which results from different methods are correlated with each other [Moody, 2008]. This procedure allows to test if a new method achieves a performance similar to a previously validated one, but there is no way to extract conclusions about the discordances between methods.

2.3.2 Clinical evaluation

The ultimate goal of TWA testing is to identify those patients at a higher risk of suffering cardiac arrest. After measuring TWA in the ECG, clinical indices are extracted from the results of TWA analysis, and the cardiac risk of the patient is assessed according to these indices using a specific set of rules. Common clinical indices are the presence or absence of TWA, the duration of TWA episodes, the amplitude of TWA, and the heart rate at which TWA appears. The set of rules is different for each TWA analysis method [Narayan, 2006, de Vilhena Garcia, 2008]. Therefore, after a new TWA analysis method is methodologically validated, a set of clinical indices and rules that allows the risk stratification of patients needs to be derived. We will refer to this process as *clinical evaluation*.

A first step toward a complete clinical evaluation is the application of the TWA analysis method to specific populations of patients, either to describe the characteristics of TWA in those populations, or to distinguish between groups of patients and/or healthy subjects. Only a few recent

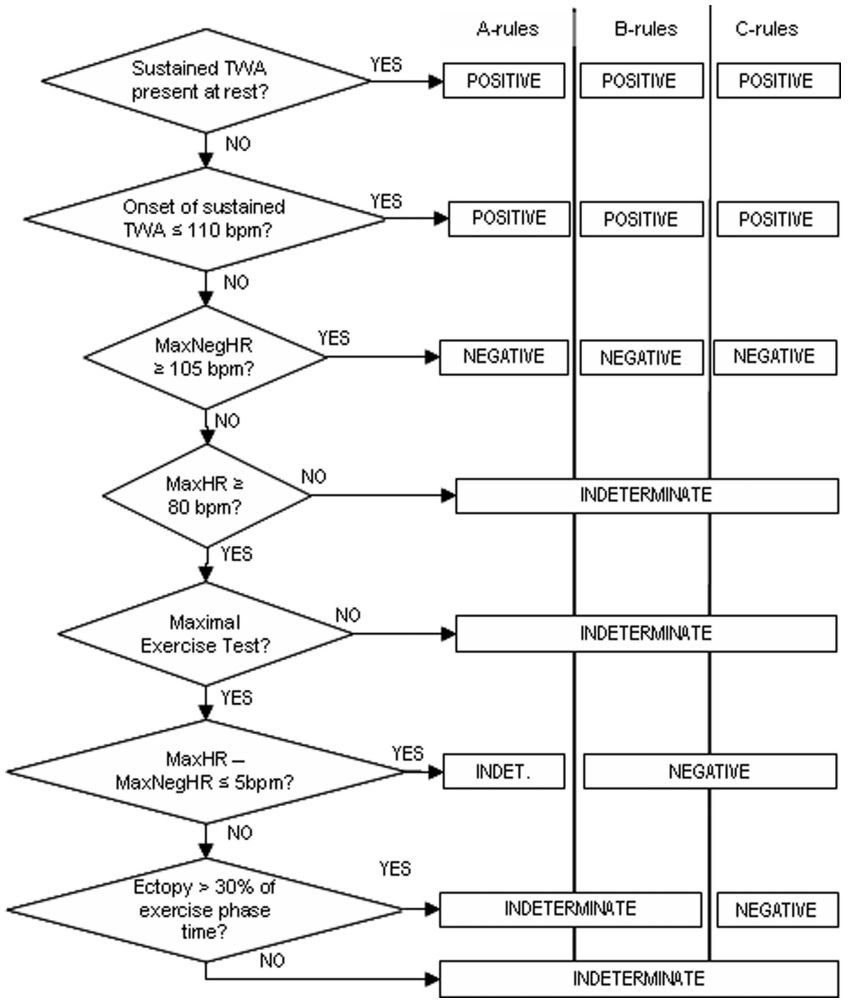

Figure 2.4: Schematic diagram showing the most used classification schemes in SM-TWA testing. Abbreviations used: MaxHR = maximum heart rate achieved in the stress test; MaxNegHR = maximum heart rate achieved with clearly no TWA. Reproduced from [de Vilhena Garcia, 2008].

TWA methods have reached this stage. In 2006, Martínez and coworkers used the LLRM to describe the time-course and the spatial distribution of TWA in CAD patients undergoing coronary angioplasty [Martínez et al., 2006]. Shusterman and coworkers studied the temporal relations between TWA and the spontaneous initiation of ventricular tachyarrhythmias in a CAD population [Shusterman et al., 2006] with the IBAM. Burattini and coworkers applied the AMFM to CAD patients and healthy subjects, and identified thresholds for TWA measures that identified 13% of CAD patients [Burattini et al., 2009b] and 24% of CAD patients [Burattini et al., 2010a]. Most recently, Nemati and coworkers applied their method [Nemati et al., 2010] to differentiate populations of healthy subjects, CHF patients, sleep apnea patients, and subjects who suffered SCD [Nemati et al., 2011].

To date, only the SM and the MMAM have been completely validated for different patient populations. The ability of the SM-TWA test to predict cardiac death, SCD, ventricular arrhythmias an ICD shocks has been evaluated in numerous studies [Gehi et al., 2005, Hohnloser et al., 2009]. These studies comprised a wide range of subject populations, including ischemic and non-ischemic congestive heart failure, post-MI patients, athletes, and healthy subjects. The SM is usually applied to stress tests ECGs, and complex sets of rules are applied to decide if the TWA test results should be considered abnormal (classified as *positive*), and therefore indicative of high cardiac risk (see figure 2.4). A complete description of the interpretation and classification of SM-TWA tests can be found in [Bloomfield et al., 2002] and [Richter et al., 2005].

The predictivity of MMAM-TWA for cardiovascular mortality and SCD has also been evaluated in various studies, enrolling more than 12000 patients from different populations [Nieminen and Verrier, 2010]. The MMAM is the preferred option for ambulatory ECGs, but the rules to decide whether a test is abnormal or not are still subject to intense research, and a consensus has not been established yet in the scientific community [Amit et al., 2009, Bansal and Berger, 2010].

Chapter 3

Common materials and methods

3.1 Introduction

This chapter contains a unified description of the methods and materials used throughout the thesis. It starts with the description of the basic single-lead analysis scheme that is usually followed by TWA methods, and details two of those methods: the LLR and the SM. Then, the chapter presents the general multilead scheme proposed in this thesis, and discusses several options to adapt the scheme to different analysis scenarios. The chapter ends with a description of the ECG datasets used to validate the methods.

3.2 Basic scheme for single-lead analysis

According to the framework proposed by Martínez and Olmos [Martínez and Olmos, 2005], TWA analysis methods can be described using a general scheme, such as the one in figure 3.1, consisting of three main processes: signal preprocessing, TWA detection, and estimation of TWA magnitude and/or waveform. The preprocessing stage prepares the raw ECG signal for TWA analysis, and then the stages of detection and estimation operate individually on each ECG lead. These stages are described next.

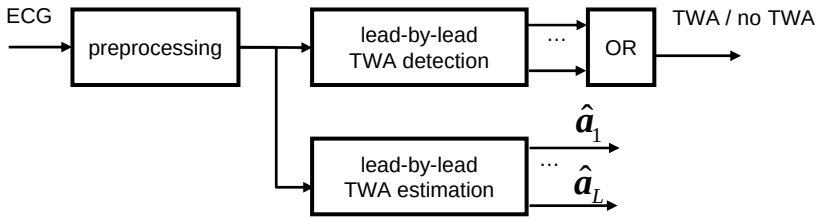

Figure 3.1: Basic single-lead scheme for TWA analysis

3.2.1 Preprocessing of the ECG signal

The objective of the preprocessing is to minimize the contamination by noise and artifacts in the signal, and to prepare it for posterior stages. Much research has been conducted on this topic, as preprocessing is an essential step in any ECG processing system. An overview on preprocessing procedures can be found in [Sörnmo and Laguna, 2005]. The description below is restricted to the procedures applied in this work.

The first step is to determine the instants of occurrence of heart beats. This is done by detecting the QRS complexes in the signal, because the QRS is the part of the beat that concentrates most of the energy. The *fiducial points*, or reference points of the QRS complexes, are found with two different techniques in this work. The first technique is based in the wavelet decomposition of the ECG signal, and works on a single-lead basis [Martínez et al., 2004]. This technique was applied to the synthetic and semi-synthetic datasets described in sections 4.2.1, 5.2.1, 5.2.2 and 5.2.4. The second technique, called ARISTOTLE [Moody and Mark, 1982], is a multilead QRS detector that provides annotations of abnormal beats. It is used for ECGs recorded during stress testing or daily activity, described in sections 3.5.3 and 3.5.6 respectively, because in such signals noise and artifacts may appear intermittently in different leads, and therefore the use of a multilead QRS detector is preferable.

The second step is to cancel the baseline wander. The baseline wander is an external, low-frequency activity in the ECG which may interfere with the signal analysis, and may result from a variety of noise sources including respiration, body movements, and poor electrode contact. A cancellation technique based on cubic-splines interpolation is used in this work [Sörnmo, 1993], which consists of subtracting an estimation of the baseline wander

from the ECG signal. The estimation is obtained by fitting a polynomial to representative samples ('knots') of the ECG, which are chosen at the PQ interval of successive beats.

The ECG signal is then low-pass filtered to eliminate the noise outside the TWA frequency band, and downsampled to reduce redundancy in the resulting low-pass signal. The frequency content of TWA is located below 15 Hz, so the signal can be filtered and downsampled to a resulting sampling frequency of $F_s > 30$ Hz without losing information. In this work, signals with original sampling frequencies of 1000 Hz and 500 Hz are downsampled by factors of 32 and 16 respectively, resulting in $F_s = 31.25$ Hz, and signals originally sampled at 200 Hz are downsampled by a factor of 6, resulting in $F_s = 33.33$ Hz.

Finally, an interval of 350 ms (or the closest value corresponding to a integer number of samples) corresponding to the ST-T complex is selected in each beat. The initial point of the interval is typically defined between 60 and 80 ms after the QRS fiducial point. This distance can be a constant if the heart rhythm is stable in the signal, or variable if the heart rhythm presents large variations. The specific choice is reported for each study in the corresponding methods section.

3.2.2 Detection and estimation of TWA

After the preprocessing stage, a TWA detector is applied to each lead of the ECG, and then the magnitude of TWA is estimated. Two single-lead methods are considered for these steps. The first one is the LLRM, which was developed in the BIO-GTC research group and has been validated both with simulation studies and with clinical datasets for the study of acute ischemia [Martínez et al., 2006]. The second one is the SM, which is widely used in clinical practice [Smith et al., 1988].

With both methods, the signal is analyzed using a sliding window of K beats. For every fragment of K beats, each lead is independently analyzed to decide if TWA is present or not, and if TWA is detected, its amplitude is estimated in that lead. The final detection is positive if TWA is detected at least in one lead. The rate at which detections and amplitude estimates are computed is determined by the shift step of the sliding window, denoted by δ and measured in beats. As discussed in [Martínez and Olmos, 2005], short windows (low K) allow better tracking of abrupt TWA changes and transient episodes than long windows (high K), whereas longer windows

produce a greater smoothing on the beat-to-beat series under analysis, which reduces the noise in the detection statistics and amplitude estimators. In this thesis, values of K ranging from 16 to 128 are considered, depending on the noise characteristics of signals. The influence of the sliding step δ was also discussed in [Martínez and Olmos, 2005]; a value of δ equal to one beat allows a beat-to-beat sampling of the TWA evolution, whereas greater values such as $\delta = K/2$ or $\delta = K$ provide less correlated measures, which can be useful for the statistical characterization of the methods' performance. The way LLRM and SM operate is summarized next.

Laplacian Likelihood Ratio method

The LLRM computes beat-to-beat the maximum likelihood estimation (MLE) of the TWA under the assumption of Laplacian noise, and applies a generalized likelihood ratio test (GLRT) to decide whether TWA is present or not.

Let K be the number of beats under analysis, N the number of samples of each ST-T complex, and L the number of leads. The ST-T complex of the kth beat and the lth lead is represented with a row vector as

$$\mathbf{x}_{k,l} = \Big[x_{k,l}(0) \quad \dots \quad x_{k,l}(N-1) \Big]^T . \tag{3.1}$$

The LLR method assumes the following model for each complex

$$x_{k,l}(n) = s_l(n) + \frac{1}{2} a_l(n)(-1)^k + v_{k,l}(n), \quad n = 0 \dots N-1 \tag{3.2}$$

which in vector notation is

$$\mathbf{x}_{k,l} = \mathbf{s}_l + \frac{1}{2} \boldsymbol{a}_l (-1)^k + \mathbf{v}_{k,l} \tag{3.3}$$

where $\boldsymbol{s}_l$ is the background ST-T complex, which is periodically repeated in every beat, $\boldsymbol{a}_l$ is the TWA waveform, defined as the difference between odd and even beats, and $\mathbf{v}_{k,l}$ is additive random noise (vectors in (3.3) are defined as in (3.1)).

Background ST-T complexes can be canceled with a *detrending* filter that computes the difference between each complex and the previous one

$$\mathbf{x}'_{k,l} = \mathbf{x}_{k,l} - \mathbf{x}_{k-1,l}, \ k = 1 \ \dots \ K-1 \tag{3.4}$$

The noise present in $\mathbf{x}'_{k,l}$ is assumed to be independent and identically distributed Laplacian with zero mean and unknown standard deviation σ_l. The

MLE of $\boldsymbol{a}_l$ for this model is given by [Martínez and Olmos, 2003, Martínez et al., 2006]

$$\hat{a}_l(n) = \text{median}\left(\left\{x'_{k,l}(n)(-1)^k\right\}_{k=1}^{K-1}\right) \quad n = 0 \ldots N-1 \tag{3.5}$$

and the TWA amplitude is calculated as the root mean square (RMS) value across the estimated TWA waveform as

$$V_{alt_l} = \sqrt{\frac{1}{N}\sum_{n=0}^{N-1}\hat{a}_l^2(n)} \ \ (\mu V). \tag{3.6}$$

The GLRT statistic can be expressed as

$$Z_l = \frac{\sqrt{2}}{\hat{\sigma}_l NK}\sum_{n=0}^{N-1}\left(\sum_{k=1}^{K-1}\left|x'_{k,l}(n)\right| - \sum_{k=1}^{K-1}\left|x'_{k,l}(n) - \hat{a}_l(n)(-1)^k\right|\right) \tag{3.7}$$

where $\hat{\sigma}_l$ is the MLE of the standard deviation of the noise

$$\hat{\sigma}_l = \frac{\sqrt{2}}{NK}\sum_{k=1}^{K-1}\left\|\mathbf{x}'_{k,l} - \hat{\boldsymbol{a}}_l(-1)^k\right\|_1. \tag{3.8}$$

Details of the derivation of the MLE and GLRT are included in appendix 3.A, and can also be found in [Martínez and Olmos, 2003, Martínez et al., 2006].

To decide whether TWA is present or not, the GLRT statistic Z_l is compared to a threshold γ. TWA detection is positive if $Z_l > \gamma$, and negative otherwise. Since the detection statistic (3.7) is invariant to amplitude scaling of $\mathbf{x}'_{k,l}$ (it is a constant false alarm rate (CFAR) detector), the value of γ can be set to obtain a fixed probability of false alarm (P_{FA}) regardless of the noise level [Kay, 1998].

Spectral Method

The SM [Smith et al., 1988, Rosenbaum et al., 1994] is based on Fourier analysis of each beat-to-beat series of synchronized samples within the ST-T complex. The TWA component is obtained by evaluating the Fast Fourier transform (FFT) at the alternans frequency, which is 0.5 cycles per beat (cpb), or equivalently, 1 cycle every two beats. Following the notation in [Martínez and Olmos, 2005], the detection statistic can be expressed as $Z_l = (1/N)\sum_{n=0}^{N-1} z_l(n)$, where $z_l(n) = (1/K)\left|\text{FFT}\left\{x_{k,l}(n)\right\}\right|^2_{f=0.5}$ is the 0.5 cpb frequency bin of the short-time periodogram computed from the

beat-to-beat series of the nth sample. A significance measure called TWA ratio (TWAR) is defined as

$$\mathrm{TWAR}(l) = \frac{Z_l - m_l}{s_l} \tag{3.9}$$

where m_l and s_l are the mean and the standard deviation of the spectral noise measured in the spectral window [0.33 - 0.48 cpb]. To evaluate whether TWA is significant, TWAR is compared to a fixed threshold (typically $\gamma = 3$). Finally, TWA amplitude is estimated as

$$V_{alt_l} = \sqrt{Z_l - m_l} \quad (\mu V)\,. \tag{3.10}$$

3.3 General scheme for multilead analysis

The key idea of multilead analysis is to combine the information of the ECG leads to increase the Alternans-Signal-to-Noise ratio (ASNR) in the signal, that is, to improve the visibility of TWA over noise. A higher ASNR improves the detectability and the estimation of TWA, and is obtained by means of a linear transformation that separates TWA from noise in the ECG. The different ways of calculating the transformation will be summarized in section 3.4.

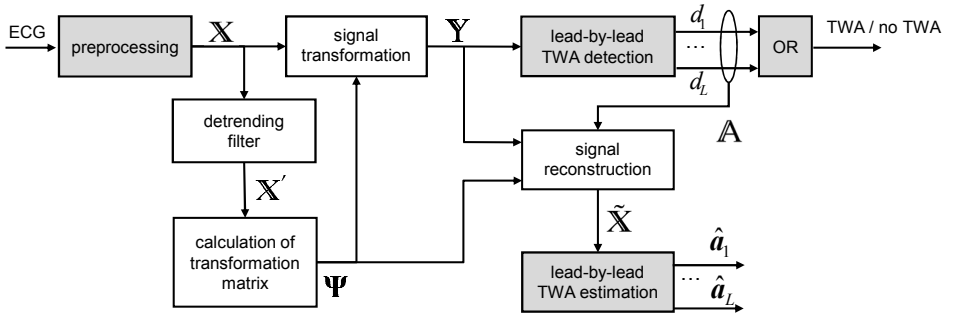

Figure 3.2: General multilead scheme for TWA analysis. Blocks in gray are the ones used by the single-lead scheme, in which $\mathbf{Y} = \mathbb{X} = \tilde{\mathbf{X}}$.

In the multilead scheme, the leads of the ECG are combined before TWA detection and estimation. Therefore, this scheme can be interpreted as an extension of a basic single-lead scheme with new intermediate stages. A diagram of the multilead scheme is shown in figure 3.2, where the original stages of a basic single-lead scheme appear in gray. Since detection and

estimation stages do not change, it is possible to combine the extended multilead scheme with any TWA analysis method that performs detection and estimation in separate stages. In particular, the multilead scheme can be combined with LLRM and SM just by computing the significance measures (GLRT or TWAR) and the amplitude estimates (eqs. (3.6) and (3.10)) in the detection and the estimation stages respectively.

The stages of the general multilead scheme are summarized below. The LLRM has been selected as the basic TWA analysis method for the description, and an example of application to a synthetic signal with simulated TWA has been included for illustration. The simulated signal belongs to the synthetic dataset described in section 4.2.1 and is depicted in figure 3.3(a).

3.3.1 Preprocessing of the ECG signal

The preprocesing stage consists of the same QRS detection, baseline cancellation, downsampling, and ST-T selection steps as the single-lead scheme. It was designed this way to facilitate the comparison of the analysis results obtained with the two schemes. As exactly the same preprocessing is applied to the input signal, the preprocessing errors that may appear (QRS detection errors, residual baseline wander, etc.) will equally affect the single and the multilead schemes, and therefore it will be correct to attribute the differences in the detection and estimation of TWA to the multilead transformation of the signal.

At the end of the preprocessing stage, two multilead data matrices, $\mathbf{X}$ and $\mathbf{X}^{(m)}$, are constructed as follows. Following the notation of the single-lead scheme, the ST-T complex of the kth beat and the lth lead is represented by the row vector

$$\mathbf{x}_{k,l} = \begin{bmatrix} x_{k,l}(0) & \dots & x_{k,l}(N-1) \end{bmatrix}^T .$$

For each lead l, ST-T segments are concatenated to form the $(1 \times KN)$ lead vectors:

$$\begin{aligned} \tilde{\mathbf{x}}_l &= \begin{bmatrix} \mathbf{x}_{0,l} & \dots & \mathbf{x}_{K-1,l} \end{bmatrix} \\ \tilde{\mathbf{x}}_l^{(m)} &= \begin{bmatrix} \mathbf{x}_{m,l} & \dots & \mathbf{x}_{m+K-1,l} \end{bmatrix} \end{aligned} \tag{3.11}$$

where $\tilde{\mathbf{x}}_l^{(m)}$ is the equivalent to $\tilde{\mathbf{x}}_l$ obtained after sliding the analysis window m beats forward. Two $(L \times KN)$ matrices are finally constructed by putting

together all the leads:

$$\mathbf{X} = \begin{bmatrix} \tilde{\mathbf{x}}_1 \\ \vdots \\ \tilde{\mathbf{x}}_L \end{bmatrix} \quad ; \quad \mathbf{X}^{(m)} = \begin{bmatrix} \tilde{\mathbf{x}}_1^{(m)} \\ \vdots \\ \tilde{\mathbf{x}}_L^{(m)} \end{bmatrix} \tag{3.12}$$

where $\mathbf{X}^{(m)}$ is a delayed version of $\mathbf{X}$, and is necessary for one of the transformations described in section 3.4. For simplicity, it is omitted in figure 3.2.

3.3.2 Signal transformation

The second stage aims to find a spatial transformation of the original leads set that separates TWA from noise as much as possible. First, background ST-T segments are canceled with a *detrending* filter

$$\mathbf{x}_{k,l}^{'} = \mathbf{x}_{k,l} - \mathbf{x}_{k-1,l},\ k = 1\ \ldots\ K-1 \tag{3.13}$$

and the *detrended* beats $\mathbf{x}_{k,l}^{'}$ are arranged as in (3.11) and (3.12) to form matrices $\mathbf{X}^{'}$ and $\mathbf{X}^{(m)'}$. The application of the *detrending* filter is intended to eliminate the background ECG, so that signals $\mathbf{X}^{'}$ and $\mathbf{X}^{(m)'}$ only contain a mixture of TWA and noise. This is necessary because otherwise the separation techniques described later would tend to separate the background ECG, not the TWA, from noise, since the background ECG has greater power than the TWA component. Then, the transformation $\mathbf{\Psi}$ is calculated using a technique that separates TWA from the rest of the ECG components.

Various techniques are employed to find the transformation matrix $\mathbf{\Psi}$ in the thesis: PCA, πCA, Spectral Ratio Maximization (SRM), and Independent Component Analysis (ICA). These techniques are described in section 3.4. Once the transformation matrix is computed, it is applied to the original data $\mathbf{X}$

$$\mathbf{Y} = \mathbf{\Psi}^T \mathbf{X} \tag{3.14}$$

to obtain the transformed signal $\mathbf{Y}$, whose leads (rows of $\mathbf{Y}$) will be denoted as transformed leads.

The objective of the linear transformation is to increase the separation between TWA and noise by projecting most of the TWA component onto one subset of transformed leads, and most of the noise onto a different subset of leads. Therefore, TWA and noise will appear more separated in

the transformed signal than in the original signal, and the detection of TWA will be easier. This effect is illustrated in figure 3.3(b), where TWA becomes easily detectable in the transformed signal after PCA transformation.

3.3.3 Detection of TWA

The detection of TWA is performed exactly as in the single-lead scheme, but in this case the LLRM and SM operate on the transformed leads. The result of the lead-by-lead detection is denoted by d_l: if TWA is detected in the lth lead, then $d_l = 1$, and $d_l = 0$ otherwise. The final detection will be positive if TWA is detected in one or more transformed leads ('OR' block in figure 3.2). In the example of figure 3.3(b), TWA is detected in transformed leads 5, 6, and 7 with the LLRM.

3.3.4 Signal reconstruction

Signal transformation can be interpreted as a change of coordinate system in the space. This means, for the example in figure 3.3(b), that the transformed lead T*1* does not correspond to the original lead V*1*. However, clinicians use the amplitudes of TWA in the standard 12-lead system or in the Frank lead system to decide about the results of clinical TWA tests. Therefore, in certain clinical scenarios it will be necessary to "reverse" the transformation before estimating TWA. To solve this problem, a reconstruction stage is included in the analysis scheme, where a new signal in the original lead set is reconstructed after TWA detection. In this way, TWA amplitude measurements can be computed in the original leads set, which also facilitates the comparison with the single-lead scheme.

To exactly reverse the transformation, we would need to do

$$\mathbf{X} = (\mathbf{\Psi}^T)^{-1}\mathbf{Y} = \mathbf{\Psi}\mathbf{Y},$$

where the second equivalence holds true if $\mathbf{\Psi}$ is orthonormal. However, such reconstruction would not improve the estimation of TWA over a single-lead scheme, since TWA would be estimated on the same original signal $\mathbf{X}$ as in the single-lead case. With the multilead scheme, the transformed leads where no TWA is detected are discarded first, and then a signal in the original domain is reconstructed using only those transformed leads with TWA. Discarding the transformed leads without TWA has a denoising effect that improves the estimation of TWA in the reconstructed signal, as the following chapters will show.

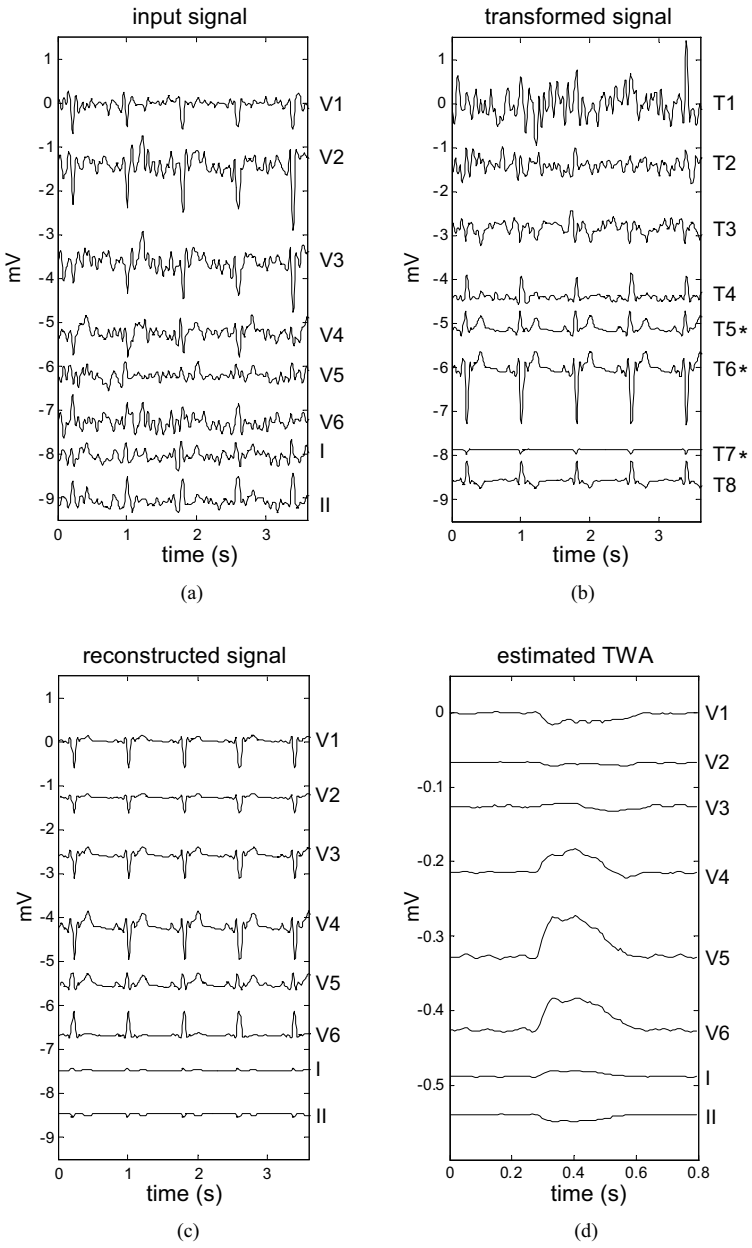

Figure 3.3: (a) Simulated signal with TWA embedded in noise (ASNR $= -20$ dB). (b) Signal transformed with PCA. Asterisks indicate the transformed leads where TWA is detected ($d_5 = d_6 = d_7 = 1$). (c) Reconstructed signal. (d) Estimated TWA waveform.

Therefore, a diagonal matrix is defined from the lead-by-lead detection as

$$\mathbb{A} = \begin{bmatrix} d_1 & & 0 \\ & \ddots & \\ 0 & & d_L \end{bmatrix} \tag{3.15}$$

and the reconstruction matrix $(\mathbf{\Psi}^T)^{-1}$ is truncated as follows

$$\mathbf{\Psi}_{\text{TR}} = (\mathbf{\Psi}^T)^{-1}\mathbb{A}. \tag{3.16}$$

Matrix $\mathbf{\Psi}_{\text{TR}}$ has zeros in columns corresponding to leads without TWA. A reconstructed signal is then obtained from the leads with detected TWA as

$$\tilde{\mathbf{X}} = \mathbf{\Psi}_{\text{TR}}\mathbf{Y}. \tag{3.17}$$

The reconstructed data matrix $\tilde{\mathbf{X}}$ consists of the concatenation of the multilead single-beat matrices $\tilde{\mathbf{X}}_k$:

$$\tilde{\mathbf{X}} = \begin{bmatrix} \tilde{\mathbf{X}}_0 & \tilde{\mathbf{X}}_1 & \dots & \tilde{\mathbf{X}}_{K-1} \end{bmatrix} \tag{3.18}$$

where

$$\tilde{\mathbf{X}}_k = \begin{bmatrix} \tilde{\mathbf{x}}_{k,1} & \dots & \tilde{\mathbf{x}}_{k,L} \end{bmatrix}^T \tag{3.19}$$

with $\tilde{\mathbf{x}}_{k,l}$ corresponding to the reconstructed ST-T complex of the kth beat in the lth lead. Note that $\tilde{\mathbf{X}} = \left((\mathbf{\Psi}^T)^{-1}\mathbb{A}\mathbf{\Psi}^T\right)\mathbf{X}$ is equivalent to a spatially filtered version of $\mathbf{X}$, where the aim of the equivalent filter is to preserve the TWA content, not to obtain a perfect signal reconstruction. When no detection is obtained, $\tilde{\mathbf{X}} = 0$. Figure 3.3(c) shows the reconstructed signal for the example case.

3.3.5 Estimation of TWA

Finally, TWA waveform and amplitude are estimated as in (3.5) and (3.6), but from the reconstructed signal $\tilde{\mathbf{X}}$ instead of from the original signal $\mathbf{X}$. The estimated TWA for the example case is depicted in figure 3.3(d).

3.3.6 Variations of the general scheme

Throughout the thesis, several modifications of the general multilead scheme are considered, depending on the requirements of each particular study. In cases where the objective is to compare the detection power of different

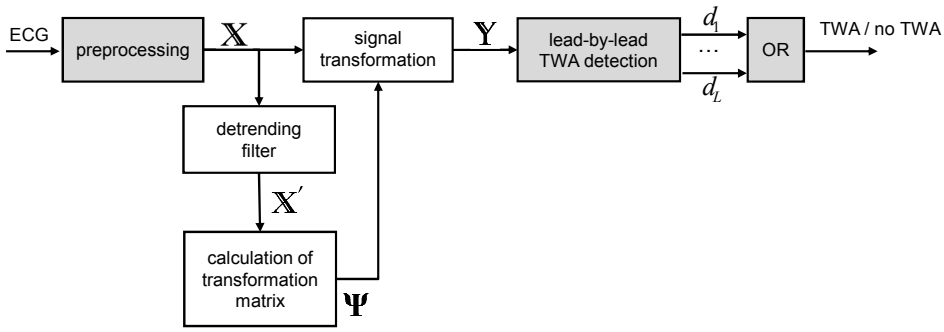

Figure 3.4: Simplified multilead scheme for TWA detection.

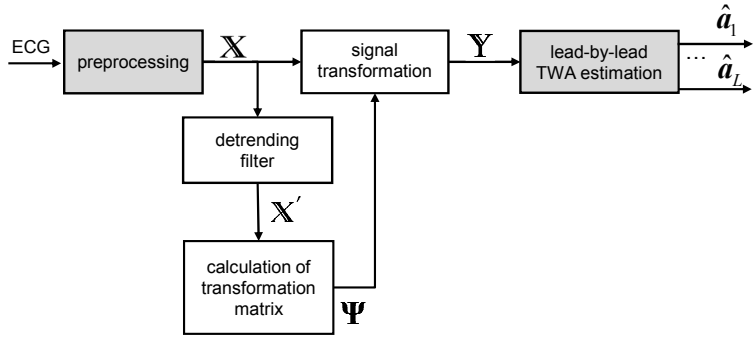

Figure 3.5: Modified multilead scheme for TWA analysis in situations where no detection threshold can be determined.

alternatives, such as in studies reported in sections 4.4.3 and 5.4.3, a simplified version of the general multilead scheme is used, in which reconstruction and estimation stages are omitted (figure 3.4).

For those cases where a detection threshold γ can not be set under realistic assumptions, such as the clinical study with ambulatory records (see chapter 6), a modified version is proposed in which TWA is estimated in the transformed leads (figure 3.5).

3.4 Signal transformation techniques

3.4.1 Principal Component Analysis

Principal component analysis (PCA) is a statistical technique which converts a set of correlated variables into a set of uncorrelated variables ("principal components"). In general, the objective of PCA is to condense the information of a large set of variables into a few variables, while maintaining the variability present in the dataset [Joliffe, 2002]. In this thesis, however, the main objective of PCA is to separate TWA from noise as much as possible, since TWA and noise originate from different physical processes, and therefore it is sensible to assume that they are uncorrelated.

The derivation of principal components assumes that the signal $\mathbf{X}'$ is a zero-mean random process with a spatial (inter-lead) correlation $\mathbf{R}_{\mathbf{X}'} = E\{\mathbf{X}'\mathbf{X}'^T\}$. The principal components of $\mathbf{X}'$ result from applying an orthogonal linear transformation $\mathbf{\Psi} = [\boldsymbol{\psi}_1\ \boldsymbol{\psi}_2\ \ldots\ \boldsymbol{\psi}_L]$ to $\mathbf{X}'$,

$$\mathbf{Y}' = \mathbf{\Psi}^T\mathbf{X}', \tag{3.20}$$

so that the rows of $\mathbf{Y}'$ (that is, the transformed leads) become mutually uncorrelated and sorted in descending order of variance. The first principal component is obtained as a scalar product $\tilde{\mathbf{y}}_1' = \boldsymbol{\psi}_1^T\mathbf{X}'$, where the vector $\boldsymbol{\psi}_1$ is chosen so that the variance of $\tilde{\mathbf{y}}_1'$,

$$E\{\tilde{\mathbf{y}}_1'\tilde{\mathbf{y}}_1'^T\} = E\{\boldsymbol{\psi}_1^T\mathbf{X}'\mathbf{X}'^T\boldsymbol{\psi}_1\} = \boldsymbol{\psi}_1^T\mathbf{R}_{\mathbf{X}'}\boldsymbol{\psi}_1 \tag{3.21}$$

is maximized subject to the constraint that $\boldsymbol{\psi}_1^T\boldsymbol{\psi}_1 = 1$. The maximum variance is obtained when $\boldsymbol{\psi}_1$ is chosen as the normalized eigenvector corresponding to the largest eigenvalue of $\mathbf{R}_{\mathbf{X}'}$, denoted as λ_1. In that case, the resulting variance is

$$E\{\tilde{\mathbf{y}}_1'\tilde{\mathbf{y}}_1'^T\} = \boldsymbol{\psi}_1^T\mathbf{R}_{\mathbf{X}'}\boldsymbol{\psi}_1 = \lambda_1\boldsymbol{\psi}_1^T\boldsymbol{\psi}_1 = \lambda_1. \tag{3.22}$$

Subject to the constraint that $\tilde{\mathbf{y}}_1^{'}$ and the second principal component $\tilde{\mathbf{y}}_2^{'}$ should be uncorrelated, $\tilde{\mathbf{y}}_2^{'}$ is obtained by choosing $\boldsymbol{\psi}_2$ as the eigenvector corresponding to the second largest eigenvalue of $\mathbf{R}_{\mathbf{X}'}$, and so on. Accordingly, to obtain the whole set of L different principal components, the eigenvector equation for $\mathbf{R}_{\mathbf{X}'}$ needs to be solved,

$$\mathbf{R}_{\mathbf{X}'}\boldsymbol{\Psi} = \boldsymbol{\Psi}\boldsymbol{\Lambda} \tag{3.23}$$

where $\boldsymbol{\Lambda}$ denotes a diagonal matrix with the eigenvalues $\lambda_1 \ \ldots \ \lambda_L$ sorted in descending order, and $\boldsymbol{\Psi}$ denotes the corresponding eigenvector matrix. Since $\mathbf{R}_{\mathbf{X}'}$ is unknown in practice, it can be approximated by the sample correlation matrix, defined as

$$\hat{\mathbf{R}}_{\mathbf{X}'} = \frac{1}{(K-1)N}\mathbf{X}'\mathbf{X}'^{T}. \tag{3.24}$$

Figure 3.3(b) shows the input signal in (a) after transformation with PCA.

3.4.2 Periodic Component Analysis

Periodic Component Analysis (πCA) is an eigenvalue technique for analyzing periodic structure in multichannel signals. It was first proposed for speech analysis [Saul and Allen, 2000] and then applied to the analysis of ECGs, for ECG compression and also for maternal and fetal ECG separation [Sameni et al., 2008].

This technique aims to find the projection $\tilde{\mathbf{y}}^{'} = \mathbf{w}^{T}\mathbf{X}'$ that maximizes the periodic structure of the signal at the TWA frequency, with $\mathbf{w} = [w_1 \ w_2 \ \ldots \ w_L]^T$ being a column vector with L real weights. To do so, a cost function is defined as

$$\epsilon(\mathbf{w}, m) = \frac{\left\|\tilde{\mathbf{y}}'^{(m)} - \tilde{\mathbf{y}}'\right\|^2}{\left\|\tilde{\mathbf{y}}'\right\|^2} \tag{3.25}$$

where $\tilde{\mathbf{y}}'^{(m)} = \mathbf{w}^{T}\mathbf{X}'^{(m)}$, with $\mathbf{X}'^{(m)}$ defined in (3.12), and $m = 2$ beats is the period of the TWA. This cost function is an inverse measure of periodicity: if the resulting signal $\tilde{\mathbf{y}}^{'}$ is periodic with period m, $\tilde{\mathbf{y}}^{'} = \tilde{\mathbf{y}}'^{(m)}$ and therefore $\epsilon(\mathbf{w}, m) = 0$.

Expanding the right hand side of (3.25) in terms of the weights $\mathbf{w}$ gives

$$\begin{aligned}\epsilon(\mathbf{w},m) &= \frac{\left\|\mathbf{w}^T\mathbf{X}'^{(m)} - \mathbf{w}^T\mathbf{X}'\right\|^2}{\|\mathbf{w}^T\mathbf{X}'\|^2} = \frac{\left\|\mathbf{w}^T(\mathbf{X}'^{(m)} - \mathbf{X}')\right\|^2}{\|\mathbf{w}^T\mathbf{X}'\|^2} \\ &= \frac{\mathbf{w}^T(\mathbf{X}'^{(m)} - \mathbf{X}')(\mathbf{X}'^{(m)} - \mathbf{X}')^T\mathbf{w}}{\mathbf{w}^T\mathbf{X}'\mathbf{X}'^T\mathbf{w}^T} = \frac{\mathbf{w}^T\hat{\mathbf{A}}_{\mathbf{X}'}(m)\mathbf{w}}{\mathbf{w}^T\hat{\mathbf{R}}_{\mathbf{X}'}\mathbf{w}}\end{aligned}$$

where $\hat{\mathbf{A}}_{\mathbf{X}'}(m)$ is the spatial sample correlation of $\left(\mathbf{X}^{(m)\prime} - \mathbf{X}'\right)$, and $\hat{\mathbf{R}}_{\mathbf{X}'}$ is the spatial sample correlation of $\mathbf{X}'$, defined in (3.24).

In the resulting expression,

$$\epsilon(\mathbf{w},m) = \frac{\mathbf{w}^T\hat{\mathbf{A}}_{\mathbf{X}'}(m)\mathbf{w}}{\mathbf{w}^T\hat{\mathbf{R}}_{\mathbf{X}'}\mathbf{w}} \tag{3.26}$$

the numerator and denominator are both quadratic forms in the weights $\mathbf{w}$. Such ratio is known as a *Rayleigh quotient*. By the Rayleigh-Ritz theorem of linear algebra, the weights $\mathbf{w}$ that minimize (3.26) are given by the generalized eigenvector corresponding to the smallest generalized eigenvalue of the matrix pair $\left(\hat{\mathbf{A}}_{\mathbf{X}'}(m), \hat{\mathbf{R}}_{\mathbf{X}'}\right)$ (see appendix 3.B for details).

Therefore, the transformation matrix $\mathbf{\Psi}$ is chosen as the generalized eigenvector matrix of $\left(\hat{\mathbf{A}}_{\mathbf{X}'}(m), \hat{\mathbf{R}}_{\mathbf{X}'}\right)$, with the eigenvectors (columns of $\mathbf{\Psi}$) sorted according to the corresponding eigenvalues in ascending order of magnitude. In this way, the transformation $\mathbf{Y} = \mathbf{\Psi}^T\mathbf{X}$ projects the most periodic component into the first row of $\mathbf{Y}$, that is, TWA—if present—is projected onto the first transformed lead, and therefore the first column of $\mathbf{\Psi}$ can be interpreted as the spatial direction from which the periodic content of the signal is better observed.

3.4.3 Spectral Ratio Maximization

Spectral Ratio Maximization (SRM) is a novel technique proposed in this thesis to improve the detection of TWA. Like πCA, SRM tries to find a projection $\tilde{\mathbf{y}}' = \mathbf{w}^T\mathbf{X}'$ that maximizes the periodicity of the transformed signal, but the measure of periodicity is now defined in the spectral domain as

$$\xi(\mathbf{w}) = \frac{S_{\tilde{\mathbf{y}}}(f_{0.5})}{\int S_{\tilde{\mathbf{y}}}(f)\, df} \tag{3.27}$$

where $S_{\tilde{\mathbf{y}}}(f)$ is the power spectral density of the transformed signal, estimated with the modified periodogram, and $f_{0.5}$ is the frequency of TWA (0.5 cycles per beat).

To find the $\mathbf{w}$ that maximizes (3.27), a gradient-based optimization algorithm is applied as implemented in MATLAB Optimization toolbox function *fminunc* [Mat, 2002]. The algorithm follows a quasi-Newton approach and uses the Broyden-Fletcher-Goldfarb-Shanno (BFGS) method for updating the Hessian matrix (second partial derivatives of the objective function), which is widely believed to be the most effective technique for general use [Broyden, 1970, Fletcher, 1970, Goldfarb, 1970, Shanno, 1970]. Unlike PCA or πCA, in this case the transformed signal $\mathbf{Y}$ will only contain one transformed lead.

To evaluate the sensitivity of the technique to the initial conditions, two options are considered to initialize the iterative algorithm: the vector $\mathbf{w} = [1\ 0\ \ldots\ 0]^T$, which represents a projection on the first lead axis of the input signal (**SRM** scheme), and the projection $\mathbf{w}$ obtained with πCA as described above (π**CA-SRM** scheme).

3.4.4 Independent Component Analysis

Independent component analysis (ICA) is increasing in popularity in the field of biomedical signal processing. It is generally used when it is required to separate measured biomedical signals into their constituent underlying components. Most applications of ICA are to multichannel time series measurements. In that case, the term blind source separation (BSS) can be used as a more generic identifier of the separation process [James and Hesse, 2005].

The basic BSS problem that ICA attempts to solve assumes a set of L observations, in our case the matrix $\mathbf{X}'$ defined in (3.12), to be a combination of M unknown sources,

$$\mathbf{S} = \begin{bmatrix} \mathbf{s}_1 \\ \vdots \\ \mathbf{s}_M \end{bmatrix} \tag{3.28}$$

where the sources $\mathbf{s}_i$ are $(1 \times KN)$ row vectors. The mixing of the sources is generally assumed to be linear, and the mixing matrix describing the linear combination of the sources is given by the full-rank $(L \times M)$ matrix $\mathbf{U}$ such that

$$\mathbf{X}' = \mathbf{US}. \tag{3.29}$$

It is also generally assumed that the number of underlying sources is less than or equal to the number of measurement channels ($M \leq L$). In our case, it will be assumed that $M = L$.

The task of ICA algorithms is to recover the original sources $\mathbf{S}$ from the observations $\mathbf{X}^{'}$, and this translates to that of finding a de-mixing matrix $\mathbf{W}$ such that

$$\hat{\mathbf{S}} = \mathbf{W}\mathbf{X}^{'}, \tag{3.30}$$

where $\hat{\mathbf{S}}$ are the resulting estimates of the underlying sources. To compute the de-mixing matrix, ICA algorithms assume that the resulting sources must be mutually independent. Statistical independence is a stronger assumption that uncorrelatedness, and while statistically independent sources are always uncorrelated, the contrary does not necessarily happen. This means that independent variables are uncorrelated and have no higher order correlations.

Besides uncorrelatedness, statistical independence is based on higher order statistics (HOS). It is possible to obtain an estimate $\hat{\mathbf{S}}$ of the sources $\mathbf{S}$ if the sources are non-Gaussian [Hyvärinen et al., 2001]. In practice, it is enough to make the estimates $\hat{\mathbf{S}}$ as non-Gaussian as possible because, according to the central limit theorem, sums of independent non-Gaussian random variables are closer to Gaussian than the originals. In this way, looking for independent sources is equivalent to looking for non-Gaussian sources.

In this thesis, two widely referenced techniques for implementing ICA following a HOS approach are used: FastICA and JADE. FastICA is one of the most referenced ICA techniques in the literature [Hyvärinen, 1999] and it is freely distributed in http://www.cis.hut.fi/projects/ica/fastica/ (Last accessed: April 2011). The FastICA algorithm finds the transformation that maximizes the independence of the components by minimizing their mutual information with a fixed point algorithm.

JADE is a widely used algorithm [Cardoso and Souloumiac, 1993] that finds the transformation that maximizes the independence of the signal components by jointly diagonalizing fourth-order cumulant tensors. The JADE algorithm is publicly available in http://perso.telecom-paristech.fr/~cardoso/guidesepsou.html (Last accessed: April 2011).

For the multilead scheme, the transformation matrix $\mathbf{\Psi}$ is chosen as the de-mixing matrix obtained with FastICA or JADE algorithms.

3.5 ECG Databases

Various datasets, consisting of both real ECGs and synthetic signals, are used along the thesis for the evaluation of the methods described in previous sections. This section presents the ECG databases that are either analyzed in the evaluation studies, or used as a basis for the generation of synthetic signals.

3.5.1 STAFF-III Database

The STAFF-III database contains the ECGs from 102 patients at the Charleston Area Medical Center in West Virginia. Nine standard leads (V1-V6, I, II, and III) were recorded using equipment by Siemens-Elema AB (Solna, Sweden) and digitized at a sampling rate of 1 kHz.

ECGs were recorded while patients underwent percutaneous transluminal coronary angioplasty (PTCA), which is a procedure for opening damaged or obstructed coronary arteries that involves the inflation of a balloon inside the artery to open it up. This inflation produces acute ischemia in the cells of the myocardium, which can induce TWA. The STAFF-III database was used in [Martínez et al., 2006] to characterize the relation between TWA and acute ischemia.

In this thesis, real TWA episodes were extracted from STAFF-III signals to create the evaluation datasets described in sections 4.2.1 and 5.2.2.

3.5.2 PTB Diagnostic ECG Database

The PTB Diagnostic ECG Database was compiled by the National Metrology Institute of Germany and is publicly available at http://www.physionet.org/physiobank/database/ptbdb/. The database contains 549 ECGs collected from healthy volunteers and patients with different heart diseases. Each ECG record includes the conventional 12 leads, together with the 3 Frank leads, and is digitized at a sampling rate of 1 kHz.

In this thesis, records from healthy volunteers were used to recreate realistic noise conditions in the synthetic signals described in section 4.2.1.

3.5.3 Stress Test Database

This data set was compiled at the University Hospital Lozano Blesa of Zaragoza (Spain) [Bailón et al., 2003]. It contains 12-lead ECGs recorded during treadmill exercise test following Bruce protocol, at 1 kHz sampling rate with an amplitude resolution of 0.6 μV. Records belong to three different groups: 211 patients with a negative clinical and electrical exercise test (*non-ischemic* group), 66 asymptomatic volunteers from the Spanish Army who underwent the exercise test with negative results for coronary artery disease (*volunteer* group), and 79 patients with significant stenosis in at least one major coronary artery as shown by coronary angiography (*ischemic* group).

In this thesis, records from *volunteer* and *non-ischemic* groups were used to create the evaluation dataset described in section 5.2.2. Records from *volunteer* and *ischemic* groups were analyzed to evaluate the clinical utility of the multilead schemes, as reported in sections 4.4.4 and 5.4.4.

3.5.4 Physionet TWA Database

The Physionet T-Wave alternans database is a publicly available resource compiled for the PhysioNet/Computers in Cardiology Challenge 2008 [Moody, 2008]. It contains one hundred real and synthetic ECG records, sampled at 500 Hz and with an approximate duration of two minutes. The synthetic subset of the database consists of thirty-two 12-lead ECGs containing artificial TWA in calibrated amounts. The remaining 68 records are real signals from different databases, 56 of which belong to patients with known cardiac risk factors. Synthetic records have 12 leads, and real records have 2, 3 or 12 leads.

In this thesis, the analysis of this database with the multilead schemes based on PCA and πCA is reported in section 5.4.5 as an example of application to a publicly available dataset.

3.5.5 MIT-BIH Noise Stress Test Database

This database includes 12 half-hour ECG recordings and 3 half-hour recordings of noise typical in ambulatory ECG recordings [Moody et al., 1984]. The noise recordings were made using physically active volunteers and standard ECG recorders, leads, and electrodes; the electrodes were placed on the limbs in positions in which the subjects' ECGs were not visible. The

three noise records were assembled from the recordings by selecting intervals that contained predominantly baseline wander (in record 'bw'), muscle artifact (in record 'ma', with a spectrum which overlaps that of the ECG, but which extends to higher frequencies), and electrode motion artifact (in record 'em', usually the result of intermittent mechanical forces acting on the electrodes).

In this thesis, noise records 'bw', 'ma' and 'em' were used to create synthetic signals with realistic noise, as described in sections 4.2.1 and 5.2.1.

3.5.6 MUSIC database

This database contains ambulatory ECGs and clinical follow-up information of more than 900 patients with symptomatic chronic heart failure (CHF), who were enrolled in the MUSIC (MUerte Súbita en Insuficiencia Cardiaca) study, a prospective, multicenter study designed to assess risk predictors for cardiovascular mortality in patients with CHF [Vázquez et al., 2009]. Twenty-four-hour ECGs with the XYZ orthogonal leads and a sampling rate of 200 Hz were recorded using SpiderView recorders (ELA Medical, Sorin Group, Paris, France).

In this thesis, a total of 650 patients with sinus rhythm were considered for the clinical study presented in chapter 6.

Appendix 3.A: GLRT and MLE derivation for the LLRM

The derivation of the GLRT and the MLE for the LLRM presented here has been taken from [Martínez and Olmos, 2003, 2005] and [Martínez et al., 2006].

As explained in section 3.2.2, the LLRM assumes the following model for the observed signal

$$\mathbf{x}_k = \mathbf{s} + \frac{1}{2}\boldsymbol{a}(-1)^k + \mathbf{v}_k \tag{3.31}$$

which is the same equation that (3.3), but where the lead index l has been omitted for simplicity, since the LLRM is applied to each lead independently. After applying the detrending filter in (3.4), we obtain

$$\mathbf{x}_k^{'} = \mathbf{x}_k - \mathbf{x}_{k-1} = \boldsymbol{a}(-1)^k + (\mathbf{v}_k - \mathbf{v}_{k-1}) = \boldsymbol{a}(-1)^k + \mathbf{w}_k, \tag{3.32}$$

where the TWA waveform, $\boldsymbol{a}$, is deterministic but unknown, and the rest of undesired components are grouped into the noise term $\mathbf{w}_k = \mathbf{v}_k - \mathbf{v}_{k-1}$. The LLRM assumes that the noise samples in $\mathbf{w}_k$ follow a zero-mean Laplacian distribution with unknown standard deviation σ. In this model, both the TWA waveform $\boldsymbol{a}$ and the noise level σ are assumed to be stationary within the analysis window, but are allowed to change as the analysis window runs through the record, allowing adaptation to changes in signal and noise.

Departing from this model, the TWA detection problem can be expressed as the hypothesis test

$$\begin{aligned} H_0 &: \boldsymbol{a} = 0 \\ H_1 &: \boldsymbol{a} \neq 0. \end{aligned} \tag{3.33}$$

A data matrix is created by putting together all the observations in the analysis window,

$$\mathbf{X}' = \left[\mathbf{x}_1'^T, \ldots, \mathbf{x}_{K-1}'^T\right], \tag{3.34}$$

were each column contains one observation of the data (that is, the samples corresponding to one detrended beat). We can express the likelihood function for this data matrix as

$$p\left(\mathbf{X}'; \boldsymbol{a}, \sigma\right) = \left(\frac{1}{\sqrt{2}\sigma}\right)^{KN} \exp\left\{-\frac{\sqrt{2}}{\sigma}\sum_{k=1}^{K-1}\left\|\mathbf{x}_k^{'} - \boldsymbol{a}(-1)^k\right\|_1\right\}. \tag{3.35}$$

The GLRT is given by the likelihood ratio

$$L_G = \frac{p\left(\mathbf{X}'; \hat{\boldsymbol{a}}, \hat{\sigma}_1, H_1\right)}{p\left(\mathbf{X}'; \hat{\sigma}_0, H_0\right)} \underset{H_0}{\overset{H_1}{\gtrless}} \gamma, \tag{3.36}$$

where the unknown parameters $\boldsymbol{a}$ and σ are replaced by their MLE under each hypothesis ($\hat{\boldsymbol{a}}$ is the MLE of $\boldsymbol{a}$ under H_1, and $\hat{\sigma}_1$ and $\hat{\sigma}_0$ are the MLE of σ under H_1 and H_0 respectively).

Under H_1, the MLE of $\boldsymbol{a}$ must fulfill the condition

$$\hat{\boldsymbol{a}} = \arg\max_{\boldsymbol{a}} \, p\left(\mathbf{X}^{'}; \boldsymbol{a}, \sigma, H_1\right), \tag{3.37}$$

and, since finding the maximum of the likelihood function is equivalent to finding the minimum of

$$-\ln p\left(\mathbf{X}^{'}; \boldsymbol{a}, \sigma, H_1\right) = -\ln\left(\frac{1}{\sqrt{2}\sigma}\right)^{KN} + \frac{\sqrt{2}}{\sigma}\sum_{k=1}^{K-1}\left\|\mathbf{x}_k^{'} - \boldsymbol{a}(-1)^k\right\|_1, \tag{3.38}$$

the condition in (3.37) can be rewritten as

$$\hat{\boldsymbol{a}} = \arg\min_{\boldsymbol{a}} \sum_{k=1}^{K-1}\left\|\mathbf{x}_k^{'} - \boldsymbol{a}(-1)^k\right\|_1. \tag{3.39}$$

It can be shown [Kay, 1993] that this condition is accomplished when $\hat{\boldsymbol{a}}$ is the median of the demodulated series

$$\hat{\boldsymbol{a}} = \text{median}\left(\left\{\mathbf{x}_k^{'}(-1)^k\right\}_{k=1}^{K-1}\right) \tag{3.40}$$

which is the vector-notation equivalent to the expression given in (3.5).

Equaling to zero the partial derivatives of (3.35) with respect to σ under both hypothesis, we obtain the MLEs

$$\hat{\sigma}_0 = \frac{\sqrt{2}}{KN}\sum_{k=1}^{K-1}\left\|\mathbf{x}_k^{'}\right\|_1 \tag{3.41}$$

and

$$\hat{\sigma}_1 = \frac{\sqrt{2}}{KN}\sum_{k=1}^{K-1}\left\|\mathbf{x}_k^{'} - \boldsymbol{a}(-1)^k\right\|_1, \tag{3.42}$$

which is the expression given in (3.8). Substituting the MLEs in (3.36), we get the GLRT

$$L_G = \left(\frac{\hat{\sigma}_0}{\hat{\sigma}_1}\right)^{KN} \underset{H_0}{\overset{H_1}{\gtrless}} \gamma. \tag{3.43}$$

Applying the monotonically increasing function $f(x) = x^{(1/KN)} - 1$ to both sides of (3.43) we get the equivalent test

$$Z = \frac{\sqrt{2}}{\hat{\sigma}_1 KN}\sum_{n=0}^{N-1} z(n) \underset{H_0}{\overset{H_1}{\gtrless}} \gamma^{'}, \tag{3.44}$$

where

$$z(n) = \sum_{k=1}^{K-1} \left|x'_k(n)\right| - \sum_{k=1}^{K-1} \left|x'_k(n) - \hat{a}(n)(-1)^k\right| \tag{3.45}$$

and $\gamma^{'} = \gamma^{(1/KN)} - 1$ is the new threshold. The combination of (3.44) and (3.45) results in the expression given in (3.7).

Appendix 3.B: Generalized eigenvalues and the Rayleigh quotient

The **generalized eigenvalues** problem can be stated as follows: given matrices $\mathbf{A}, \mathbf{B} \in \mathbb{R}^{n \times n}$, find $\mathbf{e} \in \mathbb{R}^n, \lambda \in \mathbb{R}$ so that

$$\mathbf{A}\mathbf{e} = \lambda \mathbf{B}\mathbf{e}. \tag{3.46}$$

If $\mathbf{B}$ is non-singular, the solutions can be obtained by solving the equivalent (standard) eigenvalue problem

$$\mathbf{B}^{-1}\mathbf{A}\mathbf{e} = \lambda \mathbf{e}. \tag{3.47}$$

Now let us assume that both $\mathbf{A}$ and $\mathbf{B}$ are symmetric and, in addition, $\mathbf{B}$ is also positive definite. The ratio

$$r(\mathbf{w}) = \frac{\mathbf{w}^T\mathbf{A}\mathbf{w}}{\mathbf{w}^T\mathbf{B}\mathbf{w}}, \tag{3.48}$$

which is known as Rayleigh quotient, is closely related to the generalized eigenvalues problem stated above. Let us determine the extremum points of $r(\mathbf{w})$, that is, the points $\mathbf{w}^*$ satisfying $\nabla r(\mathbf{w}^*) = 0$. The gradient $\nabla r(\mathbf{w})$ is calculated as

$$\nabla r(\mathbf{w}) = \frac{2\mathbf{A}\mathbf{w}(\mathbf{w}^T\mathbf{B}\mathbf{w}) - 2(\mathbf{w}^T\mathbf{A}\mathbf{w})\mathbf{B}\mathbf{w}}{(\mathbf{w}^T\mathbf{B}\mathbf{w})^2} = \frac{2\mathbf{A}\mathbf{w} - 2r(\mathbf{w})\mathbf{B}\mathbf{w}}{\mathbf{w}^T\mathbf{B}\mathbf{w}}. \tag{3.49}$$

Setting $\nabla r(\mathbf{w})$ to 0, we obtain,

$$\mathbf{A}\mathbf{w} = r(\mathbf{w})\mathbf{B}\mathbf{w}, \tag{3.50}$$

which can be identified with (3.46). Thus, the extremum points $\mathbf{w}^*$ (extremum values $r(\mathbf{w}^*)$) are obtained as the eigenvectors $\mathbf{e}$ of the corresponding generalized eigenproblem. A formal prove of this result (the *Rayleigh-Ritz* theorem) can be found in [Strang, 1988].

Chapter 4

Evaluation of the multilead scheme based on Principal Component Analysis

4.1 Introduction

ECG signals present a high spatial redundancy that can be exploited with techniques based on the eigenanalysis of input data, such as PCA or Karhunen-Loève transform (KLT) [Castells et al., 2007]. These techniques have been applied to ECG data compression and noise reduction [Olmos et al., 1999, Acar and Köymen, 1999, Paul et al., 2000, Wei et al., 2001], characterization and diagnosis of ischemia [García et al., 1999, 2003], repolarization heterogeneity [Pueyo et al., 2009, Okin et al., 2002, Acar et al., 1999], atrial fibrillation [Faes et al., 2001, Castells et al., 2005] and separation of maternal and fetal ECG [Kanjilal and Palit, 1997].

This chapter describes the evaluation of the multilead scheme for TWA analysis that combines PCA with the LLRM. As stated in chapter 2, methodological evaluation of a new technique (that is, the quantification of its detection power and its estimation accuracy) is a desirable prior step to clinical validation (which quantifies the adequateness of the TWA test as a risk stratifier). The performance of the proposed scheme is evaluated by means of a simulation study, where the multilead scheme is compared to the single-lead scheme which is the usual approach to TWA analysis. Besides, an example of application to real signals is provided, to show that the performance improvement observed in simulation can also be obtained

in real datasets.

4.2 Data sets

4.2.1 Simulated data

Biomedical signal processing techniques are usually evaluated on standard databases, where the output of the technique is compared to reference annotations established by experts. However, the main problem in the case of TWA analysis is the lack of validation databases, mainly because TWA is often non-visible due to its low amplitude. Therefore, in this work a Monte Carlo simulation approach was adopted. To evaluate the multilead scheme and to compare it with the single-lead scheme, a simulation study was designed, where synthetic ECG signals were generated with a high degree of realism, and where TWA parameters (amplitude, waveform) were known *a priori*.

Multilead ECG signals were generated by adding noise and TWA to a clean background ECG (see figure 4.1). A standard beat from a 12-lead ECG record was selected to create the background ECG. A TWA waveform was detected and extracted from another 12-lead record using the LLRM. Both records belonged to the STAFF-III database (see section 3.5.1). From the 12-lead set, only the eight independent leads were selected ($L = 8$).

Four types of noise were considered: Gaussian (gs), Laplacian (lp), electrode motion (em) and muscular activity (ma). Noise types gs and lp were randomly generated. Types em and ma, which are typical noises present in the ECG, were extracted from two real noise records of the MIT-BIH Noise Stress Test Database (see section 3.5.1).

Each Monte Carlo trial was generated as the sum of the background ECG beat repeated K times, the TWA waveform repeated K times with alternating sign, and a random realization of noise. Each realization of noise was generated as follows. First, L segments of KN samples were simulated (gs or lp noise) or extracted from the records beginning at a random position (em or ma noise). Baseline wander was removed from em and ma noises, because em and ma records contain low frequency variations of high amplitude that can distort the level of noise actually added to the simulated ECG. Noise segments were normalized to a 1 μV RMS value and

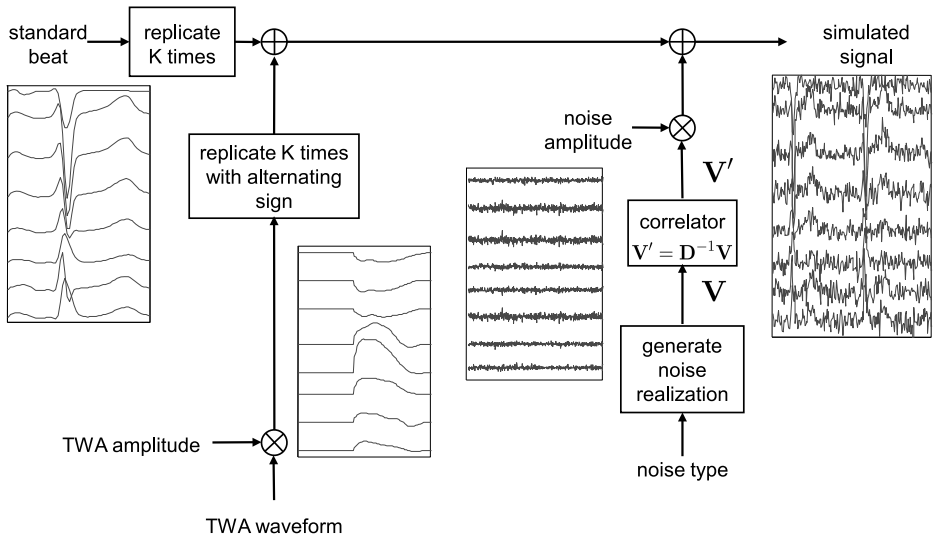

Figure 4.1: Simulation of multilead ECG signals with TWA and noise. Signals scale is not preserved for better visualization.

piled to form a multilead matrix $\mathbf{V}$

$$\mathbf{V} = \begin{bmatrix} \mathbf{v}_1 & \dots & \mathbf{v}_L \end{bmatrix}^T \tag{4.1}$$

Due to the noise generation setup, noise segments $\mathbf{v}_l$ are spatially uncorrelated ($\mathbf{R}_V = \mathbb{I}$). However, noise in real signals is spatially correlated. To correlate $\mathbf{V}$ in a realistic way, the first step was to estimate the spatial correlation of real ECG noise using 10 multilead ECG records of the PTB Diagnostic ECG database (see section 3.5.2). Figure 4.2 illustrates the process followed to estimate the correlation. A total of 2000 segments of noise were selected from each independent lead by taking the 50 ms interval prior to a P wave onset for each segment, since that interval is assumed to be isoelectric. DC level was removed, and segments corresponding to each lead were concatenated. The resulting noise leads were piled as in (4.1) to form a noise matrix $\mathbf{N}$. The spatial correlation of $\mathbf{N}$ was estimated as

$$\hat{\mathbf{R}}_N = \frac{1}{M}\mathbf{N}\mathbf{N}^T \tag{4.2}$$

where M is the number of samples of each noise lead. The Cholesky decomposition [Golub and Van Loan, 1989] was applied to the inverse of the

noise correlation matrix to obtain a whitening matrix $\mathbf{D}$

$$\hat{\mathbf{R}}_N^{-1} = \mathbf{D}^T\mathbf{D} \tag{4.3}$$

where $\mathbf{D}$ is an upper triangular matrix with strictly positive diagonal entries. The inverse of $\mathbf{D}$ was used to spatially correlate the generated noise $\mathbf{V}$

$$\mathbf{V}' = \mathbf{D}^{-1}\mathbf{V} \tag{4.4}$$

thus obtaining a correlated noise matrix $\mathbf{V}'$ with a spatial correlation $\mathbf{R}_{\mathbf{V}'} = \hat{\mathbf{R}}_N$, that is,

$$\mathbf{R}_{\mathbf{V}'} = E\left\{\mathbf{V}'\mathbf{V}'^T\right\} = \mathbf{D}^{-1}E\left\{\mathbf{V}\mathbf{V}^T\right\}(\mathbf{D}^{-1})^T = \mathbf{D}^{-1}(\mathbf{D}^{-1})^T = \hat{\mathbf{R}}_N. \tag{4.5}$$

Finally, the correlated noise $\mathbf{V}'$ was scaled so that the RMS value of the least noisy lead was $V_{noise} = 200\ \mu V$. TWA was then scaled to obtain a desired Alternans-Signal-to-Noise ratio (ASNR), defined as the maximum ratio between TWA power and noise power in the L leads:

$$\text{ASNR} = 10\ \log\frac{(V_{alt}/2)^2}{V_{noise}^2} \tag{4.6}$$

where V_{alt} is the maximum RMS value of the TWA waveforms in the L leads, that is, $V_{alt} = \max\{V_{alt_1}\ \ldots\ V_{alt_L}\}$, with V_{alt_l} defined in (3.6). Multilead ECG signals were simulated with ASNR levels ranging from -60 to 10 dB, and also without TWA. For each type of noise, a total of 10^4 realizations of noise were generated to simulate signals without TWA, and 10^4 realizations for each ASNR level to generate signals with TWA.

4.2.2 Stress test signals

As an example of application to real data, TWA analysis was performed on the set of stress test ECG records presented in section 3.5.3. Records from *volunteer* and *ischemic* groups were selected for TWA analysis. *Volunteer* records had an average duration of 20 min, and the maximum heart rate (HR) over the test was 183 ± 8 beats per minute (bpm) (mean ± standard deviation). *Ischemic* records had an average duration of 16 min, and the maximum heart rate over the test was 134 ± 23 bpm.

4.3 Methods for TWA analysis

The complete simulated dataset was processed with the LLRM, following the basic single-lead scheme (see figure 3.1) and the general multilead

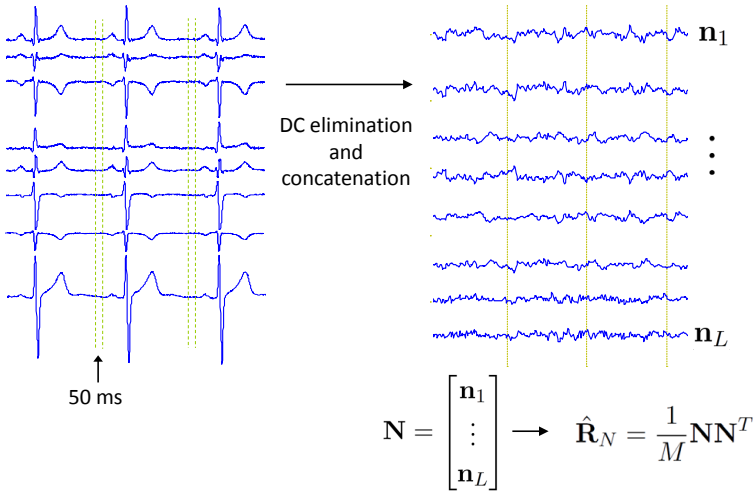

Figure 4.2: Illustration of the estimation of noise spatial correlation $\hat{\mathbf{R}}_N$ in real ECGs.

scheme (see figure 3.2), with an analysis window of $K = 32$ beats and $\delta = 1$ beat. Besides, simulated signals with *ma* noise were processed with both LLRM and SM, following the single-lead scheme and the simplified multilead scheme (see figure 3.4). For the comparison between LLRM and SM, a 128-beat analysis window was selected, since that is the window length used in commercial SM systems. In all cases the initial point of the ST-T complex was set 60 ms after the QRS fiducial point.

Stress test records were processed with the LLRM, following the single-lead scheme and the general multilead scheme, with a 128-beat analysis window and $\delta = 1$ beat. The initial points of ST-T complexes were set 80 ms after the QRS fiducial point if the mean HR in the analysis window was ≤ 100 bpm, and 60 ms after the QRS fiducial point if the mean HR was > 100 bpm.

4.4 Results

4.4.1 Detection performance

Following the terminology of detection theory [Kay, 1998], probability of false alarm (P_{FA}) was defined as the ratio between the number of positive TWA detections in signals with $V_{alt} = 0$ (false detections) and the total

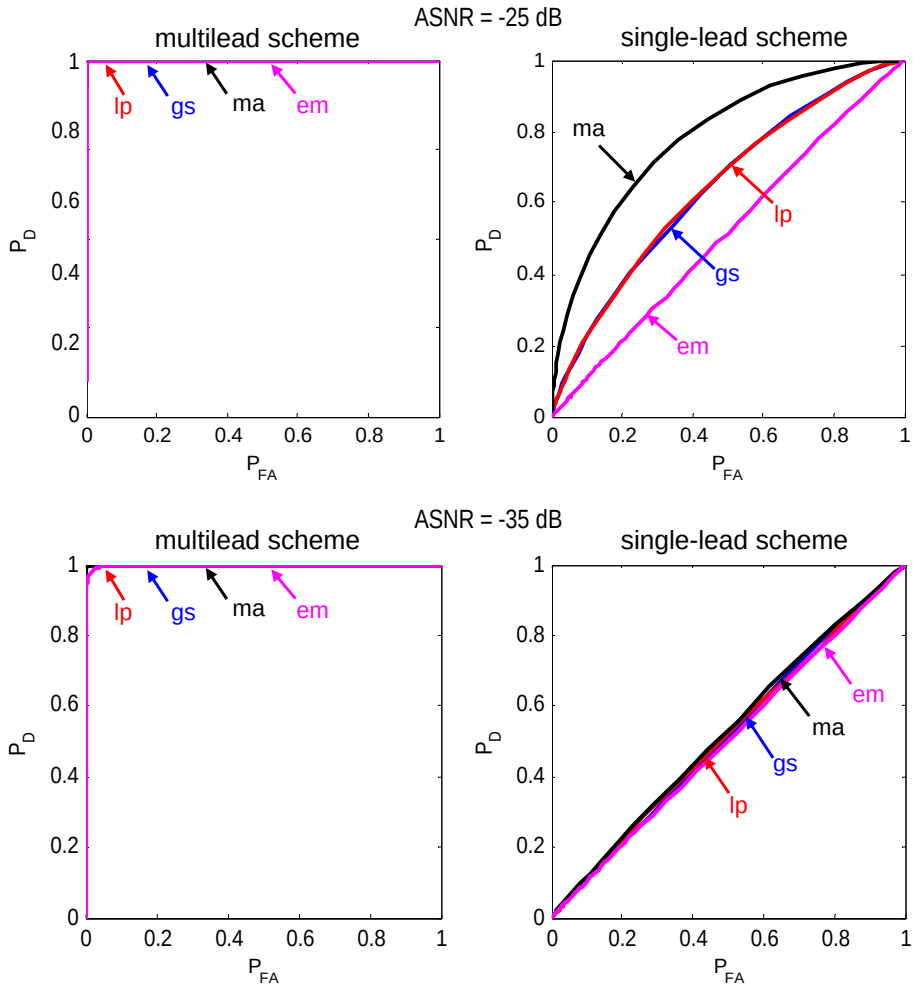

Figure 4.3: ROC curves for ASNR $= -25$ dB (corresponding to $V_{alt} = 22.5$ μV) and ASNR $= -35$ dB ($V_{alt} = 7.1$ μV) of the multilead scheme (left) and the single-lead scheme (right) combined with LLRM for Gaussian (gs), Laplacian (lp), muscular activity noise (ma) and electrode movement noise (em).

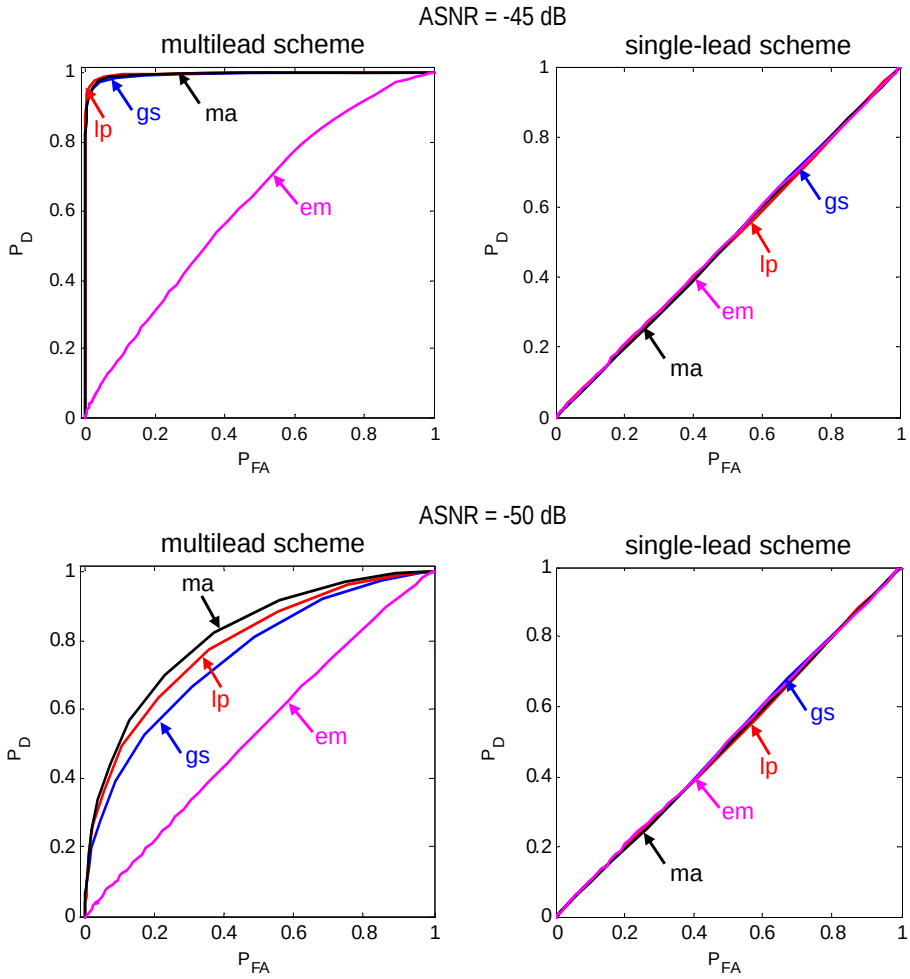

Figure 4.4: ROC curves for ASNR $= -45$ dB (corresponding to $V_{alt} = 2.2$ μV) and ASNR $= -50$ dB ($V_{alt} = 1.3$ μV) of the multilead scheme (left) and the single-lead scheme (right) combined with LLRM for Gaussian (gs), Laplacian (lp), muscular activity noise (ma) and electrode movement noise (em).

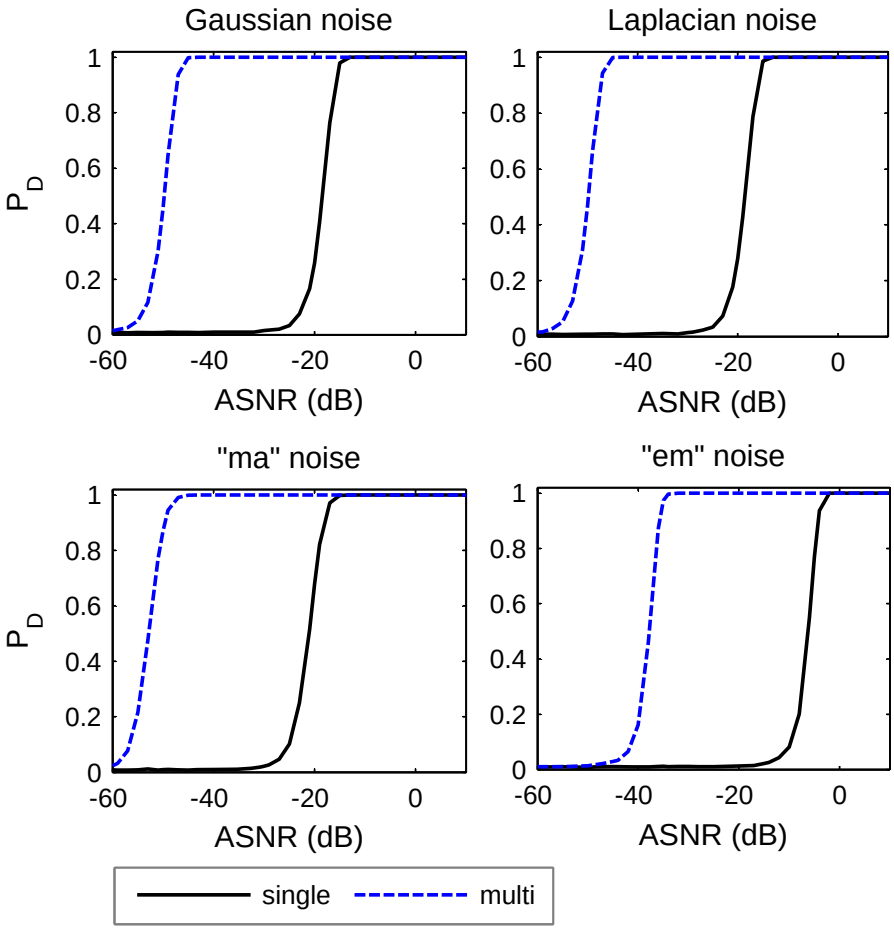

Figure 4.5: P_{D} for $P_{\mathrm{FA}} = 0.01$ of the single-lead (solid line) and the multilead scheme (dashed line) combined with LLRM vs. ASNR. Results obtained with an analysis window of 32 beats.

number of decisions made in those signals. Probability of detection (P_{D}) was defined as the ratio between the number of positive TWA detections in signals with a given V_{alt} and the total number of decisions made in those signals. Detection performance was evaluated with receiver operating characteristic (ROC) curves, which show the relationship between P_{D} and P_{FA} as a function of the detection threshold γ. Figure 4.3 shows the ROC curves corresponding to ASNR = -25 dB and -35 dB. Figure 4.4 shows the ROC curves corresponding to ASNR = -45 dB and -50 dB. For every type of noise and ASNR level, the area under the ROC curve of the multilead scheme was greater than the area under the single-lead curve.

To better analyze the behavior of the schemes for different ASNR levels, a fixed value for γ was selected so that $P_{\mathrm{FA}}= 0.01$, and the resulting P_{D} was compared. Detection thresholds were set to $\gamma = 0.06$ for *gs* noise, $\gamma = 0.06$ for *lp* noise, $\gamma = 0.06$ for *ma* noise, and $\gamma = 0.162$ for *em* noise. Figure 4.5 shows the P_{D} of the two schemes vs. ASNR for all types of noise. In all cases, the multilead scheme outperforms the single-lead scheme. The ASNR level where P_{D} achieves a value of 0.99 is 30 dB lower with the multilead scheme than with the single-lead scheme for *gs* and *lp* noises, 28 dB lower for *em* noise, and 27 dB lower for *ma* noise.

4.4.2 Estimation accuracy

The estimation performance of the two schemes was evaluated in terms of bias, variance and mean square error. Let us denote by $\hat{a}_l\,(n)$ the nth sample of the estimated TWA waveform in the lth lead, and by $a_l\,(n)$ the same sample of the true TWA waveform. For each ASNR level, the expected value of the estimation, $E\,\{\hat{a}_l\,(n)\}$, and the standard deviation of its samples, $\sigma_{\hat{a}_l}(n)$, were estimated as the samples average and the samples standard deviation of $\hat{a}_l\,(n)$ in the 10^4 realizations respectively. The bias and mean square error of the estimation were calculated for each lead l as

$$b_l(n) = E\,\{\hat{a}_l(n)\} - a_l(n),\ n = 0\ \ldots\ N-1 \tag{4.7}$$

$$e_l^2(n) = E\left\{(\hat{a}_l(n) - a_l(n))^2\right\},\ n = 0\ \ldots\ N-1 \tag{4.8}$$

where the expected values were estimated as the average of the 10^4 realizations. As explained in section 3.3.4, the reconstructed signal is $\tilde{\mathbf{X}} = 0$ if no TWA is detected, and in that case $\hat{a}_l(n) = 0,\ n = 0\ \ldots\ N-1$.

Figures 4.6 and 4.7 show the expected value and the standard deviation of the estimation for *gs* noise and various levels of ASNR. For high levels of ASNR (figure 4.6), the bias of the multilead estimation is higher than the bias of the single-lead estimation, but the standard deviation of the multilead estimation is lower. For low levels of ASNR (figure 4.7), both bias and variance are lower for the multilead estimation.

To globally quantify the accuracy of the estimation at each ASNR level, two global performance parameters, $\mathcal{R}_{b_l}$ and $\mathcal{R}_{e_l}$, were defined as

$$\mathcal{R}_{b_l}(\%) = \frac{\sqrt{\frac{1}{N}\sum_{n=0}^{N-1} b_l^2(n)}}{\sqrt{\frac{1}{N}\sum_{n=0}^{N-1} a_l^2(n)}} \times 100 \tag{4.9}$$

$$\mathcal{R}_{e_l}(\%) = \frac{\sqrt{\frac{1}{N}\sum_{n=0}^{N-1} e_l^2(n)}}{\sqrt{\frac{1}{N}\sum_{n=0}^{N-1} a_l^2(n)}} \times 100. \tag{4.10}$$

Parameter $\mathcal{R}_{b_l}$ measures the relative bias of the estimation in the lth lead, and parameter $\mathcal{R}_{e_l}$ measures the relative error caused by both the bias and the variance of the estimation. Figures 4.8 and 4.9 show the evolution of $\mathcal{R}_{b_l}$ and $\mathcal{R}_{e_l}$ vs. ASNR for *ma* noise. For ASNR ≥ -15 dB, the bias of the multilead estimation is higher than the bias of the single-lead estimation. For ASNR < -25 dB, the bias of the single-lead estimation tends to 100% for all the leads. $\mathcal{R}_b$ and $\mathcal{R}_e$ curves for *gs*, *lp*, and *em* noises are included in appendix 4.A. The same trend appears with all noise types: for high ASNR levels, $\mathcal{R}_{e_l}$ is similar for both schemes, and for low ASNR levels it is lower for the multilead scheme.

4.4.3 Comparison with the Spectral Method

As explained in the methods section, simulated signals with *ma* noise were processed with the single-lead and multilead schemes combined with LLRM (*LLR single* and *LLR multi* respectively), and also with the two schemes combined with SM (*SM single* and *SM multi*).

To ensure a fair comparison, detection thresholds were set so that the resulting P_{FA} was 0.01 for every technique (table 4.1). Detection curves for

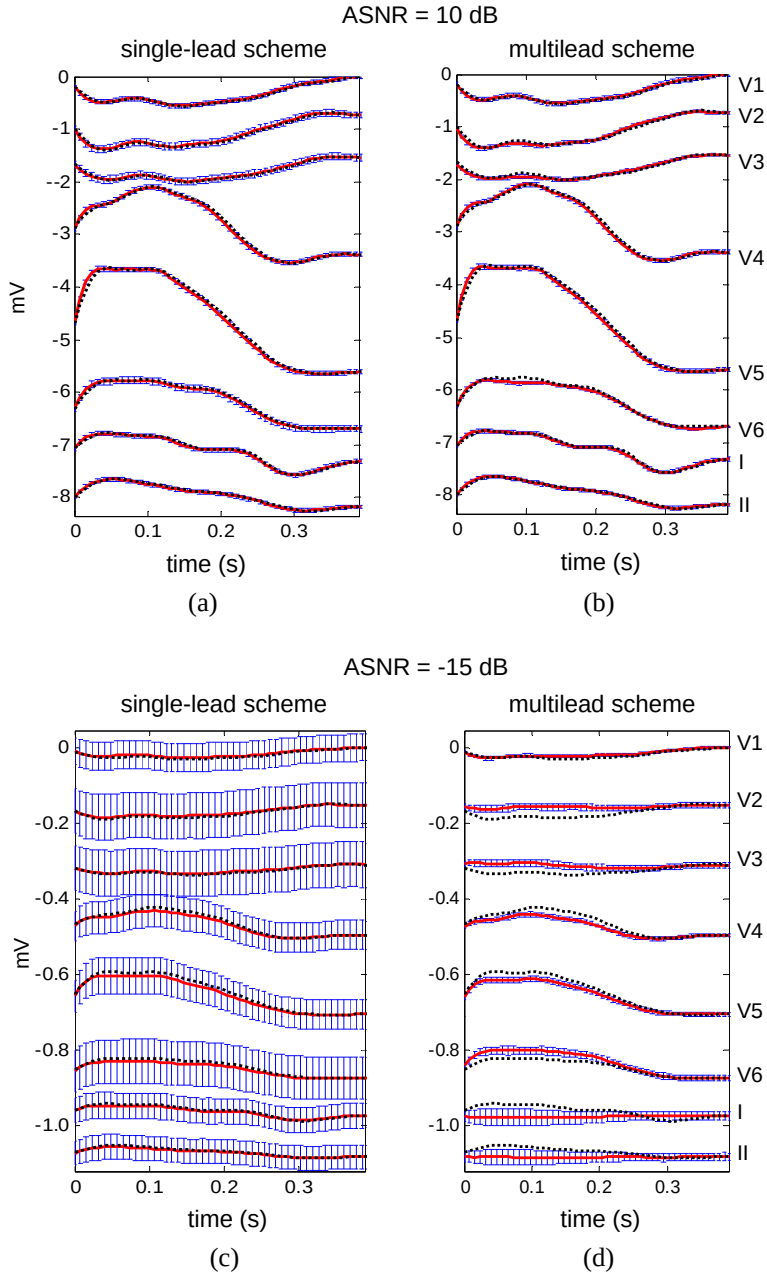

Figure 4.6: Expected value $E\{\hat{a}_l(n)\}$ (solid line) and standard deviation $\sigma_{\hat{a}_l}(n)$ (vertical bars) of the TWA waveforms estimated with the LLRM, obtained with (a) the single-lead and (b) the multilead scheme for ASNR = 10 dB, and with (c) the single-lead and (d) the multilead scheme for ASNR = -15 dB for *gs* noise. The true TWA is shown in dashed line. Leads offset is included for better visualization.

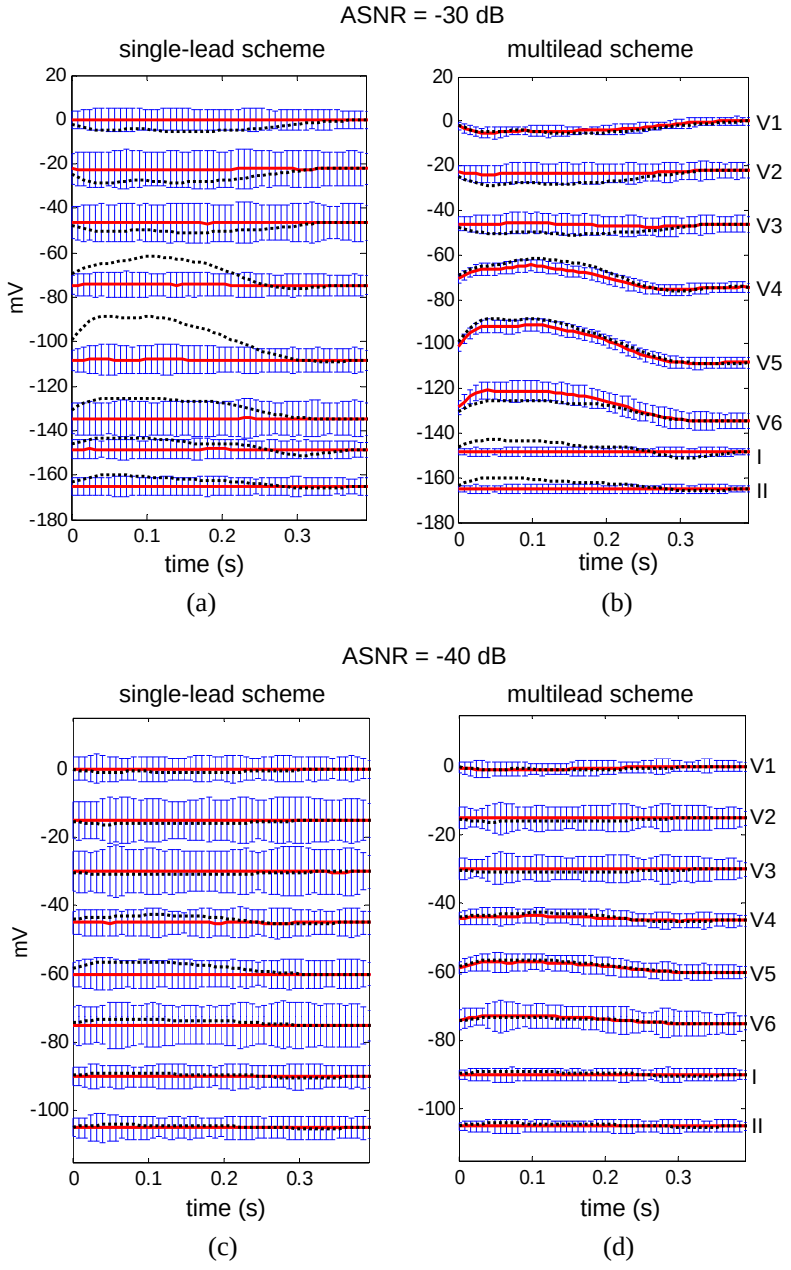

Figure 4.7: Expected value $E\{\hat{a}_l(n)\}$ (solid line) and standard deviation $\sigma_{\hat{a}_l}(n)$ (vertical bars) of the TWA waveforms estimated with the LLRM, obtained with (a) the single-lead and (b) the multilead scheme for ASNR = -30 dB, and with (c) the single-lead and (d) the multilead scheme for ASNR = -40 dB for *gs* noise. True TWA shown in dashed line. Leads offset included for better visualization.

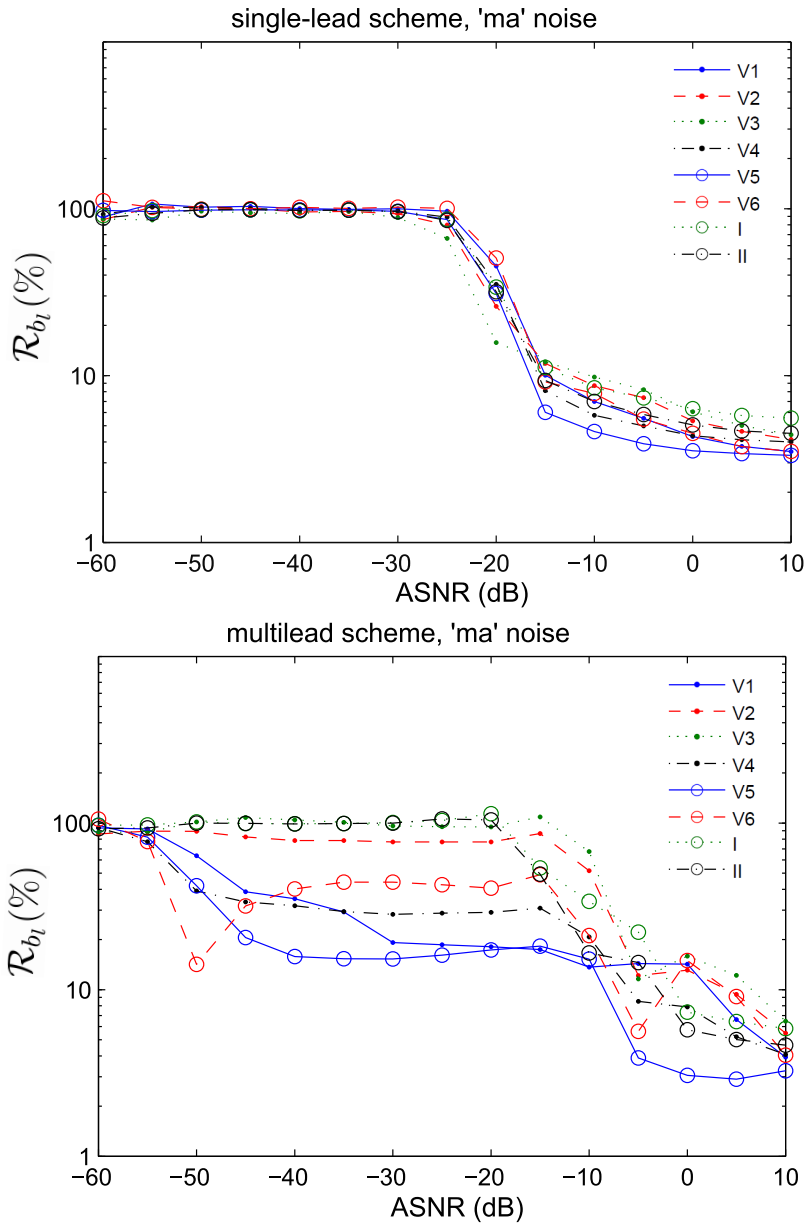

Figure 4.8: Relative bias of the TWA estimation obtained with the LLRM combined with the single-lead and (top) and with the multilead scheme (bottom) vs. ASNR for *ma* noise.

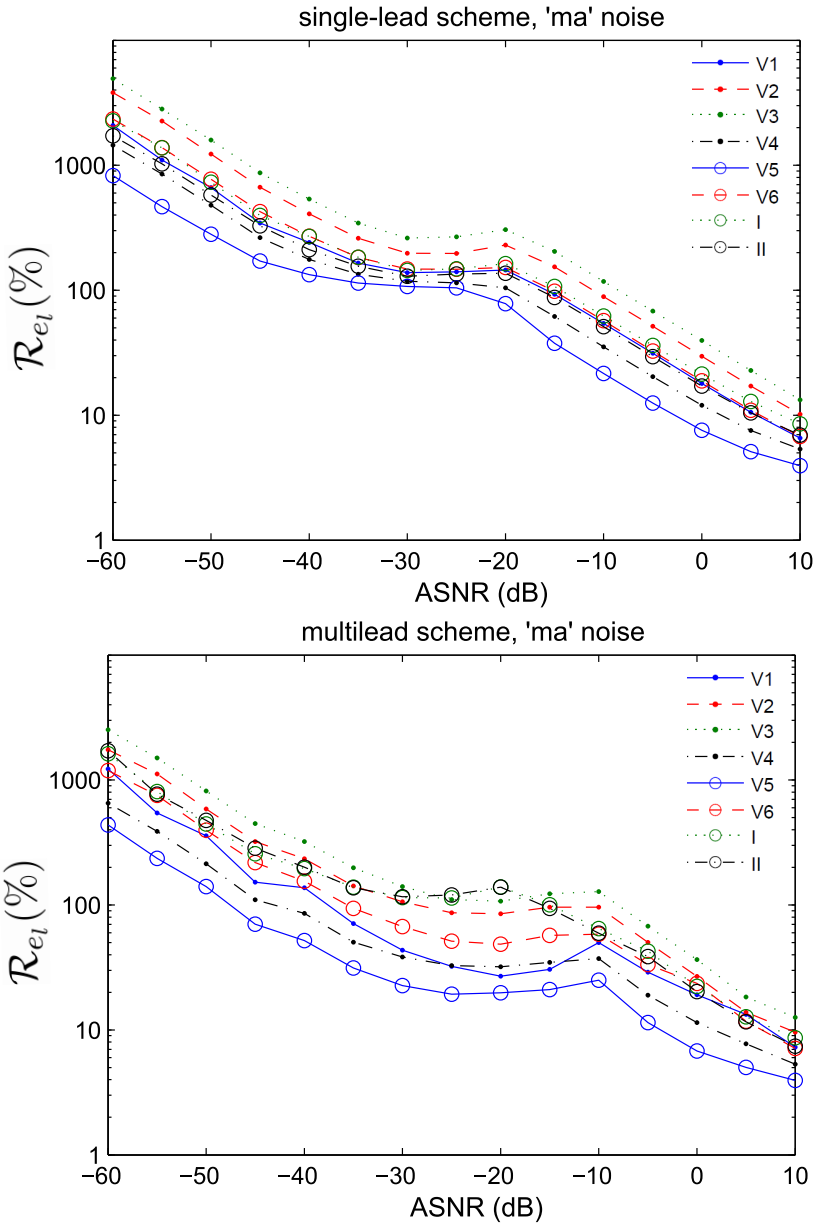

Figure 4.9: Relative error of the TWA estimation obtained with the LLRM combined with the single-lead and (top) and with the multilead scheme (bottom) vs. ASNR for *ma* noise.

	single-lead	multilead
LLRM	0.03	0.01
SM	9.47	5.95

Table 4.1: Detection thresholds which are necessary to obtain a $P_{\mathrm{FA}} = 0.01$ in the simulated dataset with *ma* noise, using the different schemes and a 128-beat analysis window.

all techniques are shown in figure 4.10. The best results are obtained with the *LLR multi* technique. The ASNR level where P_{D} achieves a value of 0.99 is 8 dB lower for *LLR single* than for *SM single*, 6 dB lower for *LLR multi* than for *SM multi*, 30 dB lower for *SM multi* than for *SM single*, and 28 dB lower for *LLR multi* than for *LLR single*.

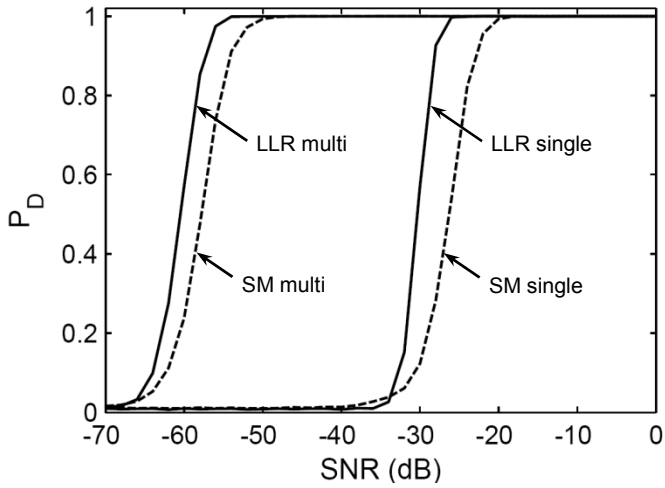

Figure 4.10: P_{D} vs. ASNR for the single lead scheme combined with LLRM (LLR single) and with SM (SM single), and for the multilead scheme combined with LLRM (LLR multi) and with SM (SM multi). $P_{\mathrm{FA}} = 0.01$ in all cases. Results obtained with an analysis window of 128 beats.

4.4.4 Application to stress test signals

TWA is a phenomenon partially related to heart rate, so TWA arises in patients at risk for SCD but also in healthy subjects at faster heart rates during stress tests. Therefore, the assumption that no TWA should be found in volunteer records at heart rates below a cut-off heart rate HR_c was made to set the same $P_{\mathrm{FA}} = 0.01$ for both analysis schemes. Volunteer's signals

	$HR_c = 100$	$HR_c = 110$
single-lead scheme	0.09	0.10
multilead scheme	0.07	0.08

Table 4.2: Detection thresholds which are necessary to obtain a $P_{\text{FA}} = 0.01$ in volunteer records at heart rates below a cut-off heart rate HR_c.

were processed, and for each scheme a threshold was calculated so that it was exceeded only by 1% of the Z values obtained before heart rate reached the HR_c, which were considered as false detections. Then, all records from both groups were processed with the resulting thresholds (table 4.2).

Table 4.3 contains the results obtained considering $HR_c = 110$ bpm to set the P_{FA}. The first row presents the total number of records of each group, and the number of records where one or more TWA episodes were detected. An episode was defined as an interval of consecutive beats in which TWA was continuously detected. For each episode, three parameters were calculated: the maximum TWA amplitude in the episode V_{max} (μV), the duration (in seconds), and the onset heart rate HR_o *(bpm)*, which was calculated as the mean heart rate of the analysis window in which the episode begins. For each group, the mean value and the standard deviation of these parameters were calculated in two ways: considering all the episodes (second row), and considering the episodes detected exclusively by one scheme and not by the other (third row). Table 4.4 shows the number of records where TWA episodes were detected before 110 bpm (P_{FA} set with a $HR_c = 110$ bpm), and the number of records where TWA episodes were detected before 100 bpm ($P_{\text{FA}} = 0.01$ set with a $HR_c = 100$ bpm).

Differences in the number of records with TWA were evaluated with the Fisher's exact test; differences in mean values of V_{max}, duration and HR_o were evaluated with the Mann-Whitney U test. A p-value < 0.05 was considered significant.

As an illustrative example, figures 4.11, 4.12 and 4.13 show how the schemes work with a signal belonging to the ischemic group (Sig1). Figure 4.11 shows the detection statistic Z obtained with the two schemes. The maximum value of Z for the multilead scheme appears at instant $t_{max} = 24$ minutes. At that time, the maximum Z with the single-lead scheme is obtained in lead V3, and with the multilead scheme in T*6*. Figure 4.12 shows the superposition of even and odd beats in those leads. Figure 4.13 shows the estimated TWA waveform in Sig1 at t_{max}. For illustration purposes,

the same detection threshold was chosen for both schemes, $\gamma = 0.1$, corresponding to the threshold obtained for the single-lead scheme in volunteer records with $HR_c = 110$ bps (table 4.2). TWA was detected only by the multilead scheme, in the transformed lead T*6*.

4.5 Discussion

According to simulation results, the high detection performance of the multilead scheme is similar for *gs*, *lp* and *ma* noises, (Figs. 4.3 and 4.4). It is worse when facing *em* noise, because the *em* bandwidth mostly overlaps the band of the TWA. Even in this case, the multilead scheme performs better than the single-lead scheme. Note that in figures 4.3 and 4.4 the single-lead scheme is not capable of detecting anything for ASNR ≤ -35 dB in any type of noise.

As shown in figure 4.5, the multilead scheme surpasses widely the performance of the single-lead scheme, detecting TWA with an ASNR from 27 to 30 dB lower than the single-lead scheme for a fixed P_{D}. The multilead scheme performs better, specially at low ASNR levels, because it separates TWA from most of the noise. For instance, in figure 3.3(c) we can see that, at ASNR $= -20$ dB, noise is mainly concentrated in leads T*1* - T*3*, so TWA becomes detectable in leads T*5* - T*7*.

In the example signal Sig1, the values of the detection statistic Z are higher with the multilead scheme than with the single-lead scheme (figure 4.11). Since the GLRT detector is CFAR, a higher P_{D} can be obtained for a fixed threshold, or a lower number of false detections for a given P_{D}. The main effect of PCA in this case is concentrating the noise in the first transformed leads, making TWA detectable in lead T*6* (note that TWA is clearly visible in T*6*, but not in V*3* in figure 4.12). With real signals, PCA will work differently depending on the spatial autocorrelation of noise and TWA, and the cross-correlation between them. It may concentrate mainly the noise, the TWA, or both. In the worst situation, when the correlations of noise and TWA are similar, they won't be separated at all. In that case the multilead scheme will not improve the analysis, but it will not make the result worse either.

Since the improvement obtained with the multilead scheme is mainly due to the effect of PCA, similar detection gains can be expected when combining the multilead scheme with other TWA techniques. For example,

		multilead scheme		single-lead scheme	
		volunteer	ischemic	volunteer	ischemic
Detection					
	records	66	70	66	70
	records with TWA	26	27	19	20
	% records with TWA	39.4	38.6	28.8	28.6
TWA characteristics					
all episodes	V_{max} *(μV)*	85±114‡	95±128	133±133‡	135±146
detected	*duration (s)*	26±26	48±59	29±24	51±39
by each	HR_o *(bpm)*	124±30†	106±20†	121±30†	105±20†
scheme	*episodes*	38	33	26	22
episodes	V_{max} *(μV)*	21±15†‡	37±22†	52±35‡	66±35
detected by one	*duration (s)*	7±7	30±71	17±16	18±21
scheme and not	HR_o *(bpm)*	127±27†	107±19†	112±7	105±18
by the other	*episodes*	17	18	5	7

Table 4.3: Results of TWA analysis in stress test data, calculated considering all episodes regardless of when they are detected. ($P_{\text{FA}} = 0.01$ for the two schemes). Data expressed as (mean ± one standard deviation). † indicates a significant difference between volunteer and ischemic groups; ‡ indicates a significant difference between multilead and single-lead schemes.

	multilead scheme		single-lead scheme	
	volunteer	ischemic	volunteer	ischemic
$HR_o < 110$ bpm				
records	66	70	66	70
records with TWA	6†	14†	6	12
% records with TWA	9.1†	20.0†	9.1	17.1
$HR_o < 100$ bpm				
records	66	70	66	70
records with TWA	6†	14†	5	10
% records with TWA	9.1†	20.0†	7.5	14.2

Table 4.4: Results of number of records with TWA in stress test data, calculated considering the episodes detected before heart rate reaches 110 bpm (first row) and 100 bpm (second row). $P_{\text{FA}} = 0.01$ for the two schemes. † indicates a significant difference in the number of records with TWA in volunteer and ischemic groups.

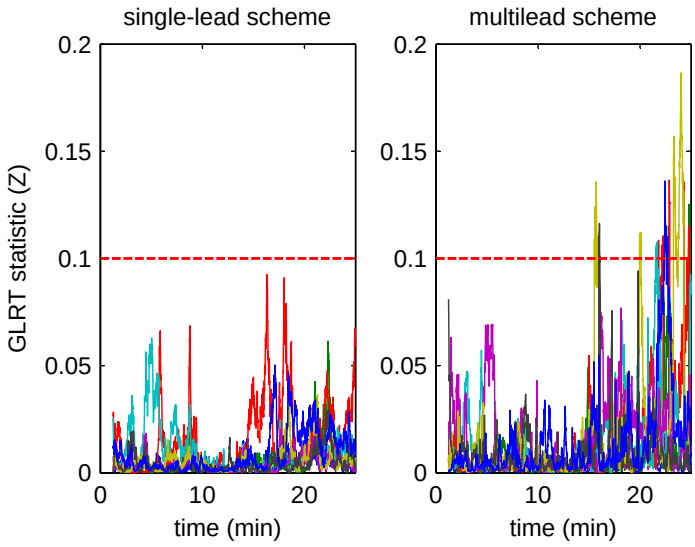

Figure 4.11: Detection statistic Z of LLRM computed with a 128-beat window in signal Sig1. Left panel: Z obtained with the single-lead scheme in leads V1-V6, I and II after the preprocessing stage. Right panel: Z obtained with the multilead scheme in transformed leads T*1*-T*8* after PCA transformation. Threshold $\gamma = 0.1$ is shown in dashed line.

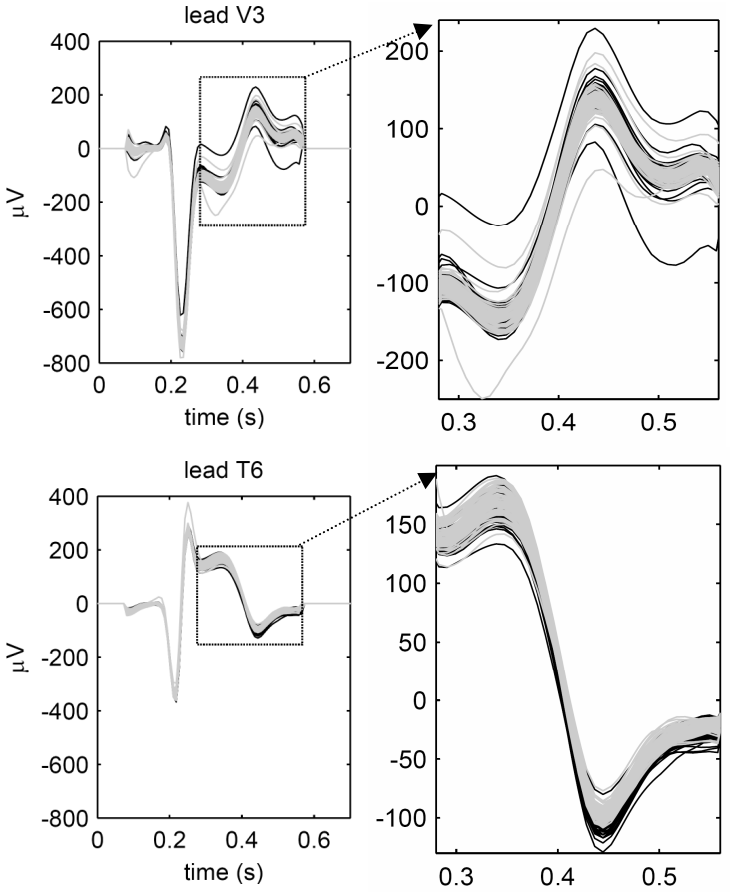

Figure 4.12: Superposition of odd (black) and even (gray) beats of a 128-beat analysis window centered on instant $t_{max} = 24\ min$ in signal Sig1. Top panel: beats of lead V3 (left), which is the lead where the maximum Z appears with the single-lead scheme, and a closer view of the ST-T complexes (right). Bottom panel: same views for lead $T6$, where the maximum Z appears with the multilead scheme. In this case, the morphology of the ST-T complex is consistently different in odd and even beats, making TWA visible to the naked eye.

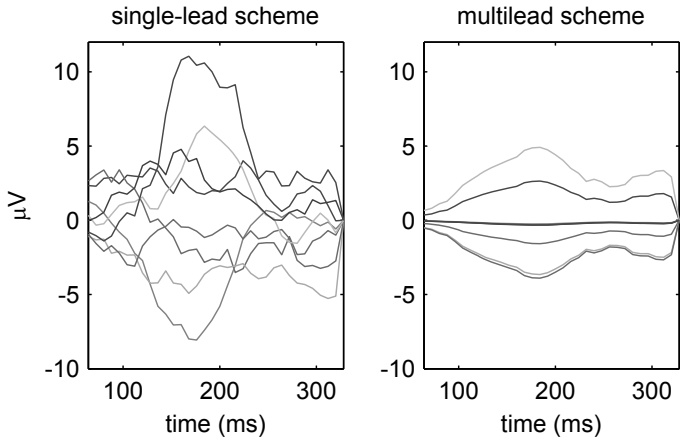

Figure 4.13: TWA waveform estimated in Sig1 at $t_{max} = 24\ min$ with the single-lead scheme (left), and the multilead scheme with $\gamma = 0.1$ (right).

in simulated data with *ma* noise, applying the multilead scheme to the SM yields an improvement of 30 dB over the single-lead approach, which is similar to the improvement obtained by applying the multilead scheme to the LLRM (28 dB) (see figure 4.10).

In the comparison of SM and LLRM, it is interesting to note that the derived threshold for the *SM single* scheme ($\gamma = 9.47$) is much higher than the usual SM significance threshold (TWAR = 3). In fact, the application of the *SM single* scheme with an equivalent $\gamma = 3$ would yield a $P_{\text{FA}} = 0.20$ in the simulated dataset, which means that one out of five TWA episodes detected by the SM would be a "false positive" due to noise. In practice, SM false positives are rejected by requiring detected TWA episodes to fulfill additional requisites, such as a minimum duration of 60 seconds among others [Bloomfield et al., 2002]. The present study does not intend to derive such rules for the LLRM, or to compare the false positives rate of LLRM and SM as implemented in commercial equipments, but these results highlight the influence of the detection thresholds in the results of TWA analysis methods.

The multilead scheme also improves the estimation accuracy, although not so remarkably as the probability of detection. For high ASNR levels, the bias of the multilead estimation is higher than the bias of the single-lead estimation due to the truncation carried out in the reconstruction stage. As only a subset of transformed leads is used to reconstruct the signal, the reconstructed TWA lacks the content of the truncated leads, which may

still contain a small alternant component. However, the lower variance of the multilead estimation compensates the bias, so the final relative error $\mathcal{R}_{e_l}$ is similar to the error of the single-lead estimation for high ASNR levels (see figure 4.9).

For low ASNR levels, on the other hand, the relative bias of the single-lead estimation tends to 100% in all the leads, that is, the estimation tends to zero. This is because as ASNR decreases, the P_{D} of the single-lead scheme starts falling (see figure 4.5), so the estimated value is zero in more and more realizations. In this case the behavior of the multilead scheme is better because the relative bias of the multilead estimation varies differently for each lead, and for some of them it is still lower than 50% at very low ASNR levels. For example, $\mathcal{R}_{b_l} < 50$ % in V1, V4, V5 and V6 until ASNR $= -45$ dB for *ma* noise (see figure 4.8). When ASNR < -25 dB, $\mathcal{R}_{e_l} > 100\%$ in the eight leads for the single-lead estimation, whereas with the multilead estimation such degradation only appears with ASNR < -50 dB. In the example signal Sig1 (figure 4.13), the estimation obtained with the multilead scheme may have bias, but is still useful to study the TWA distribution along the ST-T complex. With the single-lead scheme, this episode would not be detected with $\gamma = 0.1$ (see figure 4.11), and even with a low enough threshold, the single-lead estimation would be much noisier, reducing its clinical value.

In simulation, the multilead scheme yields an improvement of the probability of detection, and a more accurate estimation; results obtained in the real dataset prove that these benefits can also be obtained with real signals. As shown in table 4.3, the multilead scheme detects more episodes than the single-lead scheme in both groups (26 vs. 19 in volunteers, 27 vs. 20 in ischemics). Since the P_{FA} of both schemes is the same, this means that the detection power of this scheme is higher than the detection power of the single-lead scheme. When considering the episodes detected only by the multilead scheme, episodes from volunteers have a significantly lower amplitude than episodes from ischemics (21$\pm$15 vs. 37$\pm$22 μV) and they appear at a higher HR_o (127$\pm$27 vs. 107$\pm$19 bpm). This differences are not significant with the single-lead scheme. In volunteers, episodes detected only by the multilead scheme have a significantly lower amplitude than episodes detected only by the single-lead scheme (21$\pm$15 vs. 52$\pm$35 μV), and a higher HR_o (127$\pm$27 vs. 112$\pm$7 bpm); this suggests that the multilead scheme detects low amplitude episodes near the peak effort that the single-lead scheme cannot detect.

The percentage of records with TWA is similar in volunteer and ischemic groups, both with the multilead scheme (around 39% in both groups) and with the single-lead scheme (around 28% in both groups). This can be due to the fact that volunteers reach a higher peak heart rate during the test. To distinguish between groups according to the risk of SCD, it is necessary to analyze only those results obtained before the heart rate reaches a cut-off point. When the multilead scheme is applied, the percentage of records with TWA is significantly higher in the ischemic group for any cut-off point between 100 and 110 bpm, whereas this difference is not significant with the single-lead scheme (table 4.4). This suggest that the multilead scheme can improve the prognostic utility of TWA in stress testing.

Several limitations of this study must be acknowledged. Regarding simulated data, physiological features of ECG repolarization such as shape variation due to heart rate variability, or amplitude modulation due to the respiration, have not been included in the simulation setup. Moreover, the noise spatial correlation and the TWA waveform used in the simulation are two particular cases, but strong differences can be found in the lead distribution of noise and TWA in real ECG signals [Martínez et al., 2006].

4.6 Conclusions

In this chapter, a multilead analysis scheme that combines PCA with the LLRM is evaluated and compared to a single-lead scheme by means of a simulation study, in which different types of simulated and physiological noise are considered under realistic conditions. Simulation results show that the multilead scheme can detect TWA with a ASNR 30 dB lower, and allows the estimation of TWA with a ASNR 25 dB lower than the single-lead scheme in 12-lead ECGs. The two analysis schemes are also applied to stress test ECG records. Results show that the multilead scheme provides a higher detection power, and that TWA detections obtained with this scheme are significantly different in healthy volunteers and ischemic patients, whereas they are not with the single-lead scheme.

Appendix 4.A: Additional simulation results

This appendix includes additional results of the evaluation of the PCA-based multilead scheme.

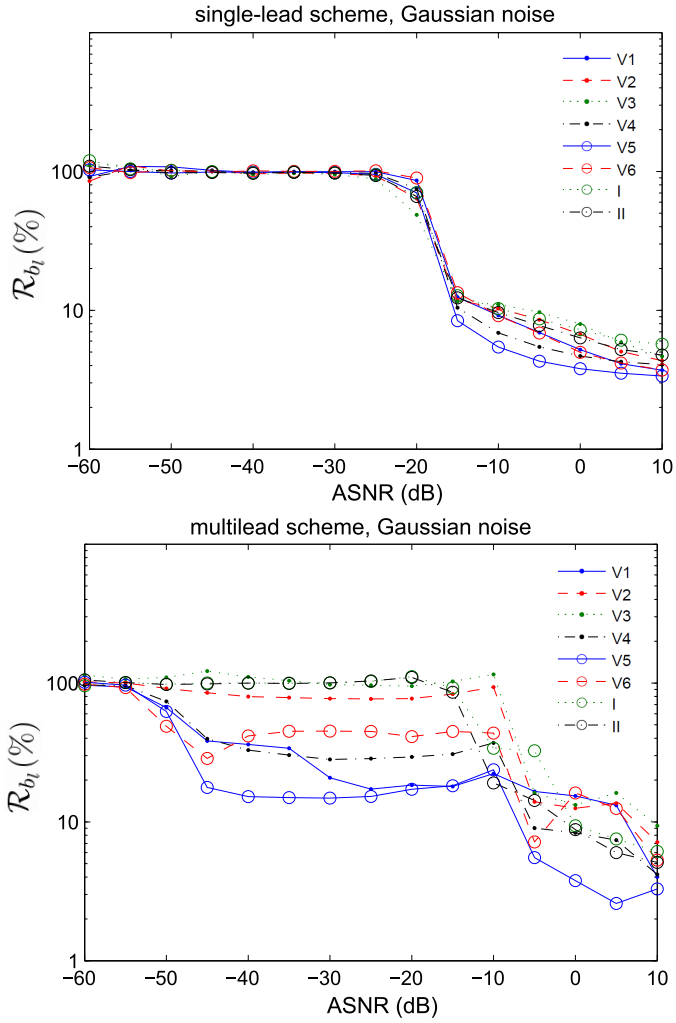

Figure 4.14: Relative bias of the TWA estimation obtained with the LLRM combined with the single-lead and (top) and with the multilead scheme (bottom) vs. ASNR for Gaussian noise.

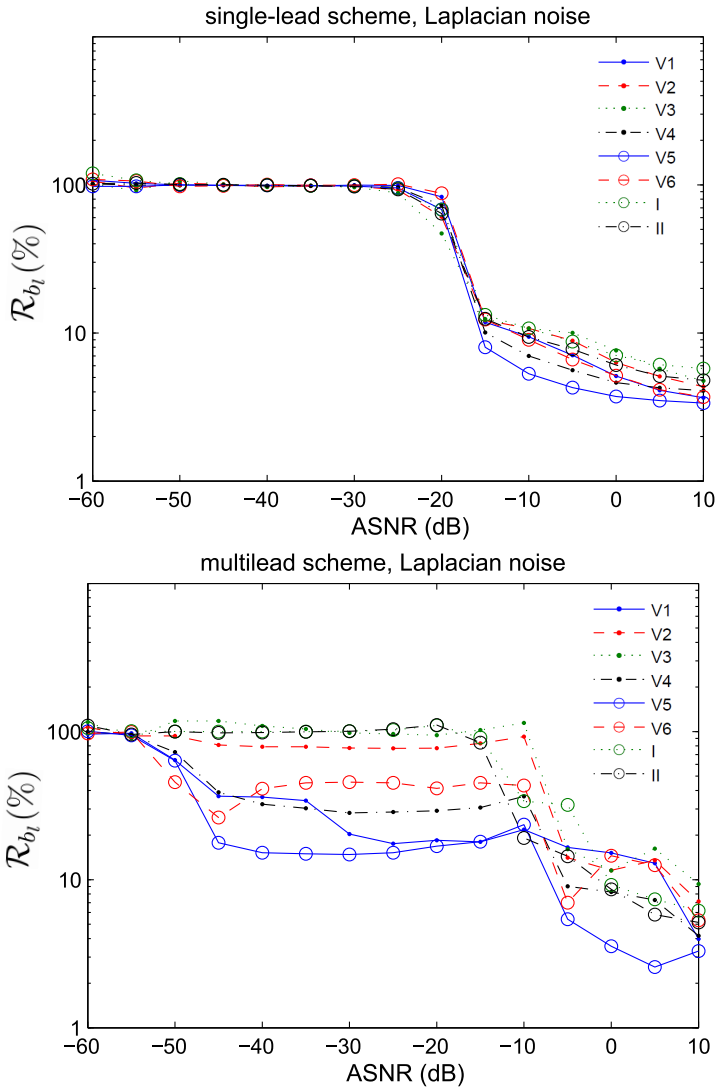

Figure 4.15: Relative bias of the TWA estimation obtained with the LLRM combined with the single-lead and (top) and with the multilead scheme (bottom) vs. ASNR for Laplacian noise.

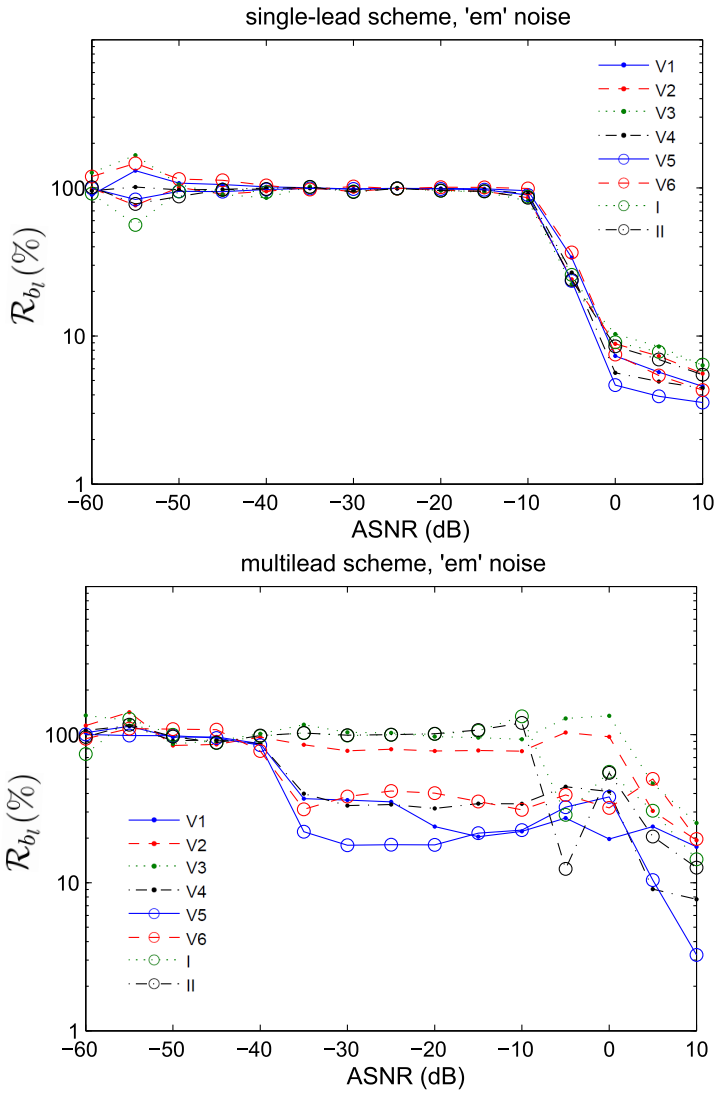

Figure 4.16: Relative bias of the TWA estimation obtained with the LLRM combined with the single-lead and (top) and with the multilead scheme (bottom) vs. ASNR for *em* noise.

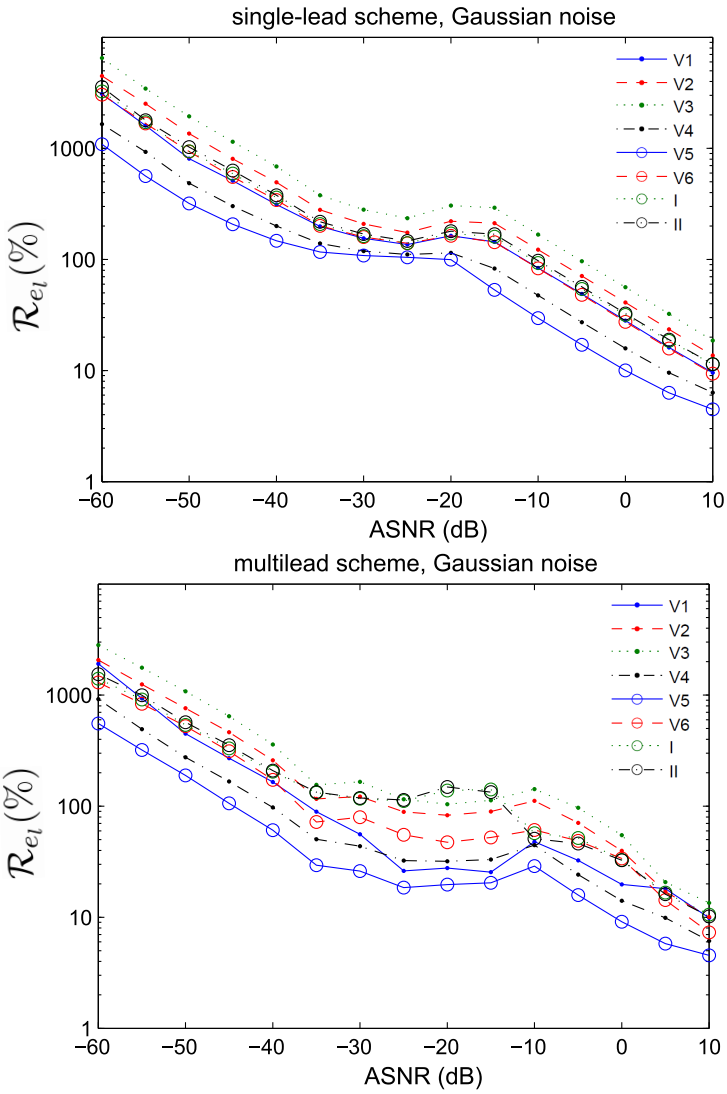

Figure 4.17: Relative error of the TWA estimation obtained with the LLRM combined with the single-lead and (top) and with the multilead scheme (bottom) vs. ASNR for Gaussian noise.

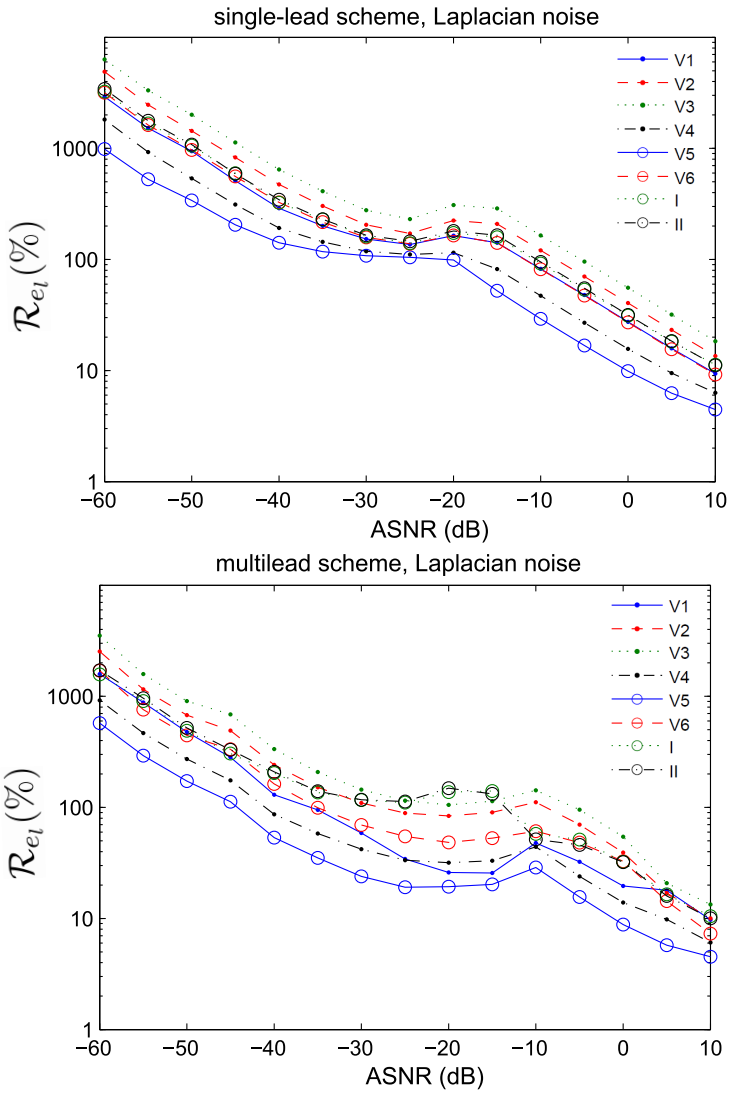

Figure 4.18: Relative error of the TWA estimation obtained with the LLRM combined with the single-lead and (top) and with the multilead scheme (bottom) vs. ASNR for Laplacian noise.

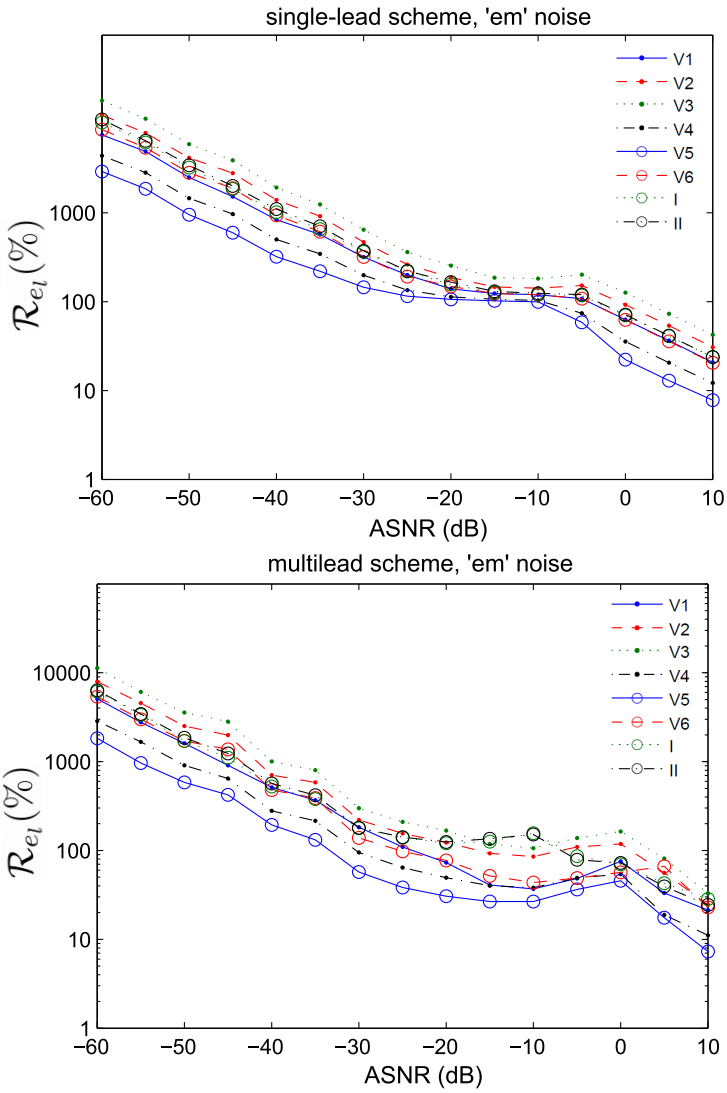

Figure 4.19: Relative error of the TWA estimation obtained with the LLRM combined with the single-lead and (top) and with the multilead scheme (bottom) vs. ASNR for *em* noise.

Chapter 5

Evaluation of the multilead scheme based on Periodic Component Analysis

5.1 Introduction

The evaluation study in the previous chapter demonstrated that the multilead scheme based on PCA improves the estimation and detection performance of SM and LLR single-lead techniques. This improvement, however, is limited by the fact that PCA uses a maximum-variance criterion to separate signal and noise into orthogonal subspaces, which may not be the best way of differentiating between the constituent sources of an ECG signal, particularly if they are not orthogonal [Clifford et al., 2006].

In this chapter, the use of Periodic Component Analysis (πCA) for the multilead scheme is evaluated. πCA is a technique that was first proposed for speech analysis [Saul and Allen, 2000] and then applied to the analysis of ECGs, for ECG compression and also for maternal and fetal ECG separation [Sameni et al., 2008]. With this technique, the variance criterion of PCA is replaced by a periodical structure criterion to separate TWA from non-alternant components, which is a more reasonable assumption from a physiological point of view because periodicity is the defining characteristic of TWA.

In this study, two multilead schemes, one based on πCA and one based on PCA, are combined with the LLR method, and are compared to a con-

ventional single-lead approach, in which each ECG lead is analyzed independently. Results on simulated signals with different types of noise, real signals with added TWA, and stress test signals, show that the πCA-based scheme provides the best detection power and has the potential to improve the prognostic value of TWA tests.

In addition to PCA and πCA, the use of other source separation techniques is explored in this chapter. In particular, the spectral ratio maximization (SRM), which is a new separation technique based on the periodicity of the signal, and two ICA algorithms are considered. These source separation techniques were presented in section 3.4. In the present chapter, the detection performance obtained with each technique is compared by analyzing a set of ECG signals with known TWA.

5.2 Data sets

To compare the analysis schemes in a variety of scenarios, three data sets with increasing degree of realism were analyzed. The first data set was composed of synthetic ECG signals with simulated TWA. In the second data set, known TWA was added to real ECG signals. The third data set contained real stress test ECGs from healthy volunteers and ischemic patients. Both second and third sets were composed of the stress test ECGs from the 211 patients of the *non-ischemic* group, the 66 asymptomatic volunteers of the *volunteer* group, and the 79 patients of the *ischemic* group in the stress test database described in section 3.5.3. Finally, the Physionet TWA database (see section 3.5.4) was analyzed to facilitate future reproduction or comparison with the methods presented here, since this dataset is publicly available.

5.2.1 Synthetic signals

Synthetic 3 Frank lead ECGs were generated using an artificial multilead ECG model which can exhibit realistic TWA [Clifford et al., 2010]. This model generates the cardiac dipole as a sum of Gaussian kernels, and then derives the XYZ orthogonal leads. Natural morphology changes due to inter-beat interval (RR) and respiration are incorporated from varying the Gaussian amplitude and width parameters of the dipole generator. The TWA effect is modeled as a disturbance on the T-loop of the dipole. An example of a synthetic ECG generated with this model is shown in figure

5.1.

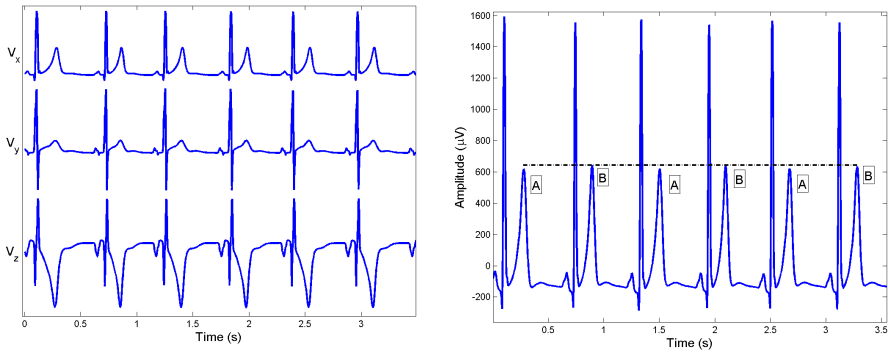

Figure 5.1: Left: example of synthetic ECG generated by the multilead ECG model. Right: example of TWA simulated by the multilead ECG model. Figures reproduced from [Clifford et al., 2008].

Five-minute signals were created with TWA amplitudes ranging from 0 μV to 200 μV. For a given TWA amplitude, a total of 50 ECG records were generated at a sampling frequency of 500 Hz. Individual records differed in that the underlying ECGs were generated using an stochastic model of heart rate variability (70±5 beats per minute (bpm)). Furthermore, a sum of noises was added to the signal, containing electrode motion noise (*em*), muscular activity noise (*ma*) and baseline wander (*bw*), all of them obtained from the MIT-BIH Noise Stress Test Database (see section 3.5.5). For each synthetic ECG signal, two-lead segments of 5 minutes were extracted from *em*, *ma* and *bw* records beginning at a random position. These records only contain two leads, so a third lead of spatially correlated noise was computed as the first principal component of the two available leads. Finally, the three noise leads were scaled to obtain an SNR of 20 dB with respect to the ECG, and added to the synthetic signal.

5.2.2 Real signals with added TWA

This data set contained real 12-lead ECGs from the stress test database (see section 3.5.3) with artificially added TWA. ECG fragments where the presence of TWA was unlikely were selected from all *non-ischemic* and *volunteer* records. The TWA phenomenon is partially related to heart rate, and can appear in healthy subjects at fast heart rates [Cutler and Rosenbaum, 2009, Turitto et al., 2001]. Therefore, only the initial fragment in which the heart

rhythm was < 100 bpm was selected from each record. These fragments were then divided into segments of 32 consecutive beats, resulting in a total of 1744 ECG segments.

Then, TWA was added to ECGs, with amplitudes (V_{alt}) ranging from 0 to 200 μV. To do this, the LLR method was employed to identify a real 12-lead TWA waveform (*twa1)* in an ECG of a patient undergoing a percutaneous coronary intervention. The way of obtaining this waveform was already described in section 4.2.1. For each V_{alt} value, the TWA waveform was scaled and repeated with alternating sign to create a 32 beat-long TWA signal, and then the TWA signal was added to the 1744 ECG segments. This process was repeated with two more TWA waveforms, denoted as *twa2* and *twa3*, which were extracted from two records of the STAFF-III database in the same way as *twa1*. Figure 5.2 shows an excerpt of a real ECG of a volunteer from the stress test database, and the resulting signal after adding TWA of 200 μV to all the leads.

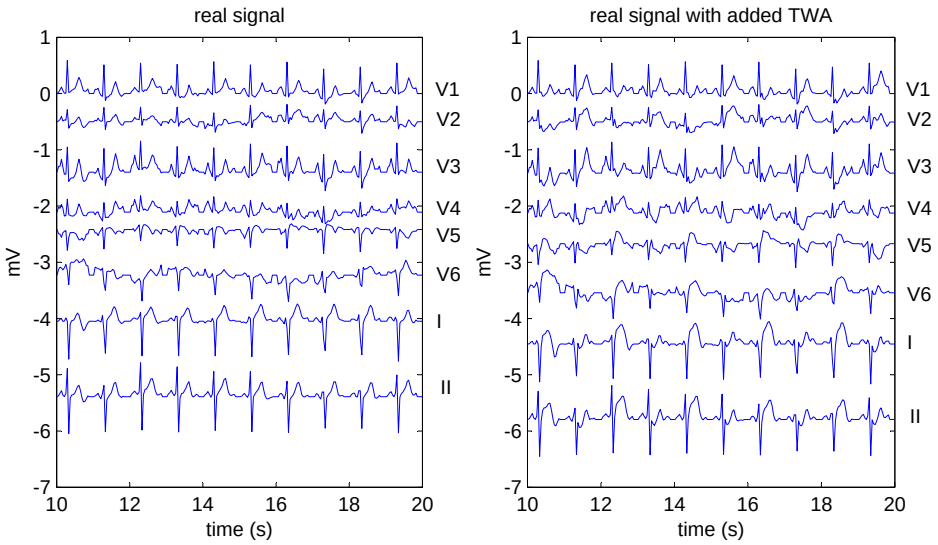

Figure 5.2: Left: excerpt of a real ECG from the stress test database. Right: the same ECG after adding TWA of 200 μV using waveform *twa1*.

5.2.3 Stress test signals

The third data set comprised all ECGs from *ischemic* and *volunteer* groups of the stress test database. This is the same data set that was analyzed in chapter 4 (section 4.2.2).

5.2.4 Signals from the Physionet TWA database

The fourth data set of this study comprises the synthetic records of the Physionet T-Wave alternans database (see section 3.5.4), a total of the thirty-two 12-lead ECGs containing artificial TWA in calibrated amounts, with an approximate duration of two minutes.

5.3 Methods for TWA analysis

First, three different approaches were evaluated: a multilead scheme (figure 3.2) with πCA as transformation technique (we will denote this scheme as *multi-πCA*), the multilead scheme with PCA (*multi-PCA*) already evaluated in chapter 4, and the single-lead scheme (*single*). To compare the detection and estimation performances of the three schemes, the first dataset—synthetic signals—was analyzed with a 16-beat analysis window ($\delta = 16$ beats), and the second dataset—real signals with added TWA—was analyzed using analysis windows of $K = 32, 64$ or 128 beats ($\delta = \mathrm{K}/2$ in all cases).

Second, the simplified multilead scheme for TWA detection (figure 3.4) was combined with PCA, πCA, SRM, πCA-SRM, FastICA and JADE to evaluate the effect of each separation technique in the detection performance. In this case, the first dataset was analyzed with a 16-beat analysis window and $\delta = 16$ beats with all the techniques. For the first and the second analyses, the initial point of ST-T complexes was set 60 ms after the QRS fiducial point.

Third, stress test records were processed with *multi-πCA* and *single* schemes. Comparison between *multi-PCA* and *single* schemes was reported in the previous chapter, so the *multi-PCA* scheme was excluded from this study. From the 12-lead set, only the eight independent leads (V1 to V6, II and II) were processed using a sliding analysis window of 128 beats and $\delta = 1$ beat.

Fourth, the synthetic signals from the Physionet TWA database were processed with *multi-πCA*, *multi-PCA* and *single* schemes, using an analysis window of 32 beats. For the third and the fourth analyses, the initial points of ST-T complexes were set 80 ms after the QRS fiducial point if HR $\leq$ 100 bpm and 60 ms after the QRS fiducial point if HR $>$ 100 bpm.

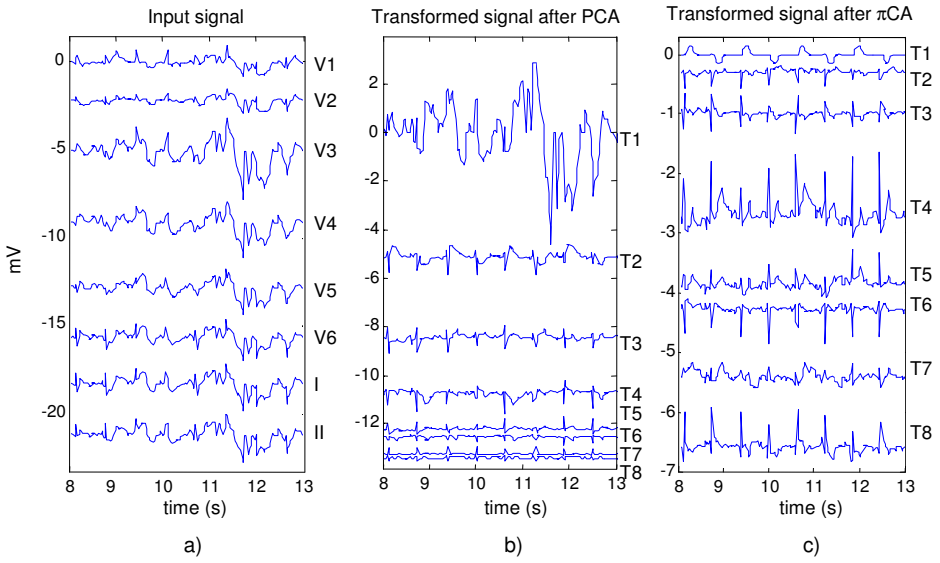

Figure 5.3: (a) The eight independent leads of a real 12-lead ECG where TWA of 200 μV was artificially added. TWA is invisible to the naked eye due to noise and artifacts. (b) Signal in (a) after PCA transformation. TWA is now visible in T2 through exaggerated oscillations in the amplitude of the T wave. (c) Signal in (a) after πCA transformation. TWA is clearly visible in T1.

5.4 Results

5.4.1 Detection performance

As in the previous chapter, probability of false alarm (P_{FA}) was defined as the ratio between the number of positive TWA detections in signals with $V_{alt} = 0$ (false detections) and the total number of decisions made in those signals. Probability of detection (P_{D}) was defined as the ratio between the number of positive TWA detections in signals with a given V_{alt} and the total number of decisions made in those signals. For each scheme, the detection threshold γ was set so that the probability of false alarm (P_{FA}) was 0.01, and the resulting P_{D} was compared.

Detection thresholds for *multi-πCA*, *multi-PCA*, and *single* schemes in the synthetic dataset are presented in table 5.1. The resulting P_{D} is presented in figure 5.4. In the range 30 μV $\leq V_{alt} \leq$ 100 μV, the *multi-πCA* scheme detected alternans with amplitudes at least 15 μV lower than the

	detection threshold γ
single	0.15
multi-PCA	0.19
multi-πCA	0.19
SRM	0.20
πca-SRM	0.20
FastICA	0.18
JADE	0.17

Table 5.1: Detection thresholds which are necessary to obtain a $P_{\text{FA}} = 0.01$ in the synthetic data set, using different schemes and a 16-beat analysis window ($\delta = 16$).

	$K = 32$	$K = 64$	$K = 128$
single	0.60	0.24	0.09
multi-PCA	0.49	0.23	0.07
multi-πCA	0.85	0.38	0.13

Table 5.2: Detection thresholds which are necessary to obtain a $P_{\text{FA}} = 0.01$ in real signals with added TWA, using different schemes and analysis window lengths K.

single scheme for a given P_{D}. For example, the *multi-πCA* scheme detected TWA of 59 μV with a $P_{\text{D}} = 0.8$, while that P_{D} was achieved by the *single* scheme only for $V_{alt} > 76$ μV, which can be interpreted as a detection gain of 2.20 dB.

Real signals with added TWA were processed in the same way as synthetic signals. For each scheme, the detection threshold γ was set so that P_{FA}=0.01 (see table 5.2). Using an analysis window of 32 beats (figure 5.5), TWA of 5 μV was detected with a $P_{\text{D}} = 1\%$ by the *single* scheme, with a $P_{\text{D}} = 60\%$ by the *multi-PCA* scheme, and with a $P_{\text{D}} = 98\%$ by the *multi-πCA* scheme. Similar detection differences were found by repeating the analysis with the two other TWA waveforms, *twa2* and *twa3* (figure 5.6).

To better understand the effects of PCA and πCA transformations, the evolution of the GLRT statistic (Z) in the transformed leads vs. TWA amplitude was analyzed for all signals. Figures 5.8, 5.9 and 5.10 show the evolution of Z when it is computed on an ECG without any transformation, on the same ECG after PCA transformation, and on the same ECG after

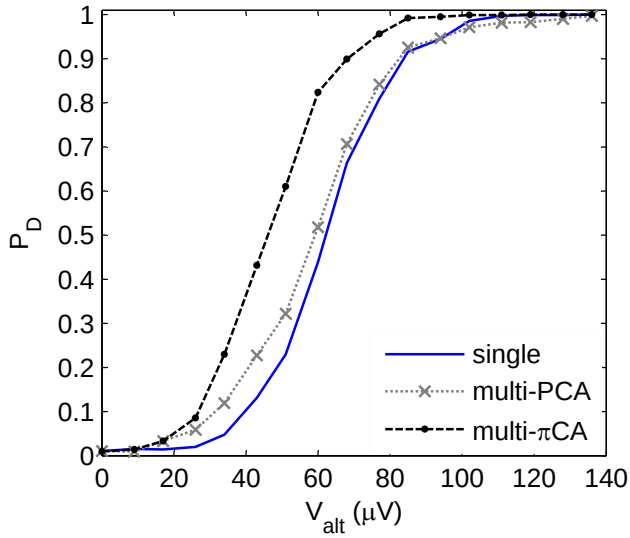

Figure 5.4: P_{D} of *multi-PCA*, *multi-πCA* and *single* schemes obtained in 3-lead synthetic signals vs. simulated TWA amplitude. $P_{\mathrm{FA}} = 0.01$ for all schemes.

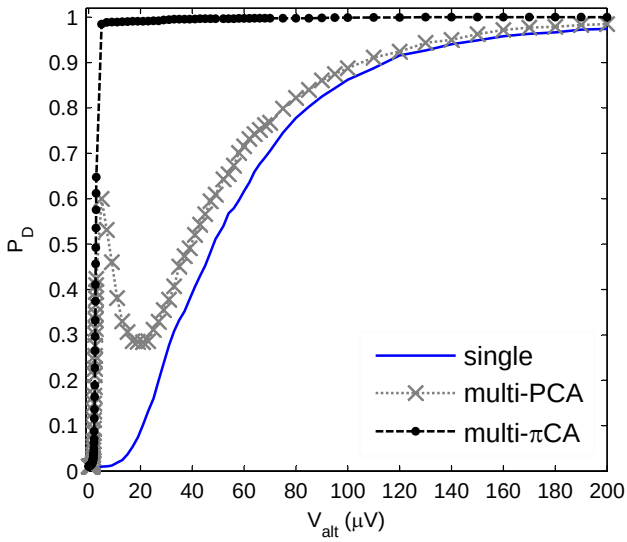

Figure 5.5: P_{D} in 12-lead real signals with added TWA with *multi-PCA*, *multi-πCA* and *single* schemes vs. TWA amplitude. Analysis window of 32 beats and $P_{\mathrm{FA}} = 0.01$ for all schemes. TWA simulated with waveform *twa1*.

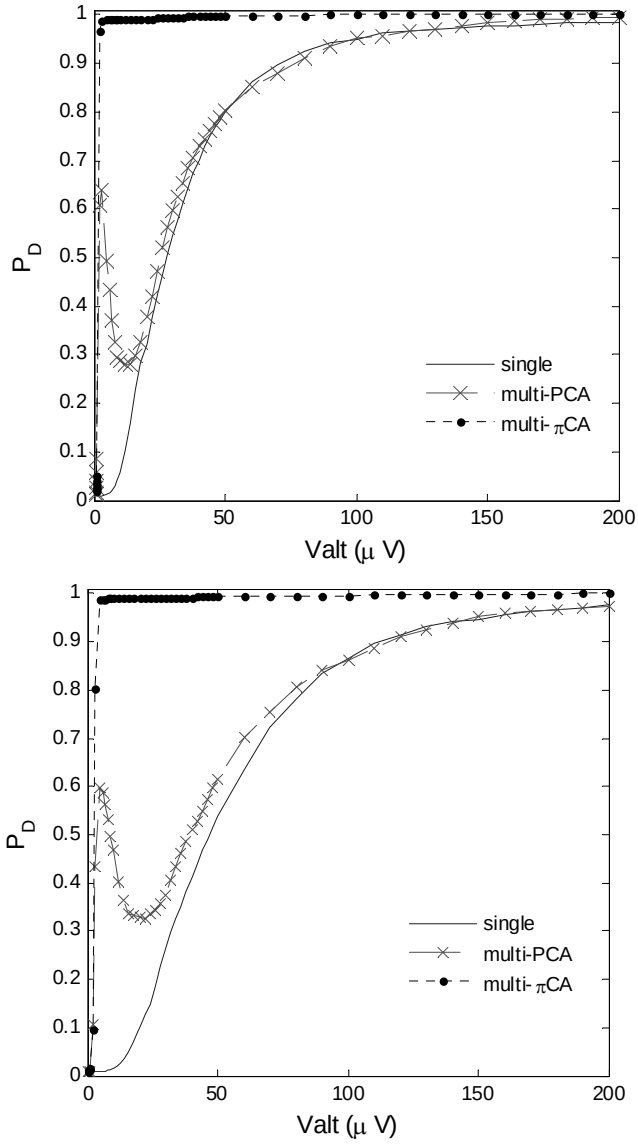

Figure 5.6: P_{D} in real signals with added TWA with *multi-PCA*, *multi-π CA* and *single* schemes vs. TWA amplitude. $P_{\mathrm{FA}} = 0.01$ for all schemes. TWA simulated with waveform *twa2* (top) and *twa3* (bottom)

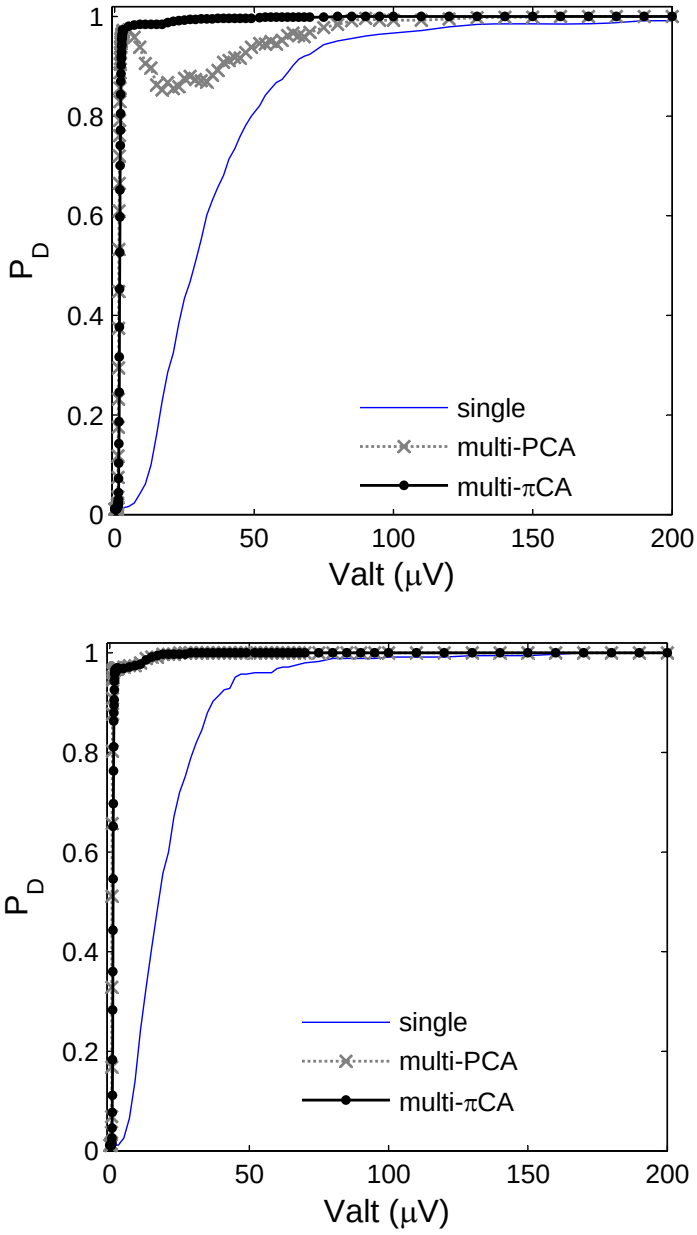

Figure 5.7: P_{D} in real signals with added TWA with *multi-PCA*, *multi-πCA* and *single* schemes vs. TWA amplitude. $P_{\mathrm{FA}} = 0.01$ for all schemes. Analysis window of 64 beats (top) and 128 (bottom). TWA simulated with waveform *twa1*.

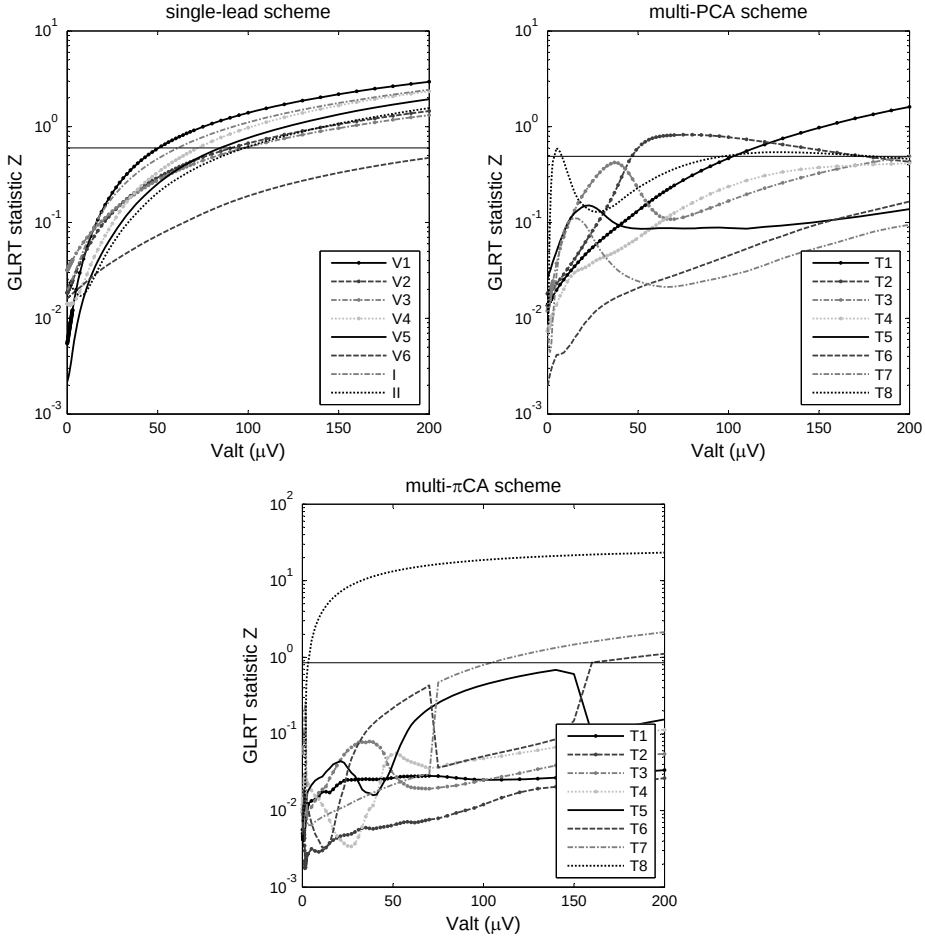

Figure 5.8: Comparison of *single* (top left), *multi-PCA* (top right) and *multi-π CA* (bottom) schemes applied to the same ECG signal with different magnitudes of TWA. The detection threshold is indicated with an horizontal straight line ($P_{\mathrm{FA}} = 0.01$ for each scheme). Analysis window of 32 beats.

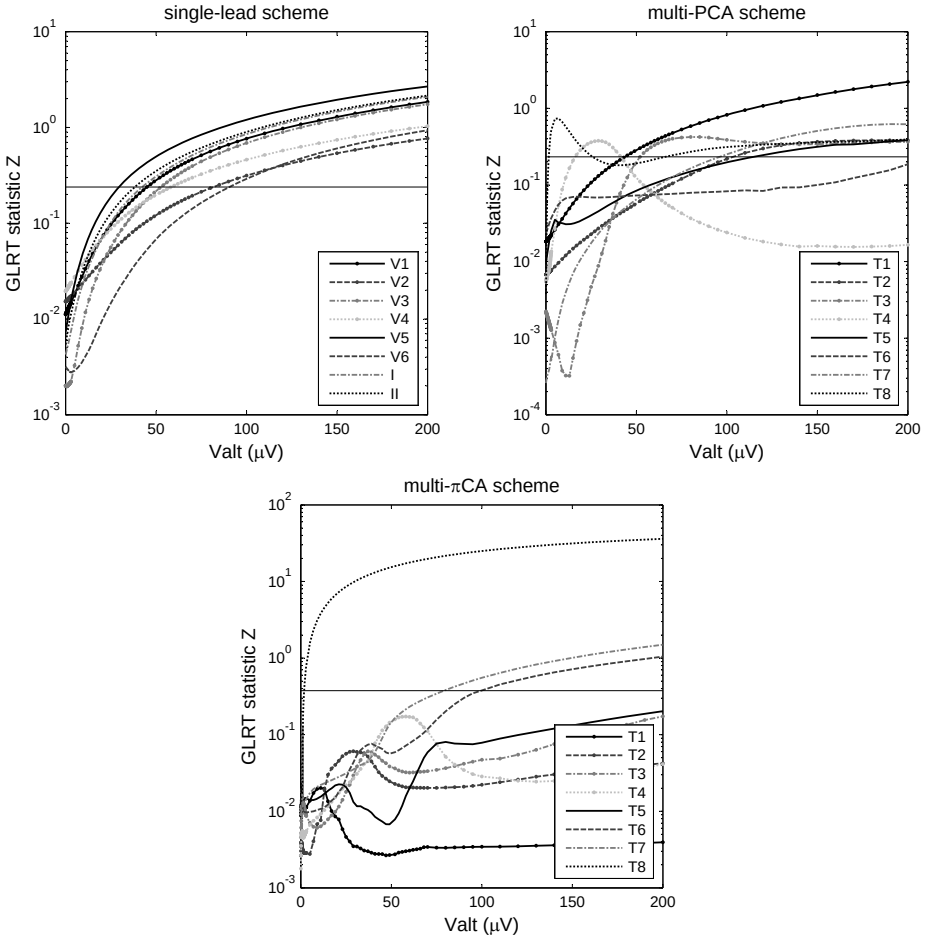

Figure 5.9: Comparison of *single* (top left), *multi-PCA* (top right) and *multi-πCA* (bottom) schemes applied to the same ECG signal with different magnitudes of TWA. Detection threshold indicated with an horizontal straight line. $P_{\mathrm{FA}} = 0.01$ for each scheme. Analysis window of 64 beats.

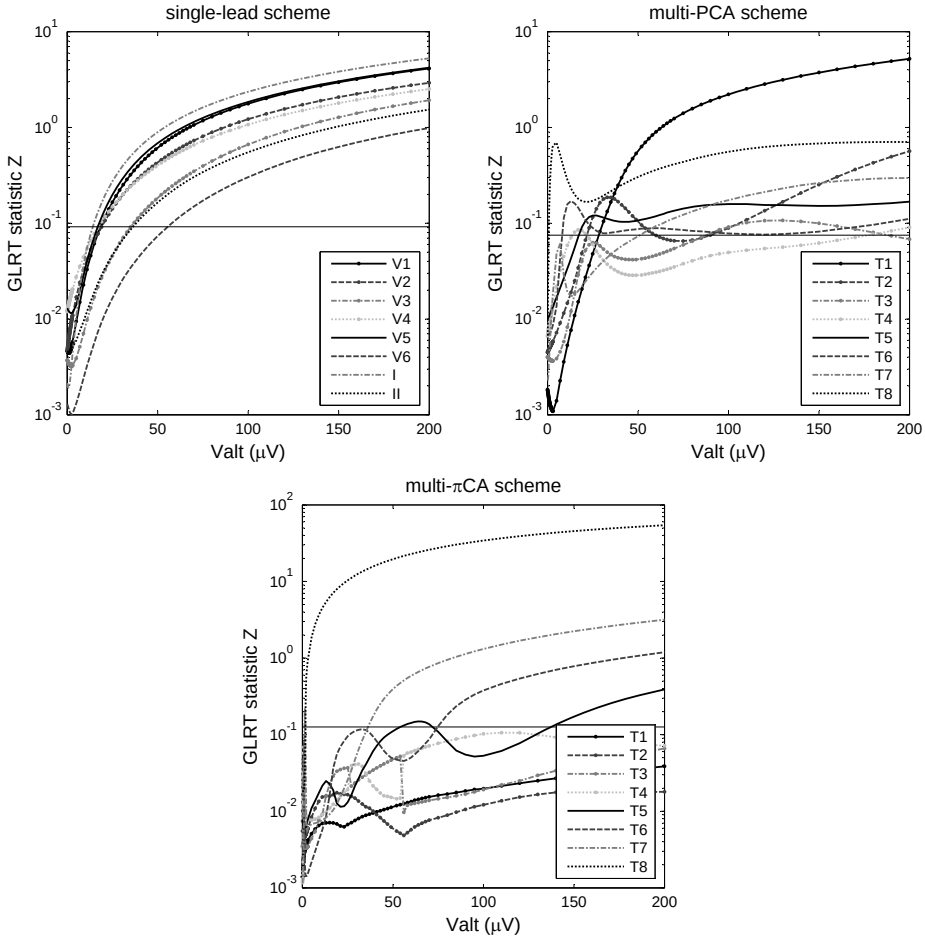

Figure 5.10: Comparison of *single* (top left), *multi-PCA* (top right) and *multi-πCA* (bottom) schemes applied to the same ECG signal with different magnitudes of TWA. Detection threshold indicated with an horizontal straight line. $P_{\mathrm{FA}} = 0.01$ for each scheme. Analysis window of 128 beats.

πCA transformation, using different window lengths. In all cases, TWA is detected when Z exceeds the threshold (horizontal black line) in one or more leads. For example, using an analysis window of $K = 32$ beats (figure 5.8), TWA was detected by the multi-PCA scheme for $V_{alt} < 5$ μV, become undetected for $5 < V_{alt} < 50$ μV, and then was detected again in T*2* for $V_{alt} = 50$ μV. With πCA, TWA was detected for $V_{alt} \geq 3.5$ μV.

5.4.2 Estimation accuracy

The estimation accuracy of the schemes was also compared. For each simulated amplitude, the mean value and the standard deviation of the estimated amplitude V_{alt} was computed considering only those cases where detection was positive (figure 5.11). In absence of TWA, TWA was falsely detected in 1% of the cases with a mean estimated amplitude of 142.6 μV (*single* scheme) and 58.9 μV (*multi-πCA* scheme). For a simulated amplitude of 136 μV, the bias and standard deviation of the estimation were 0.6 μV and 18.2 μV respectively (*single* scheme), and 2.7 μV and 16.0 μV (*multi-πCA* scheme).

5.4.3 Comparison to other source separation techniques

The detection performance of the different transformation techniques—PCA, πCA, SRM, πCA-SRM, FastICA and JADE, presented in section 3.4—was compared in the synthetic dataset, defining P_{D} and P_{FA} as in previous sections. The best performance was obtained with schemes πCA, SRM and πCA-SRM, that presented similar P_{D} for every V_{alt} (figure 5.12).

The execution time (in seconds) for the analysis of the entire synthetic dataset was 64 s with PCA, 68 s with πCA, 6678 s with SRM, 5345 s with πCA-SRM, 1254 s with FastICA and 129 s with JADE.

The projection directions obtained with πCA, SRM and πCA-SRM schemes were studied. For each V_{alt} value, the vectors $\mathbf{w}$ obtained with each scheme were normalized and averaged (see sections 3.4.2 and 3.4.3). The average directions obtained with SRM and πCA-SRM schemes coincided in all cases. The directions of πCA and SRM schemes were similar for low V_{alt} (figure 5.13(a)), and the difference between them decreased as V_{alt} increased (figure 5.13(b)).

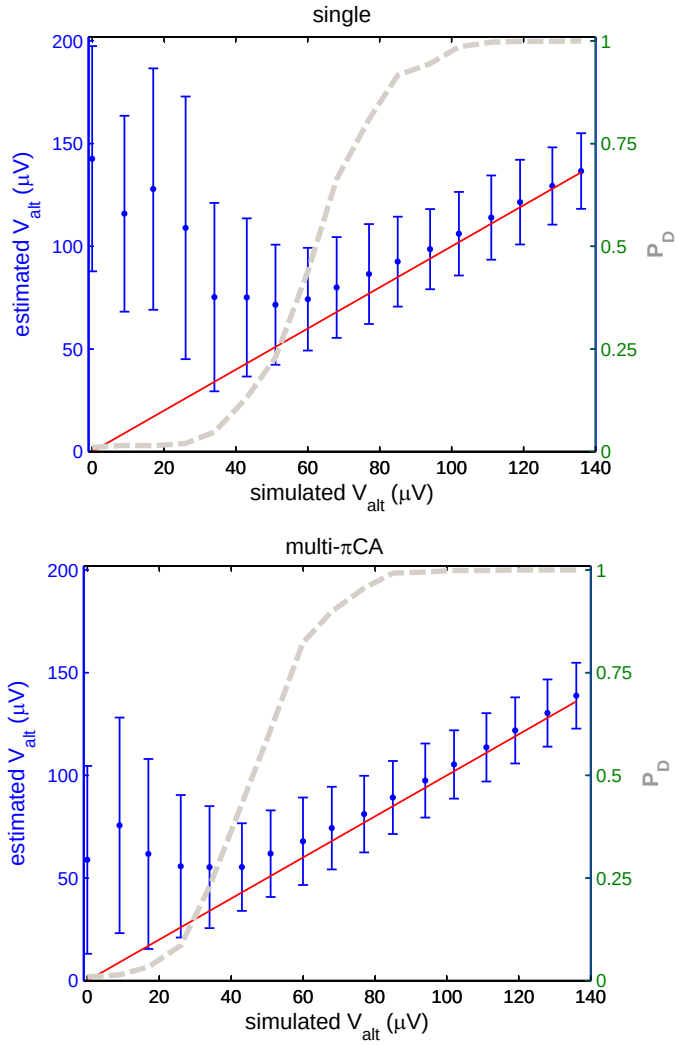

Figure 5.11: Estimated vs. simulated TWA amplitude in synthetic signals using the *single-lead* (top), and *multi-π CA* (bottom) schemes. Dots and bars represent the average and the standard deviation of the estimated amplitude respectively, and straight line corresponds to perfect estimation (left ordinates axis). Dashed line represents the P_{D} of each scheme for $P_{\mathrm{FA}} = 0.01$ (right ordinates axis).

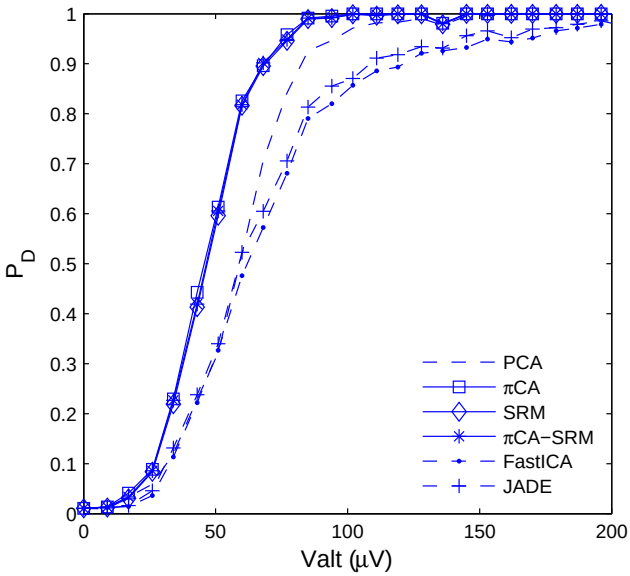

Figure 5.12: P_{D} of the different BSS schemes vs. simulated TWA amplitude. $P_{\mathrm{FA}} = 0.01$ for all schemes.

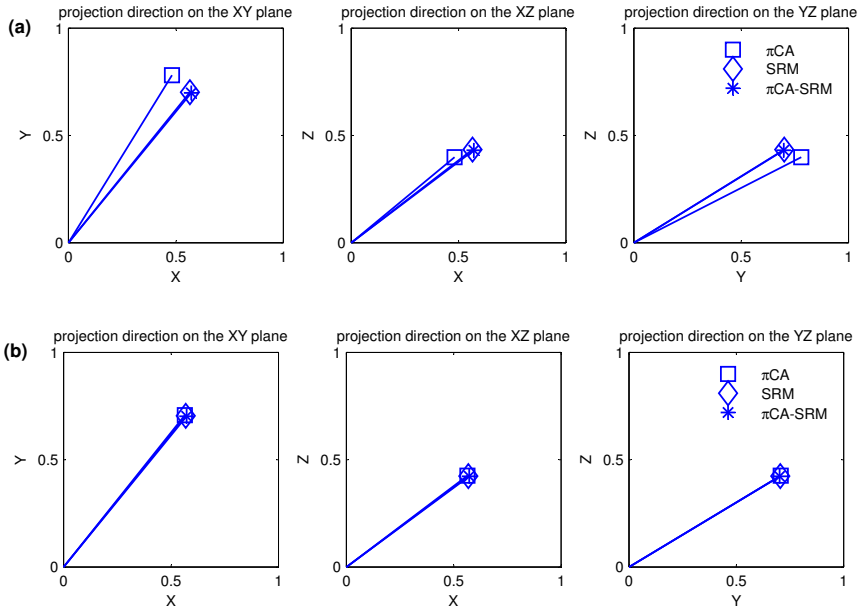

Figure 5.13: Average direction of the projections obtained with the πCA scheme (squares), the SRM scheme (diamonds) and the πCA-SRM scheme (asterisks) in signals with (a) V_{alt}=10 μV and (b) V_{alt}=60 μV.

	$HR_c = 100$	$HR_c = 110$
single	0.09	0.10
multi-πCA	0.09	0.11

Table 5.3: Detection thresholds which are necessary to obtain a $P_{\text{FA}} = 0.01$ in volunteer records at heart rates below a cut-off heart rate HR_c, with *single* and *multi-π CA* schemes.

5.4.4 Application to stress test signals

Stress test signals were analyzed as reported in the previous chapter (see section 4.3), but this time with the *multi-π CA* scheme. The same strategy was followed to make a fair comparison of the sensitivity of *multi-π CA* and *single* schemes: their specificity was made equal by setting the same $P_{\text{FA}} = 0.01$ for both schemes. To do so, the assumption that no TWA is likely to be found in volunteer records at heart rates below a cut-off value HR_c was made. Volunteers' signals were processed, and for each scheme the threshold γ was calculated so that it was exceeded only by 1% of the Z values obtained before the heart rate reached the HR_c (false detections). Then, all records from both groups were processed with the resulting thresholds, reported in table 5.3.

For each detected TWA episode, three parameters were calculated: the maximum amplitude V_{max} (μV), the duration of the episode, and the onset heart rate HR_o (bpm). Average values of amplitude, duration, and onset heart rate were compared between volunteer and ischemic groups with the Mann-Whitney U test, and the percentages of records with TWA of both groups were compared with Fisher's exact test. A p-value < 0.05 was considered significant.

First, $HR_c = 110$ bpm was chosen in order to set γ, and all detected TWA episodes were analyzed (table 5.4). The highest sensitivity to TWA was obtained with the *multi-π CA*, since it detected TWA in more records than the *single* scheme both in volunteer (43.9% vs. 28.7%) and in ischemic groups (47.1% vs. 28.5%). In volunteers, TWA appeared at a lower heart rate than in ischemic patients with both schemes (126 vs. 109 bpm with the *multi-π CA* scheme, 121 vs. 105 bpm with *single* scheme).

Then, only those TWA episodes detected before 100 bpm (first row in table 5.5) and before 110 bpm (second row in table 5.5) were analyzed. In both cases, the detection thresholds were computed considering cut-off heart

rates of $HR_c = 100$ bpm and $HR_c = 110$ bpm respectively for a $P_{\text{FA}} = 0.01$ (table 5.3). With the *multi-πCA* scheme, the percentage of records with TWA was significantly higher in the ischemic group in both cases, whereas this difference was not significant with the *single* scheme. TWA episodes detected by the two schemes in volunteers had lower amplitude and shorter duration than in the ischemic group, although these differences were not significant.

If we compare these results with those obtained in chapter 4 (table 4.4), we can observe that the separation between groups is higher with the *multi-πCA* scheme than with the *multi-PCA* scheme. With the *multi-πCA* scheme, the percentage of records with TWA (volunteers vs. ischemics) is 17% vs. 37% for $HR_o = 110$ bpm, and 7% vs. 24% for $HR_o = 110$ bpm, whereas with the *multi-PCA* these differences were lower: 9% vs. 20% for both HR_o.

5.4.5 Application to the Physionet TWA database

The Physionet T-wave alternans database (see section 3.5.4) was created for the Physionet challenge of 2008 [Moody, 2008]. It contains 100 records; 32 of them are synthetic with known amounts of TWA, and were simulated with the model described in section 5.2.1, and the remaining 68 records are real signals from different databases, 56 of which belong to patients with known cardiac risk factors. Synthetic records have 12 leads, and real records have 2, 3 or 12 leads.

This database was compiled with the intention to create a reference for evaluation of new TWA algorithms. During the challenge, participants were asked to propose a method to quantify the TWA level in the records of the database, and then records were sorted according to the median TWA level of all the entries to create a reference rank. Finally, each entry received a performance metric computed as the Kendall's correlation coefficient [Abdi, 2007] between the method's rank and the reference rank.

Although the reference rank was useful for scoring the challenge entries, it did not represent an increasing magnitude of TWA, and therefore it is not appropriate for benchmarking. If synthetic signals were ordered according to their true TWA level (correct rank), the correlation between the correct rank and the reference rank derived from all entries would be 0.698, which would have been the 8^{th} score in the competition. Furthermore, the reported method with the highest score [Bortolan and Christov, 2008] did

	multi-πCA scheme		single-lead scheme	
	volunteer	ischemic	volunteer	ischemic
% records with TWA	43.9‡	47.1§	28.7‡	28.5§
TWA characteristics				
V_{max} *(μV)*	125±143	123±163	133±133	135±146
duration (s)	33±39	45±44	29±24	51±39
HR_o *(bpm)*	126±30†	109±18†	121±30†	105±20†
number of episodes	41	42	26	22

Table 5.4: Results of TWA analysis in stress test data, considering all episodes regardless of when they are detected. $P_{\text{FA}} = 0.01$ for the two schemes. Data expressed as (mean ± one standard deviation). † indicates a significant difference between volunteer and ischemic groups; ‡ and § indicate a significant difference between multilead and single-lead schemes.

	multi-πCA scheme		single-lead scheme	
	volunteer	ischemic	volunteer	ischemic
$HR_o < 110$ bpm				
% records with TWA	16.6†	37.1†	9.1	17.1
V_{max} *(μV)*	105±107	126±169	72±55	113±55
duration (s)	32±40	49±39	31±32	53±41
number of episodes	13	27	6	11
$HR_o < 100$ bpm				
% records with TWA	7.5†	24.2†	7.5	14.2
V_{max} *(μV)*	89±87	113±143	40±20	128±130
duration (s)	42±43	63±47	25±17	65±46
number of episodes	9	21	6	10

Table 5.5: Results of number of records with TWA in stress test data, calculated considering the episodes detected before heart rate reaches 110 bpm (first row) and 100 bpm (second row). $P_{\text{FA}} = 0.01$ for the two schemes. † indicates significant differences in the number of records with TWA in volunteer and ischemic groups.

not quantify TWA magnitude, but only labeled records as with or without TWA. Besides, in the reference rank, 25 out of the 30 records with highest TWA are synthetic. This indicates that the comparison with the reference rank penalizes those methods that are able to detect TWA in real signals, and favors those methods that only measure TWA in synthetic signals with a low degree of physiological variability and with a higher number of leads. The reported method with the highest score, for instance, only detects TWA in one real signal.

These results, however, do not invalidate the use of the Physionet TWA database as a reference. Comparisons can still be made with respect to the correct rank of synthetic methods, and the fact that this dataset is publicly available facilitates reproduction of results and comparison with other methods.

In this work, the 32 synthetic signals from this database were processed with *multi-πCA*, *multi-PCA* and *single* schemes, using the detection thresholds computed for real signals with added TWA in section 5.4.1. ECG records were sorted according to the TWA amplitude estimated by each scheme, and compared each resulting rank with the correct rank that is obtained by sorting the records according to its true TWA content. The Kendall rank correlation coefficients between the estimated rankings and the correct ranking were 0.685 for the *single* scheme, 0.750 for the *multi-PCA* scheme, and 0.766 for the *multi-πCA* scheme.

5.5 Discussion

The *multi-πCA* scheme presents the best detection performance among the compared schemes, both in synthetic and real signals (figures 5.4 and 5.5). This scheme exploits the fact that ECG signals do not usually contain any component of cardiac origin at the frequency of 0.5 cpb other than TWA. If baseline wander and other low-frequency artifacts were perfectly removed, the only component projected into the first transformed lead by the πCA transformation would be the alternans. In practice, the signal may still contain residual baseline and noise after preprocessing; in that case, the transformation does not isolate TWA in the first transformed lead, but it still makes TWA stand out over noise, increasing the ASNR in that lead. This effect explains why TWA with an amplitude as low as 5 μV becomes detectable in real signals (figure 5.5), and can be clearly observed in the last panel of figure 5.8, where the detection statistic, which represents an

indirect measure of the ASNR, exceeds the threshold at $V_{alt} = 3.5$ μV.

Unlike πCA, PCA does not necessarily project the TWA component into the first transformed lead. PCA separates signal components according to their variance; therefore, PCA projects the component with the highest power into the first transformed lead. That component can be the noise if TWA power is lower than noise power.

This effect can be observed in the evolution of the GLRT statistic Z with PCA (figure 5.8). In that example, when TWA is low ($V_{alt} = 5$ μV), PCA concentrates the noise in the highest transformed leads (T*1*- T*3*), removing it from the lowest lead (T*8*). Therefore, in T*8* the ASNR rises, the statistic Z passes the detection threshold, and TWA is detected. As V_{alt} increases, TWA and noise power become similar, and PCA cannot separate them, so the ASNR in the transformed leads does not increase and TWA is not detected. Then, when V_{alt} is high enough, TWA power starts to be higher than noise power, and PCA progressively projects TWA into higher leads, making them detectable first in T*2* and finally in T*1*. This "positive-negative-positive" detection pattern was consistently found in real signals with added TWA, and is the cause of the "valley" in the P_{D} curve of the *multi-PCA* scheme (figure 5.5). This pattern was not found in the synthetic signals of the first dataset, where three leads are not rich enough in information for PCA to produce such a clear separation of TWA and noise. The value of the detection threshold for a fixed P_{FA} decreases when a longer analysis window is used, but longer windows have little effect on the spatial redistribution of TWA and noise in the transformed signal. Therefore, the "valley" in the P_{D} curve tends to disappear for longer analysis windows (see figure 5.7).

When we compare the detection gains of multilead schemes over a single-lead scheme in the different evaluation datasets, both in this chapter and in chapter 4 (figures 4.5, 5.4 and 5.5), we can observe that the detection gain is higher for 12-lead ECGs than for 3-lead ECGs, and also that the highest difference between single and multilead schemes is obtained with synthetic signals without any physiological variability (the signals generated in section 4.2.1). A lower number of leads and a more realistic noise and variability in the ECG decrement the detection gain that can be obtained with a multilead scheme.

The ICA algorithms, FastICA and JADE, present the worst detection performance among the compared schemes (figure 5.12). ICA has been successfully applied to other ECG problems in the past [Castells et al., 2007],

but, according to the results of the present study, it is not the best approach for TWA analysis. FastICA and JADE algorithms are based on the classic ICA model, which assumes that the input signal is an instantaneous stationary linear mixture of independent sources, whose number equals the number of signal channels. This is not a very realistic assumption for TWA analysis in 3-lead ECGs, in which the signal after the preprocessing stages, besides the TWA component, may still contain different types of residual noise (electrode movement, baseline wander, motion artifacts) and residual activity of the ventricles due to a non-perfect *detrending* filter. In this case, assuming only three sources could be unrealistic, and independence between sources is not assured either. ICA algorithms could yield better results with 12-lead ECGs, such as those obtained in TWA clinical stress tests, but their utility with ambulatory 2 or 3-lead ECGs seems limited.

The best detection performance is obtained with the periodicity-based schemes. Both πCA and SRM search for the direction from which the periodicity of the transformed signal is maximum, following a temporal and a spectral criterion respectively. These criteria offer equivalent detection results; the directions obtained by the two schemes tend to converge as TWA increases, and for low V_{alt} values, πCA and SRM directions are close enough to produce the same P_{D}. The projections obtained with SRM and πCA-SRM schemes coincide in all cases. Initializing the optimization algorithm with πCA —a closer point to the solution— reduces convergence time, but even in that case the computational cost is more than 70 times higher than the cost of the πCA scheme.

The main benefits of the *multi-πCA* scheme can also be expected when it is combined with single-lead techniques other than the LLR method. The improvement in the detection power is due to the signal transformation stage, and does not depend on the actual detection technique, so similar detection gains are obtained when the multilead scheme is combined with LLR and SM techniques, as it was demonstrated in the previous chapter. Furthermore, the *multi-πCA* scheme can also simplify the detection rules of existing methods such as SM, which require a complex set of lead-specific conditions to determine the presence of TWA in an ECG [Bloomfield et al., 2002]. The fact that πCA always projects TWA into the first transformed lead (T*1*) means that the detection rule needs to be applied only to that lead, making a simpler and more powerful detection scheme.

In addition to a high sensitivity to TWA, an accurate estimation of the TWA amplitude is also an important requisite of the analysis methods, since

quantitative evaluation of TWA has been shown to improve risk assessment [de Vilhena Garcia et al., 2009, Minkkinen et al., 2008, Klingenheben et al., 2005]. Results in section 5.4.1 indicate that the *multi-πCA* scheme improves the accuracy of the amplitude estimation (figure 5.11). For high V_{alt} levels, the bias of the *multi-πCA* estimation is slightly higher than the bias of the single-lead estimation due to the truncation carried out in the reconstruction stage —as only a subset of transformed leads is used to reconstruct the signal, the reconstructed TWA lacks the content of the truncated leads, which may still contain a small alternant component. However, the variance of the *multi-πCA* estimation is lower than the variance of the single-lead estimation, especially at low amplitudes, so the total mean square error is always lower than with the *single* scheme. This effect is also observed in the PhysioNet TWA database, where the use of the *multi-πCA* scheme provides the highest correlation with the correct rank of records.

Results on stress test signals confirm that the higher sensitivity to TWA of the *multi-πCA* scheme can also be expected in a real clinical dataset. Furthermore, this scheme improves the differentiation of volunteers and ischemic patients according to TWA episodes over the *multi-PCA* and the *single* schemes, which indicates the potential clinical utility of the proposed method. According to current guidelines of TWA analysis in stress test, TWA episodes are considered to indicate arrhythmic risk only if they satisfy several requirements, one of them being longer than 60 seconds [Bloomfield et al., 2002]. These guidelines have been derived after extensive application of the spectral method in clinical studies, and their application to other techniques is not straightforward, but needs to be clinically validated before extracting conclusions about the prognostic value of any new method. In our study, results indicate that TWA appears at higher heart rates in volunteers than in ischemic patients, and that under heart rates of 100 and 110 bpm, TWA episodes are less frequent and have lower amplitude and shorter duration (around 30 seconds) than in the ischemic group. These findings agree with existing clinical evidence [Nearing and Verrier, 2002, Rosenbaum et al., 1994], but it would be premature to extract conclusions about arrhythmic risk at this stage.

In this study, cut-off values of heart rate, amplitude or duration of TWA to predict cardiovascular events could not be determined in the study population because the follow-up information in terms of arrhythmic events or all-cause mortality was not available.

5.6 Conclusions

The multilead analysis scheme based on πCA is the most robust and sensitive tool for TWA analysis among the compared alternatives. Comparison in different scenarios—from synthetic signals to clinical records—shows that it provides a better detection power than the previously proposed multilead scheme based on PCA, and than the conventional single-lead approach. Furthermore, the proposed scheme improves the differentiation between healthy volunteers and patients with ischemic disease according to TWA detections.

Chapter 6

Analysis of TWA in ambulatory records

6.1 Introduction

The utility of TWA testing during ambulatory monitoring has been subject to intense investigation in recent years [Verrier et al., 2005b, Nieminen and Verrier, 2010]. In ambulatory records, the maximum amplitude of TWA has been semi-automatically quantified using the Modified Moving Average Method MMAM [Verrier et al., 2005b], and then compared to a cut point to decide if such TWA level should be considered normal or abnormal. This binary TWA index has been found to be a strong predictor of arrhythmic events and cardiac mortality in different populations [Nieminen and Verrier, 2010]. In the last years, quantitative analysis of TWA amplitude as a continuous variable has also been shown to indicate an increasing cardiac risk [Klingenheben et al., 2005, Slawnych et al., 2009].

The MMAM measures the local TWA activity at each analysis point using the powerful noise-rejection principle of recursive averaging [Verrier et al., 2005b]. However, as only one TWA measurement is usually chosen to characterize an ambulatory record, it is essential that this measurement corresponds to real TWA and that it is not caused by artifacts in the signal. Therefore, the visual verification of TWA measurements after MMAM processing becomes indispensable [Nieminen and Verrier, 2010]. Furthermore, basing the risk assessment on a single TWA measurement may reduce the reproducibility of the index, as it is very dependent on the specific activity that the patient is performing at a particular time.

One way to circumvent these limitations could be to extend the averaging approach to longer periods. It has been shown that long-term averaging of ECG measurements allows the quantification of subtle phenomena such as heart rate turbulence [Martínez et al., 2010], deceleration capacity [Bauer et al., 2006] or baroreflex sensitivity [Rienzo et al., 2001]. The hypothesis of the study in this chapter is that the application of extensive, long-term averaging to TWA quantification will produce reliable measurements of the average TWA activity over long periods, and that these measurements, being less sensitive to noise, will make it possible to perform TWA analysis for risk assessment in a fully-automated way.

This study presents a fully-automated method to analyze TWA in ambulatory records, based on the πCA multilead scheme, which was chosen as the best option among the alternatives compared in chapter 5. Results demonstrate that the average TWA activity in a 24-hour period is an independent predictor of CD and SCD in patients with chronic heart failure (CHF). Following the approaches of existing studies [Klingenheben et al., 2005, Slawnych et al., 2009, Minkkinen et al., 2009], two risk indices are proposed: a binary index that defines a positive/negative TWA test, and a quantitative continuous index that reflects an increasing degree of cardiac risk.

6.2 Study population

A total of 992 patients with symptomatic CHF corresponding to NYHA classes II to III were enrolled in the MUSIC (MUerte Súbita en Insuficiencia Cardiaca) study, a prospective, multicenter study designed to assess risk predictors for cardiovascular mortality in ambulatory patients with CHF [Vázquez et al., 2009]. The study protocol was approved by institutional investigation committees and all patients signed informed consent. The collection of clinical data for this population was reported in previous studies [Vázquez et al., 2009, Cygankiewicz et al., 2009]. No medications were withdrawn during Holter monitoring.

Twenty-four-hour ambulatory ECG recordings (XYZ orthogonal leads, 200 Hz sampling rate) were performed using SpiderView recorders (ELA Medical, Sorin Group, Paris, France). From the overall population, the 650 available records from patients with sinus rhythm were included in the present study. The clinical characteristics of studied patients as well as medication are listed in the first column of table 6.1.

6.2.1 Follow-up and end-points

Patients were followed up every 6 months for a median of 48 months, with total mortality as a primary end point, and cardiac death (CD) and sudden cardiac death (SCD) as secondary end points. Information about end points was obtained from medical records, patients' physicians, and family members.

Cardiac death was defined as death from cardiac causes, but excluding such vascular causes as pulmonary embolism, aortic aneurysm dissection/aneurysm, or stroke. Sudden cardiac death was defined as: a) a witnessed death occurring within 60 minutes from the onset of new symptoms unless a cause other than cardiac was obvious, b) an unwitnessed death ($<$ 24 hours) in the absence of preexisting progressive circulatory failure or other causes of death, or c) death during attempted resuscitation.

End points were reviewed and classified by the MUSIC Study Endpoint Committee. Table 6.2 summarizes the number of deaths in the study population during the median 48-month period.

6.3 Methods

6.3.1 Measurement of TWA

The analysis scheme chosen for this study is the multilead scheme based on πCA. Instead of using the general multilead scheme (figure 3.2), the modified scheme depicted in figure 3.5 is used, because in this case the detection threshold cannot be realistically determined. In previous studies, a threshold for the detection stage was set by analyzing signals without TWA (in data sets with artificially added TWA), or ECG segments from healthy subjects where the absence of TWA could be reasonably assumed (in stress test data). In the present study, the absence of TWA could not be assumed at any point because the population did not include a control group of healthy subjects. Choosing a threshold from previous studies was not realistic either, because thresholds depend on factors such as the number of leads to analyze, the conditions of ECG recording (rest vs. stress test, for example), and the length of the analysis window, among others. Therefore, the modified scheme in which detection is omitted was selected.

Heart beats were detected and labeled as normal or abnormal with the Aristotle ECG analysis software [Moody and Mark, 1982]. Baseline wan-

der was canceled using a cubic-splines technique [Meyer and Keiser, 1977]. Automatic TWA analysis was then performed on every ECG recording in three steps: 1) selection of signal segments which were suitable for automatic analysis, 2) estimation of the amplitude of TWA in those segments, and 3) computation of indices that reflect the general alternans activity through the record. These steps are summarized below.

Selection of segments

ECGs were analyzed in segments of 128 beats with a 50% overlap between adjacent segments ($\delta = 64$). Each segment was included in automatic TWA analysis if 1) the difference between the maximum and the minimum instantaneous heart rate (HR) during the segment was ≤ 20 beats per minute (bpm), and 2) at least 80% of the beats in the segment fulfilled all of the following conditions:

1. it was labeled as normal by the Aristotle software,
2. the difference between the RR interval of that beat and the previous RR interval was ≤ 150 ms,
3. the difference between the baseline voltage measured at the PQ segment in that beat and the one measured in the preceding beat was ≤ 300 μV.

Estimation of TWA amplitude

If an ECG segment (denoted as the k*th* segment) was suitable for analysis, a measurement of the TWA amplitude in that segment (denoted as V_k) was computed by using a multilead scheme that combined πCA with the LLRM.

First, the ECG segment was low-pass filtered at 15 Hz to eliminate part of the noise that could affect the estimation of TWA amplitudes. Figure 6.1 shows an example of an ECG signal with TWA after baseline cancellation and low-pass filtering.

Then, the three orthogonal leads of the ECG segment were linearly combined to obtain a new lead in which the visibility of TWA over noise was maximized. This combination of leads was not predetermined, but was specifically computed for each segment with the πCA technique, and depended on how the 2-beat periodic components of the signal were distributed among the ECG leads. In this study, only the first transformed

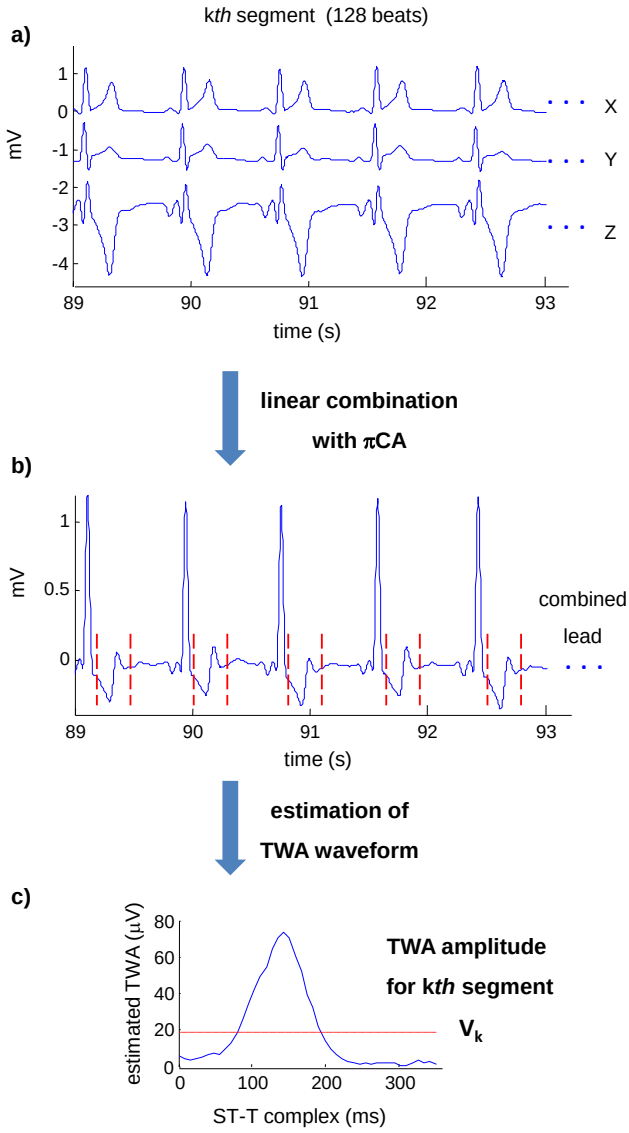

Figure 6.1: Example of TWA amplitude estimation. (a) ECG segment selected for automatic analysis after low-pass filtering and baseline cancellation. (b) New combined lead, computed with πCA. (c) Median TWA waveform in the segment, estimated with the Laplacian likelihood ratio method, and absolute TWA amplitude in the segment $V_k = 18.5\ \mu V$.

obtained with πCA was analyzed, since it is the lead where TWA is projected, as demonstrated in chapter 5. Figure 6.1(b) shows the combined lead obtained with πCA for the example ECG segment.

Finally, TWA amplitude was measured in the new combined lead (not in a reconstructed signal, this is the main difference with the general multilead scheme). In each beat, an interval of 350 ms after the end of the QRS was selected (ST-T complex, marked with dashed lines in figure 6.1(b)). The median difference between the ST-T complexes of even and odd beats was computed by using the LLRM. In this way, an estimation of the median TWA waveform in the ECG segment was obtained (figure 6.1(c)). The amplitude of TWA in the segment, denoted as V_k, was finally measured as the absolute value of the mean of the estimated TWA waveform (figure 6.1(c)).

Computation of TWA indices

Two sets of indices were computed after measuring the amplitude of TWA in all the segments of an ECG record. The first set reflected the average activity of TWA within the segments under study, and the second set quantified the maximum TWA amplitude in the segments under study.

The first set consisted of the Average Alternans Index (**AAI**) and the heart-rate-restricted Average Alternans Indices ($\mathbf{AAI}_x$). AAI was computed as the average of all V_k values in the ECG signal, and reflected the average TWA activity during the 24-hour period. Note that, for instance, a 24-hour ECG that presented TWA only during 5% of the time with an amplitude of 60 μV would have an AAI = 3 μV, which means that the AAI cannot be interpreted as a direct measurement of the amplitude of TWA at any single point. Restricted Average Alternans Indices (AAI_x) were computed as the average of only those V_k values measured in segments with average HR ranging from X-10 bpm to X bpm, with $X = \{70, 80, 90, 100, 110\}$. For instance, AAI_{90} would reflect the average TWA activity at HR between 80 and 90 bpm in the 24-hour period.

The second set consisted of the Maximum Alternans Index (**MAI**) and the restricted Maximum Alternans Indices ($\mathbf{MAI}_x$). MAI was computed as the maximum of all V_k values in the ECG signal. Restricted Maximum Alternans Indices (MAI_x) were computed as the maximum of the V_k values measured in segments with average HR ranging from X-10 bpm to X bpm, with $X = \{70, 80, 90, 100, 110\}$. For instance, MAI_{90} would represent the

maximum TWA amplitude at HR between 80 and 90 bpm in the 24-hour period. This set of indices quantifying maximum TWA amplitudes was included for comparison to the usual approach in ambulatory TWA testing.

6.3.2 Statistical analysis

Data are presented as mean ± standard deviation for continuous variables, and number and percentage for categorical variables. Two-tailed Mann-Whitney and Fisher's exact tests were used for univariate comparison of quantitative and categorical data respectively. Survival probability was estimated using Kaplan-Meier methods with comparison of cumulative events using log-rank tests. Univariate and multivariate Cox proportional hazards analyses were performed to determine the prognostic value of TWA indices in predicting the end points. Cox regression models were built considering a significance ≤ 0.05 as the criterion for entry into a model. Linear relations between quantitative TWA indices and HR were evaluated with Spearman's correlation coefficient. A p-value < 0.05 was considered statistically significant. Data were analyzed using SPSS software (version 15.0; SPSS Inc. Chicago, IL).

6.4 Results

The mean value of AAI in the study population was 3.3 ± 2.1 μV, and the 25^{th}, 50^{th} and 75^{th} percentiles were 2.4, 2.9 and 3.7 μV respectively (figure 6.2). A weak negative correlation was found between AAI and mean HR in the Holter recording (ρ = -0.083, p-value = 0.035).

Patients were divided into TWA positive (TWA+) and TWA negative (TWA-) groups by setting a cut point for AAI of 3.7 μV, corresponding to the 75^{th} percentile of the distribution of AAI in the population. Of the 650 studied patients, 493 (75.8%) were included in the TWA- group (AAI $\leq$ 3.7 μV) and 157 (24.2%) in the TWA+ group (AAI $>$ 3.7 μV). No significant differences were found upon comparison of clinical variables in TWA+ and TWA- groups (table 6.1). Survival rate was significantly higher in group TWA- for primary and secondary end points (table 6.2). Figure 6.3 shows the distribution of AAI in survivors, CD and SCD groups.

Univariate Cox analysis revealed that a TWA+ outcome was associated to all-cause mortality, to CD, and to SCD (table 6.3). No association was found between a TWA+ outcome and non-cardiac mortality. Multivari-

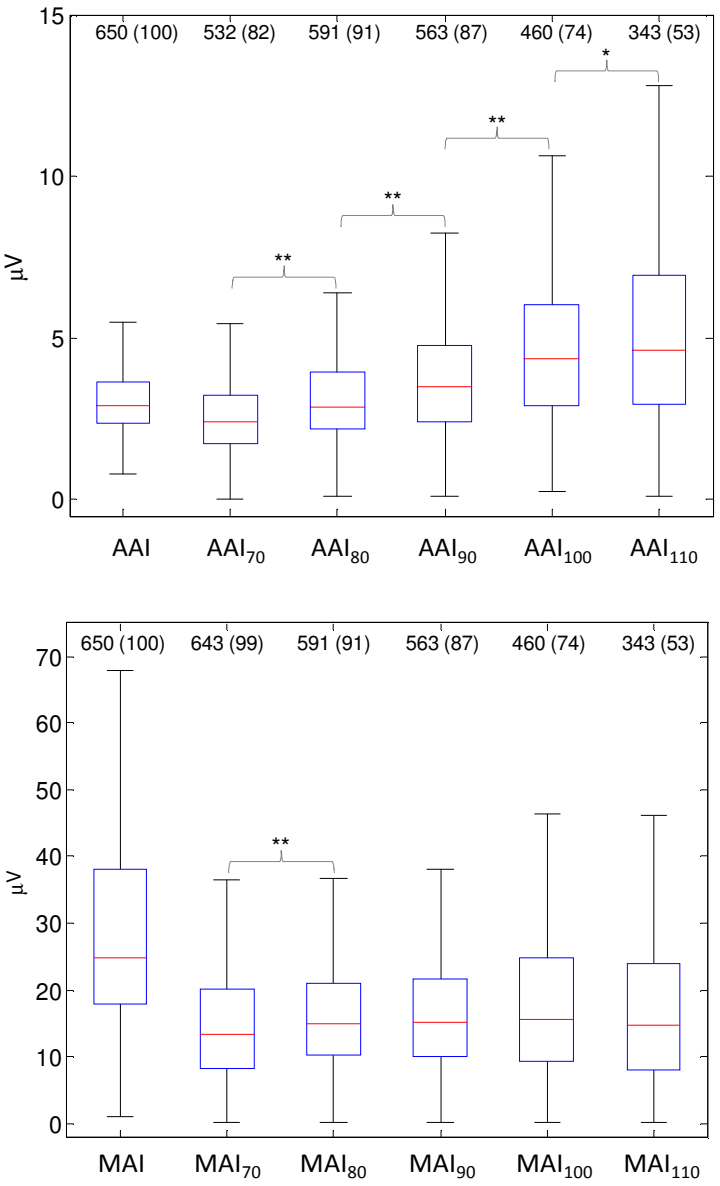

Figure 6.2: Top: boxplot of the average alternans indices computed in the 24-h period (AAI), and in intervals with HR in the range of X-10 to X bpm (AAI_x). Bottom: boxplot of the maximum alternans indices computed in the 24-h period (MAI), and in intervals with HR in the range of X-10 to X bpm (MAI_x). The number (and percentage) of records in which indices could be computed is indicated above the boxes. Significant differences between the medians of adjacent boxes are indicated by *($p < 0.05$) and **($p < 0.001$).

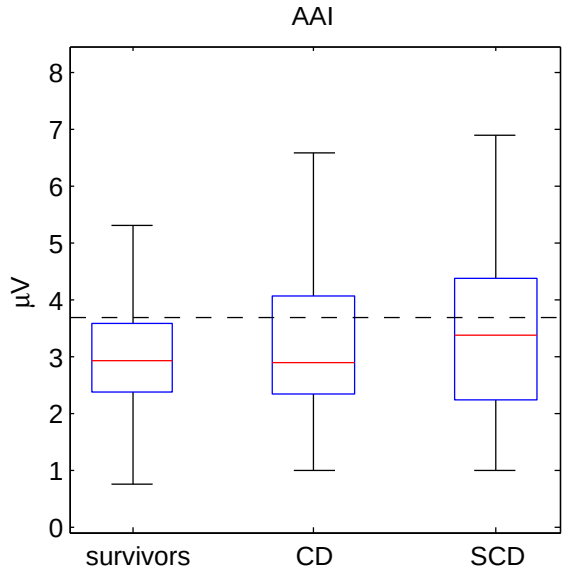

Figure 6.3: Boxplot of the average alternans index computed in the 24-h period (AAI) in survivors, CD and SCD groups. The horizontal dashed line indicates the cut point of 3.7 μV, corresponding to the 75^{th} percentile of the distribution of AAI in the overall population.

ate Cox proportional hazards models were constructed by adjusting for (1) age, gender, NYHA class, LVEF $< 35\%$, and diabetes, and (2) use of beta-blockers, amiodarone and ACE or ARB inhibitors in addition to covariables in model (1). For multivariate model (1), a TWA+ outcome was the variable most significantly associated to SCD risk, with a hazard ratio of 2.38, similar to LVEF $< 35\%$ (hazard ratio 2.55, 95% CI: 1.35 – 4.80, $p = 0.004$). For multivariate model (2), a TWA+ outcome was the covariable with the second highest hazard ratio (2.29) after LVEF $< 35\%$ (hazard ratio 2.65, 95% CI: 1.39 – 5.03, $p = 0.003$). The event-free curves for CD and SCD are shown in figure 6.4.

The mean values of AAI_x were $\text{AAI}_{70} = 2.8 \pm 1.9$ μV, $\text{AAI}_{80} = 3.3 \pm 2.3$ μV, $\text{AAI}_{90} = 3.9 \pm 2.4$ μV, $\text{AAI}_{100} = 5.0 \pm 3.1$ μV and $\text{AAI}_{110} = 6.1 \pm 5.5$ μV. Not all ECGs presented a HR spanning from 60 to 110 bpm; also, all segments within a certain HR range were discarded for TWA analysis in some recordings (according to the inclusion rules described in the Methods section). Therefore, not every AAI_x could be computed for every patient. The percentages of indeterminate values for the entire population were 18.1% for AAI_{70}, 9.1% for AAI_{80}, 13.4% for AAI_{90}, 26.1% for AAI_{100},

	Total Population (n = 650)	TWA− (n = 493)	TWA+ (n = 157)	p
Age (years)	63 ± 12	63 ± 11	64 ± 13	0.091
Gender (men)	462 (71.1%)	350 (71.0%)	112 (71.3%)	0.999
NYHA class III	117 (18.0%)	87 (17.6%)	30 (19.1%)	0.721
LVEF < 35%	356 (54.8%)	262 (53.1%)	94 (59.9 %)	0.142
Diabetes	245 (37.7%)	190 (38.5%)	55 (35.0%)	0.451
Beta-blockers	454 (69.8%)	350 (71.0%)	104 (66.2%)	0.273
Amiodarone	59 (9.1%)	43 (8.7%)	16 (10.2%)	0.632
ARB or ACE inhibitors	573 (88.2%)	441 (89.4%)	132 (84.1%)	0.088
Average HR (bpm)	75 ± 12	76 ± 12	75 ± 12	0.581
Maximum HR (bpm)	122 ± 26	123 ± 27	119 ± 25	0.100

NYHA = New York Heart Association
LVEF = Left ventricular ejection fraction
ARB = Angiotensin receptor blocker
ACE = Angiotensin-converting enzyme

Table 6.1: Characteristics of patients. Data are presented as absolute frequencies and percentages, or as mean ± standard deviation.

	Total Population (n = 650)	TWA− (n = 493)	TWA+ (n = 157)	p
Total mortality	146 (22.5%)	99 (20.1%)	47 (30.0%)	**0.012**
CD	119 (18.3%)	81 (16.4%)	38 (24.2%)	**0.033**
SCD	52 (8.0%)	30 (6.1%)	22 (14.0%)	**0.003**

Table 6.2: Events during follow-up. Data expressed as absolute frequencies and percentages.

	AAI $> 3.7\ \mu$V		AAI_{90}	
Total mortality	Hazard ratio	p	Hazard ratio	p
Univariate	1.62 (1.15 − 2.29)	**0.006**	1.04 (0.99 − 1.10)	0.150
Multivariate(1)	1.54 (1.09 − 2.19)	**0.015**	1.05 (0.98 − 1.11)	0.144
Multivariate(2)	1.48 (1.04 − 2.10)	**0.030**	1.04 (0.98 − 1.11)	0.184

	AAI $> 3.7\ \mu$V		AAI_{90}	
CD	Hazard ratio	p	Hazard ratio	p
Univariate	1.60 (1.09 − 2.35)	**0.017**	1.05 (1.00 − 1.11)	0.051
Multivariate(1)	1.54 (1.04 − 2.26)	**0.030**	1.06 (1.00 − 1.13)	**0.038**
Multivariate(2)	1.44 (0.97 − 2.13)	0.068	1.06 (1.00 − 1.13)	0.051

	AAI $> 3.7\ \mu$V		AAI_{90}	
SCD	Hazard ratio	p	Hazard ratio	p
Univariate	2.48 (1.43 − 4.30)	**0.001**	1.07 (1.01 − 1.15)	**0.041**
Multivariate(1)	2.38 (1.37 − 4.14)	**0.002**	1.07 (1.00 − 1.15)	**0.039**
Multivariate(2)	2.29 (1.31 − 4.00)	**0.004**	1.07 (1.00 − 1.15)	**0.046**

Table 6.3: Association of TWA indices with mortality. 95% confidence intervals for hazard ratios are reported in brackets. Adjusted multivariate model (1) includes age, gender, NYHA class, LVEF $< 35\%$, and diabetes. Adjusted multivariate model (2) includes covariables in (1) plus use of betablockers, amiodarone, and ARB or ACE inhibitors.

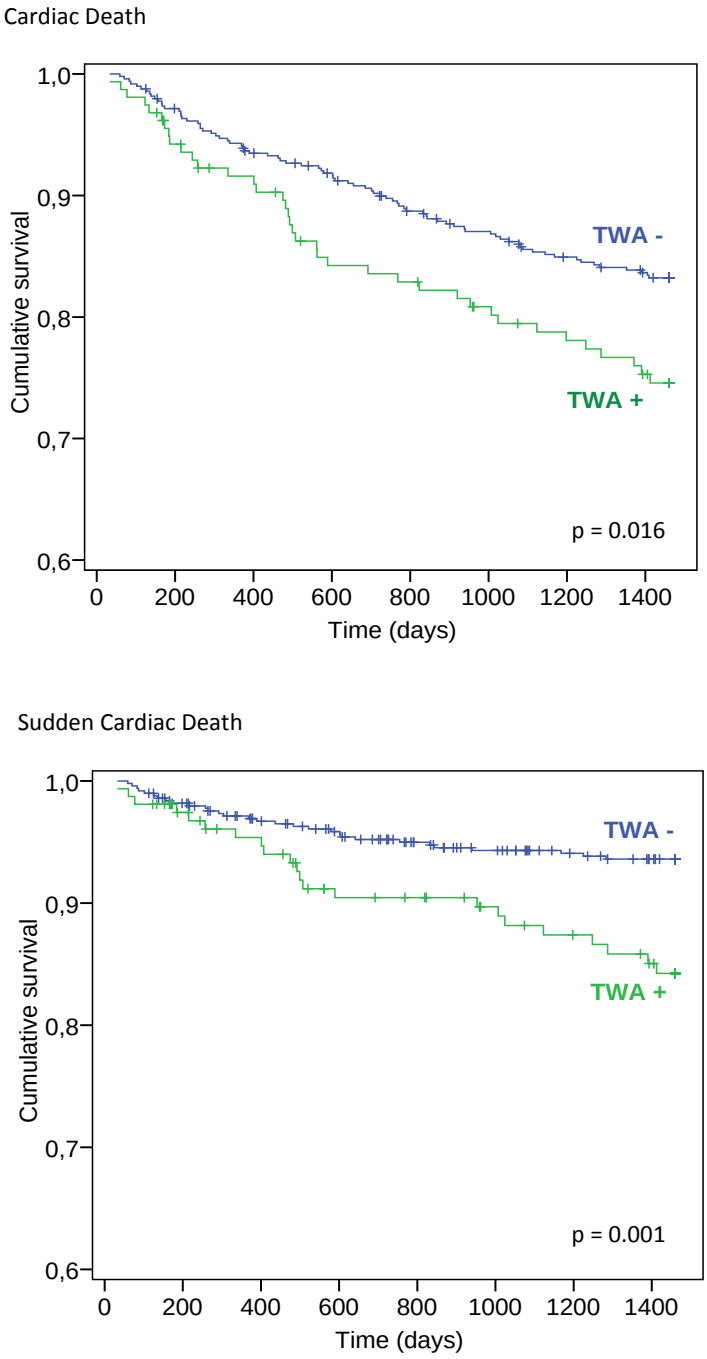

Figure 6.4: Event-free curves for CD (top) and SCD (bottom).

and 47.2% for AAI_{110}. Figure 6.2 shows the distributions of AAI_x.

The mean values of AAI_x increased with HR, and there were significant differences between indices from all adjacent HR intervals (figure 6.2). Univariate Cox analysis was performed for all AAI_x, and only AAI_{90} was found to be associated with SCD. Multivariate Cox analysis confirmed this association (table 6.3). AAI_{90} was not associated to all-cause mortality or non-cardiac mortality.

The mean value of MAI in the study population was 31.4 ± 25.3 μV, and the 25^{th}, 50^{th} and 75^{th} percentiles were 17.9, 24.7 and 38.0 μV respectively (figure 6.2). No association to CD or SCD risk was found for MAI as a continuous variable or as a categorical variable after dichotomization with the 75^{th} percentile. The mean values of MAI_x were $MAI_{70} = 16.1 \pm 13.1$ μV, $MAI_{80} = 17.2 \pm 10.6$ μV, $MAI_{90} = 17.5 \pm 12.1$ μV, $MAI_{100} = 19.7 \pm 12.1$ μV and $MAI_{110} = 20.6 \pm 22.6$ μV. MAI_x were not significantly associated to CD or SCD risk according to Cox univariate and multivariate analyses.

6.5 Discussion

This study demonstrates that the quantification of the average TWA activity over long periods is a strong, independent predictor of SCD in patients with CHF. Two indices quantifying the TWA activity in a 24-hour period, AAI and AAI_{90}, were found to independently predict CD and SCD, but did not predict non-cardiac mortality, a finding that supports the hypothesis that elevated TWA activity reflects abnormal cardiac function predisposing to cardiac death.

The average TWA activity in a 24-h period, quantified by the AAI, was the covariable most strongly associated to the risk of SCD. In our population, only a weak correlation was found between AAI and the patient's HR, which indicates that AAI is not merely a surrogate measure of the patient's HR, but also reflects the influence of HR-independent factors in TWA. Therefore, AAI may provide a measure of the extent of cardiac vulnerability, because a higher influence of HR-independent factors in TWA amplitude reflects a higher degree of cardiac electrical instability [Verrier et al., 2009].

The prognostic value of quantitative TWA measurements is increasingly being studied [Klingenheben et al., 2005, Slawnych et al., 2009, Minkkinen

et al., 2009]. In this study, an index of quantitative TWA (AAI_{90}) independently predicted SCD. When measured at moderate heart rates, higher magnitudes of TWA are known to predict a greater risk of serious outcomes [Cutler and Rosenbaum, 2009]. For TWA to predict cardiovascular events, maximum HR limits ranging from 100 to 125 bpm are usually considered [Verrier et al., 2009]. In this study, we found that the average TWA activity was associated to SCD when measured at lower rates, between 80 and 90 bpm (AAI_{90}). A possible explanation for this difference is that heart failure lowers the HR threshold to elicit TWA [Wilson et al., 2009].

Unsupervised maximum TWA amplitudes, measured by MAI and MAI_x, did not predict cardiac risk. Although the values obtained for MAI were comparable to maximum TWA amplitudes reported in the literature (between 30 and 60 μV), no significant association was found between MAI and risk of SCD or CD. This was not unexpected, since it is known that measuring TWA amplitudes without testing for its significance, either visually or automatically, can lead to inaccurate results due to noise and artifacts [Nemati et al., 2010]. In recent studies with ambulatory ECGs, the maximum TWA amplitude in a record is measured with the MMAM, either in the whole record [Maeda et al., 2009] or in segments below a maximum HR [Sakaki et al., 2009], and then needs to be visually verified to ensure that they correspond to real TWA.

In the present study, we found that quantifying the average TWA activity (AAI) instead of the maximum amplitude (MAI) eliminates the necessity of visually discarding erroneous measurements, and allows the prediction of CD and SCD in the study population. To our best knowledge, the method presented in this work is the first one that allows a multilead, fully-automated computation of TWA markers of cardiac risk in ambulatory ECGs. However, although this study indicates that the average TWA activity over a 24-hour period provides important prognostic information in patients with CHF, it would be premature to extend these observations to other groups. The use of a 75^{th} percentile cut point for TWA measures is a common starting point when a technique is first tested on a population [Verrier and Nearing, 2003, Nieminen et al., 2007], but additional prospective evaluation is still required, particularly on the applicability of the cut point derived in this study.

6.6 Conclusions

This study demonstrates that the improvements in TWA detection and estimation obtained with the πCA multilead scheme, together with the proposed strategy for computing global TWA indices, make it possible to stratify cardiac risk in Holter recordings without the need for visual validation. Results show that the average TWA activity over a 24-hour period provides important prognostic information in patients with CHF. Two novel indices, AAI and AAI_{90}, have been proposed to quantify the average TWA activity, and have been found to independently predict the risk of CD and SCD.

Chapter 7

Conclusions

This chapter summarizes the original contributions and main conclusions of the thesis, and proposes possible extensions of the work.

7.1 Summary and conclusions

As stated in chapter 1, the objective of this thesis was to develop a multilead scheme for TWA analysis that improved the detection and quantification of TWA in the ECG, and that increased the clinical value of TWA as a risk index. The work carried out to achieve this goal can be divided in three parts: design of novel multilead schemes for TWA analysis, methodological evaluation of the proposed techniques, and clinical validation of the selected multilead scheme. The original contributions and conclusions of each part are summarized next.

Design of novel multilead schemes for TWA analysis

Chapter 3 introduced a general scheme for multilead analysis of TWA. The proposed scheme is an extended version of a usual single-lead scheme, where two additional stages, transformation and reconstruction, increase the detectability of TWA, and also improve the estimation of TWA amplitude and waveform. Various techniques are proposed for the transformation stage (PCA, πCA, ICA and SRM). While πCA and ICA techniques are not new, they have been applied to TWA analysis for the first time in this work. SRM is a new technique proposed in this work which exploits the periodicity of TWA to increase its detectability in the transformed signal.

The general multilead scheme is not tied to a specific TWA analysis method, but can be combined with any single-lead method which detects and estimates TWA in separate stages. Along the thesis, it has been combined with the LLRM, and also with the SM for comparison. Besides, several modifications are proposed to adapt the general scheme to different clinical settings.

Methodological validation

Chapters 4 and 5 presented the methodological evaluation of the multilead scheme based on PCA (*multi-PCA* scheme) and based on πCA (*multi-πCA* scheme). *Multi-PCA*, *multi-πCA* and single-lead schemes were compared in various simulation studies, in which synthetic, semi-synthetic and real signals with known TWA were analyzed. Differences between schemes were quantified using two common performance metrics, probability of detection and probability of false alarm, and also using new global measures of the bias and variance of the TWA estimation. Differences in the detection power obtained with πCA and with other BSS techniques were also studied.

Simulation results in chapter 4 showed that the *multi-PCA* scheme detects TWA with a SNR 30 dB lower, and estimates TWA with a SNR 25 dB lower than the single-lead scheme for a given false alarm rate. It was also shown that a similar detection gain can be obtained by applying the *multi-PCA* scheme to the SM.

According to results in chapter 5, the *multi-πCA* is the one which provides the best detection power among the compared alternatives. In real stress-test signals with added TWA, and for a 1% false alarm rate, the *multi-πCA* scheme detects TWA of 5 μV with a probability of 98%, while the probabilities for *multi-PCA* and *single* schemes are 60% and 1% respectively.

When comparing BSS techniques, results in chapter 5 showed that the periodicity-based schemes (πCA and SRM) yield the best detection power. The maximum detection performance is obtained either using a temporal criterion (πCA) or a spectral criterion (SRM) to maximize the periodicity of the transformed signal. Therefore, using periodicity to separate TWA from noise is the best multilead strategy among the compared options. Between πCA and SRM, πCA is a better option because its computational cost is much lower.

Multi-PCA, *multi-πCA* and single-lead schemes were used to analyze

a stress test database. Results in chapter 4 showed that it is possible to distinguish between CAD patients and healthy volunteers according to the TWA detections of the *multi-PCA* scheme, whereas it is not possible with the single-lead scheme. Results in chapter 5 indicated that the *multi-πCA* scheme improves this differentiation.

Clinical validation

Chapter 6 presented a clinical study that confirmed the prognostic utility of TWA as measured by the *multi-πCA* scheme. The combination of the *multi-πCA* scheme with a procedure to select signal segments for automatic analysis produced robust TWA measurements, which were used to compute different clinical indices.

Novel indices were proposed to quantify the average TWA activity over a 24-hour period, either globally (AAI) or during intervals with limited heart rate (AAI_x). A positive/negative TWA test was defined by setting a cut point for AAI of 3.7 μV. A positive outcome (AAI $>$ 3.7 μV) was associated to all-cause mortality, CD, and SCD. The heart-rate-restricted AAI_{90} also predicted CD and SCD. Neither AAI nor AAI_{90} predicted non-cardiac mortality, which supports the hypothesis that elevated average TWA activity reflects abnormal cardiac function.

A second group of indices measuring maximum TWA amplitudes was also studied, which is a similar approach to what commercial systems commonly measure. In the present study, unsupervised measures of maximum TWA amplitudes did not predict cardiac risk.

To our best knowledge, the method presented here is the first one that allows a multilead, fully-automated computation of TWA markers of cardiac risk in ambulatory ECGs. However, although this study indicates that the average TWA activity over a 24-hour period provides important prognostic information in patients with CHF, further research is needed to confirm the validity of the cut point derived here, and to extend these observations to other populations.

7.2 Future work

Possible research lines to expand the work in this thesis are presented below.

- Evaluation of the utility of multilead TWA measures as a risk index in

stress test recordings. Starting with results in chapters 4 and 5, qualitative and quantitative TWA indices (presence, amplitude, duration, onset heart rate) can be jointly studied to find the combination that maximizes the prognostic value of the TWA stress test. This research line could not be initiated during this thesis because the stress test database did not include follow up information.

- Joint analysis of repolarization dispersion and alterations of the autonomic nervous system (ANS) to improve risk stratification. It would be interesting to test the hypothesis that combined evaluation of TWA and ANS activity increases the prognostic value of the TWA test. As a starting point, the circadian patterns of TWA, and also the relation between TWA and heart rate turbulence (HRT) could be studied in the MUSIC study database.

- Study of the relation between TWA and ischemia in ambulatory recordings. As a starting point, the multilead approach for Holter recordings presented in chapter 6 could be applied to the Long Term ST Database [Jager et al., 2003], which contains 24-hour Holter recordings with isquemia annotations. Global AAI indices could be compared to the clinical state of the patient, and also the correlation between local TWA measurements and deviations of the ST segment could be studied.

- Characterization of the spatial relation between TWA and occlusion site in CAD patients. In 2006, Martínez and coworkers analyzed TWA in patients undergoing PTCA, and found that the spatial distribution of TWA varied according to the occluded artery, which reflected the regional nature of the TWA phenomenon [Martínez et al., 2006]. As discussed in chapters 3 and 5 of this thesis, the transformation computed by πCA can be interpreted as the direction from with TWA is better observed. It would be interesting to test if the average direction obtained with πCA also correlates with the site of the occlusion during PTCA, and in that case, if the information provided by πCA can be used improve the diagnosis of CAD patients in non-invasive tests.

List of Acronyms

ACE	Angiotensin-converting enzyme
ACI	Alternans correlation index
AMFM	Adaptive matched filter method
ARB	Angiotensin receptor blocker
ASNR	Alternans-Signal-to-Noise ratio
A-V	Atrio-Ventricular (node)
bpm	beats per minute
BSS	Blind source separation
CAD	Coronary artery disease
CFAR	Constant false alarm rate
CHF	Chronic heart failure
CI	Confidence interval
CM	Correlation method
cpb	cycles per beat
CVD	Cardiovascular disease
ECG	Electrocardiogram
EP	Electrophysiologic (study)
EU	European Union
GLRT	Generalized likelihood ratio test
HR	Heart rate
IBAM	Intra-beat average method
ICA	Independent component analysis
ICD	Implantable cardioverter defibrillator
JADE	Joint approximate diagonalization of eigenmatrices
LLRM	Laplacian likelihood ratio method
LQTS	Long-QT syndrome

LVEF	Left ventricular ejection fraction
MI	Myocardial infarction
MLE	Maximum likelihood estimation
MMAM	Modified moving average method
NYHA	New York Heart Association
PCA	Principal component analysis
PTCA	Percutaneous transluminal coronary angioplasty
πCA	Periodic component analysis
ROC	Receiver operating characteristics (curve)
SA	Sinoatrial (node)
SCD	Sudden cardiac death
SM	Spectral method
SNR	Signal-to-noise ratio
SRM	Spectral ratio maximization
TWA	T-wave alternans
TWAR	T-wave alternans ratio
US	United States

Bibliography

MATLAB software, version 6. The MathWorks Inc., Natick, MA, USA, 2002.

H. Abdi. The Kendall Rank Correlation Coefficient. In Neil J. Salkind, editor, *Encyclopedia of Measurement and Statistics*. Sage, Thousand Oaks (CA), USA, 2007.

B. Acar and H. Köymen. SVD-based on-line exercise ECG signal orthogonalization. *IEEE Trans Biomed Eng*, 46(3):311–312, 1999.

G. Acar, G. Yi, K. Hnatkova, and M. Malik. Spatial, temporal and wavefront direction characteristics of 12-lead T wave morphology. *Med. Biol. Eng. Comput.*, 37:574–584, 1999.

D. R. Adam, S. Akselrod, and R. J. Cohen. Estimation of ventricular vulnerability to fibrillation through T-wave time series analysis. In *Computers in Cardiology 1981*, volume 8, pages 307–310. IEEE Comp. Soc. Press, 1981.

G. Amit, O. Costantini, and D. S. Rosenbaum. Can we alternate between T-wave alternans testing methods? *Heart Rhythm*, 6(3):338–340, Mar 2009.

A. A. Armoundas, G. F. Tomaselli, and H. D. Esperer. Pathophysiological basis and clinical application of T-wave alternans. *J Am Coll Cardiol*, 40 (2):207–217, Jul 2002.

A. A. Armoundas, S. H. Hohnloser, T. Ikeda, and R. J. Cohen. Can microvolt T-wave alternans testing reduce unnecessary defibrillator implantation? *Nat Clin Pract Cardiovasc Med*, 2(10):522–528, Oct 2005.

R. Bailón, J. Mateo, S. Olmos, P. Serrano, J. García, A. del Río, I. J. Ferreira, and P. Laguna. Coronary artery disease diagnosis based on exercise

electrocardiogram indexes from repolarisation, depolarisation and heart rate variability. *Med. Biol. Eng. Comput.*, 41(5):561–571, 2003.

S. Bansal and R. D. Berger. Microvolt T-wave alternans testing: Renewed hope? *J Cardiovasc Electrophysiol*, pages 1–2, Apr 2010.

A. Bauer, J. W. Kantelhardt, P. Barthel, R. Schneider, T. Mäkikallio, K. Ulm, K. Hnatkova, A. Schömig, H. Huikuri, A. Bunde, M. Malik, and G. Schmidt. Deceleration capacity of heart rate as a predictor of mortality after myocardial infarction: cohort study. *Lancet*, 367(9523): 1674–1681, May 2006.

M. Blanco-Velasco, F. Cruz-Roldan, J. Godino-Llorente, and K. Barner. Non-linear trend estimation of the ventricular repolarization segment for T-wave alternans detection. *IEEE Trans Biomed Eng*, Apr 2010. doi: 10.1109/TBME.2010.2048109.

D. M. Bloomfield, S. H. Hohnloser, and R. J. Cohen. Interpretation and classification of microvolt T wave alternans tests. *J Cardiovasc Electrophysiol*, 13(5):502–512, 2002.

D. M. Bloomfield, R. C. Steinman, P. B. Namerow, M. Parides, J. Davidenko, E. S. Kaufman, T. Shinn, A. Curtis, J. Fontaine, D. Holmes, A. Russo, C. Tang, and J. T. Bigger. Microvolt T-wave alternans distinguishes between patients likely and patients not likely to benefit from implanted cardiac defibrillator therapy: a solution to the multicenter automatic defibrillator implantation trial (MADIT) II conundrum. *Circulation*, 110(14):1885–1889, Oct 2004.

M. Boix, B. Cantó, D. Cuesta, and P. Micó. Using the wavelet transform for T-wave alternans detection. *Mathematical and Computer Modelling*, 50 (5-6):738 – 742, 2009. Mathematical Models in Medicine & Engineering.

G. Bortolan and I. I. Christov. Principal component analysis for detection and assessment of T-wave alternans. In *Proc. Computers in Cardiology*, pages 521–524, 14–17 Sept. 2008.

G. Bortolan, I. I. Christov, V. N. Batchvarov, and E. R. Behr. Qrs&t wave alternans and beat-to-beat ventricular repolarization variability assessed from 12-lead holters in patients with suspected brugada syndrome. In *Proc. Computers in Cardiology*, pages 305–308, 2009.

C. G. Broyden. The convergence of a class of double-rank minimization algorithms. *J. Inst. Math. Applic*, 6:76–90, 1970.

L. Burattini and R. Burattini. Heart-rate adaptive match filter based procedure to detect and quantify T-wave alternans. In *Proc. Computers in Cardiology*, pages 513–516, 14–17 Sept. 2008.

L. Burattini, W. Zareba, J. P. Couderc, E. L. Titlebaum, and A. J. Moss. Computer detection of non-stationary T wave alternans using a new correlation method. In *Proc. Computers in Cardiology 1997*, pages 657–660, 7–10 Sept. 1997.

L. Burattini, W. Zareba, E. J. Rashba, J. P. Couderc, J. Konecki, and A. J. Moss. Ecg features of microvolt T-wave alternans in coronary artery disease and long QT syndrome patients. *J Electrocardiol*, 31 Suppl:114–120, 1998.

L. Burattini, W. Zareba, and A. J. Moss. Correlation method for detection of transient T-wave alternans in digital Holter ECG recordings. *Ann Noninvasive Electrocardiol*, 4(4):416–424, 1999.

L. Burattini, S. Bini, and R. Burattini. Comparative analysis of methods for automatic detection and quantification of microvolt T-wave alternans. *Med Eng Phys*, Sep 2009a.

L. Burattini, S. Bini, and R. Burattini. Comparative analysis of methods for automatic detection and quantification of microvolt T-wave alternans. *Med Eng Phys*, 31(10):1290–1298, Dec 2009b.

L. Burattini, S. Bini, and R. Burattini. Correlation method versus enhanced modified moving average method for automatic detection of T-wave alternans. *Comput Methods Programs Biomed*, Feb 2010a. doi: 10.1016/j.cmpb.2010.01.008.

L. Burattini, W. Zareba, and R. Burattini. Identification of gender-related normality regions for T-wave alternans. *Ann Noninvasive Electrocardiol*, 15(4):328–336, Oct 2010b.

J. F. Cardoso and A. Souloumiac. Blind beamforming for non Gaussian signals. *IEE Proceedings-F*, 140(6):362–370, December 1993.

F. Castells, J. J. Rieta, J. Millet, and V. Zarzoso. Spatiotemporal blind source separation approach to atrial activity estimation in atrial tachyarrhythmias. *IEEE Trans. Biomed. Eng.*, 52(3):258–267, 2005.

F. Castells, A. Cebrián, and J. Millet. The role of independent component analysis in the signal processing of ECG recordings. *Biomedizinische Technik/Biomedical Engineering*, 52(1):18–24, 2007.

M. Chinushi, M. Restivo, E.B. Caref, and N. El-Sherif. Electrophysiological basis of arrhythmogenicity of QT/T alternans in the long-QT syndrome: tridimensional analysis of the kinetics of cardiac repolarization. *Circ Res*, 83(6):614–628, 1998.

T. Chow, S. Saghir, C. Bartone, M. Goebel, J. Schneider, T. Booth, and P. S. Chan. Usefulness of microvolt T-wave alternans on predicting outcome in patients with ischemic cardiomyopathy with and without defibrillators. *Am J Cardiol*, 100(4):598–604, Aug 2007.

G. D. Clifford, F. Azuaje, and P. McSharry. *Advanced Methods and Tools for ECG Data Analysis*. Artech House, Inc., Norwood, MA, USA, 2006. ISBN 1580539661.

G. D. Clifford, S. Nemati, and R. Sameni. An artificial multi-channel model for generating abnormal electrocardiographic rhythms. In *Proc. Computers in Cardiology*, pages 773–776, 14–17 Sept. 2008.

G. D. Clifford, S. Nemati, and R. Sameni. An artificial multi-channel model for generating abnormal electrocardiographic rhythms. *IOP Physiol. Meas.*, 31(4), Apr 2010.

O. Costantini, S. H. Hohnloser, M. M. Kirk, B. B. Lerman, J. H. Baker, B. Sethuraman, M. M. Dettmer, D. S. Rosenbaum, and A. B. C. D. Trial Investigators. The ABCD (Alternans Before Cardioverter Defibrillator) trial: strategies using T-wave alternans to improve efficiency of sudden cardiac death prevention. *J Am Coll Cardiol*, 53(6):471–479, Feb 2009.

D. Cuesta-Frau, Ma. Biagetti, P. Micó-Tormos, M. Aboy, and R. Quinteiro. T-wave alternans analysis improvement by means of curve alignment prior to distance calculation. *Conf Proc IEEE Eng Med Biol Soc*, 2007:690–693, 2007.

D. Cuesta-Frau, M. Aboy, and M. Biagetti. Response: can a simulation study of T-wave alternans (twa) resolve whether twa is T-wave amplitude dependent? *Med Biol Eng Comput*, Jan 2009.

M. J. Cutler and D. S. Rosenbaum. Explaining the clinical manifestations of T wave alternans in patients at risk for sudden cardiac death. *Heart Rhythm*, 6(3, Supplement 1):S22 – S28, 2009.

I. Cygankiewicz, W. Zareba, R. Vazquez, A. Bayes-Genis, D. Pascual, C. Macaya, J. Almendral, M. Fiol, A. Bardaji, J. R Gonzalez-Juanatey, V. Nieto, M. Valdes, J. Cinca, A. Bayes de Luna, and M. U. S. I. C. Investigators. Risk stratification of mortality in patients with heart failure and left ventricular ejection fraction $> 35\%$. *Am J Cardiol*, 103(7): 1003–1010, Apr 2009.

E. de Vilhena Garcia. T-wave alternans: reviewing the clinical performance, understanding limitations, characterizing methodologies. *Ann Noninvasive Electrocardiol*, 13(4):401–420, 2008.

E. de Vilhena Garcia, N. Samesima, H. G. Pereira Filho, C. M. Quadros, L. Tenório Cavalcante da Silva, M. Martinelli Filho, M. L. Zacharias Hannouche, W. Mathias, and C. A. Pastore. Comparison of quantitative T-wave alternans profiles of healthy subjects and ICD patients. *Ann Noninvasive Electrocardiol*, 14(2):108–118, Apr 2009.

L. Faes, G. Nollo, M. Kirchner, E. Olivetti, F. Gaita, and R. Antolini. Principal component analysis and cluster analysis for measuring the local organization of human atrial fibrillation. *Med. Biol. Eng. Comput.*, 39: 656–663, 2001.

G. M. De Ferrari and A. Sanzo. T-wave alternans in risk stratification of patients with nonischemic dilated cardiomyopathy: Can it help to better select candidates for ICD implantation? *Heart Rhythm*, 6:S29–S35, 2008.

R. Fletcher. A new approach to variable metric algorithms. *Computer Journal*, 13:317–322, 1970.

E. Frank. An accurate, clinically practical system for spatial vectorcardiography. *Circulation*, 13:737 – 749, 1956.

J. García, G. Wagner, L. Sörnmo, P. Lander, and P. Laguna. Identification of the occluded artery in patients with myocardial ischemia induced by prolonged percutaneous transluminal coronary angioplasty using traditional vs transformed ECG-based indexes. *Computers and Biomedical Research*, 32(5):470–482, 1999.

J. García, M. Anström, J. Mendive, P. Laguna, and L. Sörnmo. ECG-based detection of body position changes in ischemia monitoring. *IEEE Trans Biomed Eng*, 50(6):677–685, 2003.

A. K. Gehi, R. H. Stein, L. D. Metz, and J. A.Gomes. Microvolt T-wave alternans for the risk stratification of ventricular tachyarrhythmic events: a meta-analysis. *J Am Coll Cardiol*, 46(1):75–82, 2005.

B. Ghoraani, S. Krishnan, R. J. Selvaraj, and V. S. Chauhan. T wave alternans evaluation using adaptive time-frequency signal analysis and non-negative matrix factorization. *Medical Engineering & Physics*, In Press, 2011.

G. Gibelli, C. Fantoni, C. Anzà, P. Cattaneo, A. Rossi, A. S. Montenero, and M. Baravelli. Arrhythmic risk evaluation during exercise at high altitude in healthy subjects: role of microvolt T-wave alternans. *Pacing Clin Electrophysiol*, 31(10):1277–1283, Oct 2008.

D. Goldfarb. A family of variable metric updates derived by variational means. *Mathematics of Computing*, 24:23–26, 1970.

G. H. Golub and C. F. Van Loan. *Matrix Computations*. The Johns Hopkins University Press, Baltimore, MD, USA, second edition, 1989.

W. Grimm, M. Christ, J. Bach, H-H. Müller, and B. Maisch. Noninvasive arrhythmia risk stratification in idiopathic dilated cardiomyopathy: results of the marburg cardiomyopathy study. *Circulation*, 108(23):2883–2891, Dec 2003.

A. C. Guyton and J. E. Hall, editors. *Textbook of Medical Physiology*. W. B. Saunders Co., 11th edition, 2006. ISBN 0-8089-2317-X.

M. H. Hassan and E. S. Kaufman. Prevalence of T wave alternans in the long QT syndrome population: A study involving 25 long QT syndrome families. *Heart Rhythm*, 2(5, Supplement 1):S303 – S304, 2005.

E. D. Helfenbein, A. D. Forbes, J. M. Lindauer, S. Babaeizadeh, and S. H. Zhou. Detection of periodic variations including T-wave alternans. *Journal of Electrocardiology*, 42(6):611 – 611, 2009.

H. E. Hering. Experimentalle studien an säugethieren über das elektrocardiogramm. *Zeitschrift für die experimentelle Pathologie und Therapie*, 7: 363 – 378, 1909.

S. H. Hohnloser, T. Ikeda, and R. J. Cohen. Evidence regarding clinical use of microvolt T-wave alternans. *Heart Rhythm*, 6(3 Suppl):S36–S44, Mar 2009.

A. Hyvärinen. Fast and robust fixed-point algorithms for independent component analysis. *IEEE Trans Neural Netw*, 10(3):626–634, 1999.

A. Hyvärinen, J. Karhunen, and E. Oja. *Independent Component Analysis*. Wiley-Interscience, 1 edition, May 2001. ISBN 047140540X.

T. Ikeda, H. Saito, K. Tanno, H. Shimizu, J. Watanabe, Y. Ohnishi, Y. Kasamaki, and Y. Ozawa. T-wave alternans as a predictor for sudden cardiac death after myocardial infarction. *Am J Cardiol*, 89(1):79–82, 2002.

F. Jager, A. Taddei, G. B. Moody, M. Emdin, G. Antolic, R. Dorn, A. Smrdel, C. Marchesi, , and R. G. Mark. Long-term ST database: a reference for the development and evaluation of automated ischaemia detectors and for the study of the dynamics of myocardial ischaemia. *Med Biol Eng Comput*, 41(2):172–183, 2003.

C. J. James and C. W. Hesse. Independent component analysis for biomedical signals. *Physiological Measurement*, 26(1):R15–R39, 2005.

D. Janusek, Z. Pawlowski, and R. Maniewski. Evaluation of the T-wave alternans detection methods: a simulation study. *Anadolu Kardiyol Derg*, 7 Suppl 1:116–119, 2007.

I. T. Joliffe. *Principal Component Analysis*. Springer, New York, NY, USA, 2002.

P. P. Kanjilal and S. Palit. Fetal ECG extraction from single-channel maternal ECG using singular value decomposition. *IEEE Trans. Biomed. Eng.*, 44(1):51–59, 1997.

S. M. Kay. *Fundamentals of statistical signal processing: estimation theory*. Prentice-Hall, Inc., Upper Saddle River, NJ, USA, 1993. ISBN 0-13-345711-7.

S. M. Kay. *Fundamentals of statistical signal processing: detection theory*. Prentice-Hall, Inc., Upper Saddle River, NJ, USA, 1998. ISBN 0-13-504135-2.

T. Klingenheben, P. Ptaszynski, and S. H. Hohnloser. Quantitative assessment of microvolt T-wave alternans in patients with congestive heart failure. *J Cardiovasc Electrophysiol*, 16(6):620–624, Jun 2005.

J. Kreuz, L.M. Lickfett, and J.O. Schwab. Modern noninvasive risk stratification in primary prevention of sudden cardiac death. *J Interv Card Electrophysiol*, 23(1):23–28, 2008.

S. Luke Kusmirek and Michael R Gold. Dynamic changes of T-wave alternans: does it predict short-term arrhythmia vulnerability? *J Cardiovasc Electrophysiol*, 18(5):518–519, May 2007.

R. Lampert, R. Soufer, C. A. McPherson, W. P. Batsford, S. Tirado, C. Earley, A. Goldberg, and V. Shusterman. Implantable cardioverter-defibrillator shocks increase T-wave alternans. *J Cardiovasc Electrophysiol*, 18(5):512–517, May 2007.

S. Maeda, M. Nishizaki, N. Yamawake, T. Ashikaga, H. Shimada, M. Asano, K. Ihara, T. Murai, H. Suzuki, H. Fujii, H. Sakurada, M. Hiraoka, and M. Isobe. Ambulatory ecg-based T-wave alternans and heart rate turbulence predict high risk of arrhythmic events in patients with old myocardial infarction. *Circ J*, Oct 2009.

L. Mainardi and R. Sassi. Analysis of T-wave alternans using the dominant T-wave paradigm. *J Electrocardiol*, 44(2):119–125, 2011.

J. Marrugat, R. Elosua, and M. Gil. Epidemiología de la muerte súbita cardíaca en España. *Rev Esp Cardiol*, 52:717 – 7258, 1999.

J. P. Martínez and S Olmos. A robust T-wave alternans detector based on the GLRT for Laplacian noise distribution. In *Computers in Cardiology 2002*, volume 29, pages 677–680. IEEE Comp. Soc. Press, 2002.

J. P. Martínez and S Olmos. Detection of T wave alternans in nonstationary noise: a GLRT approach. In *Computers in Cardiology 2003*, pages 161–164. IEEE Comp. Soc. Press, 2003.

J. P. Martínez and S. Olmos. Methodological principles of T wave alternans analysis: a unified framework. *IEEE Trans Biomed Eng*, 52(4):599–613, Apr 2005.

J. P. Martínez, R. Almeida, S. Olmos, A. P. Rocha, and P. Laguna. A wavelet-based ECG delineator: evaluation on standard databases. *IEEE Trans Biomed Eng*, 51(4):570–581, April 2004.

J. P. Martínez, S. Olmos, G. Wagner, and P. Laguna. Characterization of repolarization alternans during ischemia: time-course and spatial analysis. *IEEE Trans Biomed Eng*, 53(4):701–711, April 2006.

J. P. Martínez, I. Cygankiewicz, D. Smith, A. Bayés de Luna, P. Laguna, and L. Sörnmo. Detection performance and risk stratification using a model-based shape index characterizing heart rate turbulence. *Ann Biomed Eng*, 38(10):3173–3184, Oct 2010.

O. Meste, D. Janusek, and R. Maniewski. Analysis of the T wave alternans phenomenon with ecg amplitude modulation and baseline wander. In *Proc. Computers in Cardiology*, pages 565–568, Sept. 30 2007–Oct. 3 2007.

C. R. Meyer and H. N. Keiser. Electrocardiogram baseline noise estimation and removal using cubic splines and state-space computation techniques. *Comput Biomed Res*, 10(5):459–470, Oct 1977.

M. Minkkinen, M. Kähönen, J. Viik, K. Nikus, T. Lehtimäki, R. Lehtinen, T. Kööbi, V. Turjanmaa, W. Kaiser, R. L. Verrier, and T. Nieminen. Enhanced predictive power of quantitative TWA during routine exercise testing in the Finnish cardiovascular study. *J Cardiovasc Electrophysiol*, Oct 2008.

M. Minkkinen, M. Kähönen, J. Viik, K. Nikus, T. Lehtimäki, R. Lehtinen, T. Kööbi, V. Turjanmaa, W. Kaiser, R. L. Verrier, and T. Nieminen. Enhanced predictive power of quantitative TWA during routine exercise testing in the finnish cardiovascular study. *J Cardiovasc Electrophysiol*, 20(4):408–415, Apr 2009.

G. B. Moody. The Physionet/Computers in Cardiology challenge 2008: T-wave alternans. In *Proc. Computers in Cardiology*, pages 505–508, 14–17 Sept. 2008.

G. B. Moody and R. Mark. Development and evaluation of a 2-lead ECG analysis program. In *Proc. Computers in Cardiology 1982*, pages 39–44, 1982.

G. B. Moody, W.E. Muldrow, and R. G. Mark. A noise stress test for arrhythmia detectors. In *Computers in Cardiology 1984*, volume 11, pages 381–384, 1984.

S. M. Narayan. T-wave alternans and the susceptibility to ventricular arrhythmias. *J Am Coll Cardiol*, 47(2):269–281, Jan 2006.

B. D. Nearing and R. L. Verrier. Modified moving average analysis of T-wave alternans to predict ventricular fibrillation with great accuracy. *J. Appl. Physiol.*, 92(2):541–549, 2002.

S. Nemati, O. Abdala, V. Monasterio, S. Yim-Yeh, A. Malhotra, and G. Clifford. A non-parametric surrogate-based test of significance for T-wave alternans detection. *IEEE Trans Biomed Eng*, Apr 2010. doi: 10.1109/TBME.2010.2047859.

S. Nemati, A. Malhotra, and G. D. Clifford. T-wave alternans patterns during sleep in healthy, cardiac disease, and sleep apnea patients. *J Electrocardiol*, 44(2):126–130, 2011.

T. Nieminen and R. L. Verrier. Usefulness of T-wave alternans in sudden death risk stratification and guiding medical therapy. *Ann Noninvasive Electrocardiol*, 15(3):276–288, Jul 2010.

T. Nieminen, T. Lehtimäki, J. Viik, R. Lehtinen, K. Nikus, T. Kööbi, K. Niemelä, V. Turjanmaa, W. Kaiser, H. Huhtala, R. L. Verrier, H. Huikuri, and M. Kähönen. T-wave alternans predicts mortality in a population undergoing a clinically indicated exercise test. *Eur Heart J*, 28(19):2332–2337, Oct 2007.

P. M. Okin, R. B. Devereux, R. Fabsitz, E. Lee, J. Galloway, and B. Howard. Principal component analysis of the T wave and prediction of cardiovascular mortality in american indians: The strong heart study. *Circulation*, 105:714–719, 2002.

S. Olmos, J. García, J. Jané, and P. Laguna. ECG signal compression and noise filtering with truncated orthogonal expansion. *Signal Procesing*, 79 (1):97–115, 1999.

J. M. Pastore, S. D. Girouard, K. R. Laurita, F. G. Akar, and D. S. Rosenbaum. Mechanism linking T-wave alternans to the genesis of cardiac fibrillation. *Circulation*, 99(10):1385–1394, 1999.

J. S. Paul, M. R. Reddy, and V. J. Kumar. A transform domain SVD filter for suppression of muscle noise artefacts in exercise ECGs. *IEEE Trans. Biomed. Eng.*, 47(5):654–663, 2000.

S. G. Priori, E. Aliot, C. Blomstrom-Lundqvist, L. Bossaert, G. Breithardt, P. Brugada, J. A. Camm, R. Cappato, S. M. Cobbe, C. Di Mario, B. J. Maron, W. J. McKenna, A. K. Pedersen, U. Ravens, P. J. Schwartz, M. Trusz-Gluza, P. Vardas, H. J. Wellens, D. P. Zipes, and European Society of Cardiology. Update of the guidelines on sudden cardiac death of the European Society of Cardiology. *Eur Heart J*, 24(1):13–15, 2003.

E. Pueyo, J. P. Martínez, and P. Laguna. Cardiac repolarization analysis using the surface electrocardiogram. *Philos Transact A Math Phys Eng Sci*, 367(1887):213–233, Jan 2009.

S. Richter, G. Duray, and S. H. Hohnloser. How to analyze T-wave alternans. *Heart Rhythm*, 2(11):1268–1271, Nov 2005.

M. Di Rienzo, P. Castiglioni, G. Mancia, A. Pedotti, and G. Parati. Advancements in estimating baroreflex function. *IEEE Eng Med Biol Mag*, 20(2):25–32, 2001.

V. L. Roger, A. S. Go, D. M. Lloyd-Jones, R. J. Adams, J. D. Berry, T. M. Brown, M. R. Carnethon, S. Dai, G. de Simone, E. S. Ford, C. S. Fox, H. J. Fullerton, C. Gillespie, K. J. Greenlund, S. M. Hailpern, J. A. Heit, P. M. Ho, V. J. Howard, B. M. Kissela, S. J. Kittner, D. T. Lackland, J. H. Lichtman, L. D. Lisabeth, D. M. Makuc, G. M. Marcus, A. Marelli, D. B. Matchar, M. M. McDermott, J. B. Meigs, C. S. Moy, D. Mozaffarian, M. E. Mussolino, G. Nichol, N. P. Paynter, W. D. Rosamond, P. D. Sorlie, R. S. Stafford, T. N. Turan, M. B. Turner, N. D. Wong, J. Wylie-Rosett, on behalf of the American Heart Association Statistics Committee, and Stroke Statistics Subcommittee. Heart disease and stroke statistics–2011 update: A report from the American Heart Association. *Circulation*, 123 (4):e18–209, 2011.

J. L. Rojo-Álvarez, O. Barquero-Pérez, I. Mora-Jiménez, R. Goya-Esteban, J. Gimeno-Blanes, and A. García-Alberola. Detection and estimation of T wave alternans with matched filter and nonparametric bootstrap test. In *Proc. Computers in Cardiology*, pages 617–620, 14–17 Sept. 2008.

D. S. Rosenbaum, L. E. Jackson, J. M. Smith, H. Garan, J. N. Ruskin, and R. J. Cohen. Electrical alternans and vulnerability to ventricular arrhythmias. *N Engl J Med*, 330(4):235–241, 1994.

K. Sakaki, T. Ikeda, Y. Miwa, M. Miyakoshi, A. Abe, T. Tsukada, H. Ishiguro, H. Mera, S. Yusu, and H. Yoshino. Time-domain T-wave alternans measured from Holter electrocardiograms predicts cardiac mortality in patients with left ventricular dysfunction: a prospective study. *Heart Rhythm*, 6(3):332–337, Mar 2009.

J. A. Salerno-Uriarte, G. M. De Ferrari, C. Klersy, R. F. Pedretti, M. Tritto, L. Sallusti, L. Libero, G. Pettinati, G. Molon, A. Curnis, E. Occhetta, F. Morandi, P. Ferrero, F. Accardi, and A. L. P. H. A. Study Group

Investigators. Prognostic value of T-wave alternans in patients with heart failure due to nonischemic cardiomyopathy: results of the ALPHA study. *J Am Coll Cardiol*, 50(19):1896–1904, Nov 2007.

R. Sameni, C. Jutten, and M. B. Shamsollahi. Multichannel electrocardiogram decomposition using periodic component analysis. *IEEE Trans Biomed Eng*, 55(8):1935–1940, Aug. 2008.

L. K. Saul and J. B. Allen. Periodic component analysis: an eigenvalue method for representing periodic structure in speech. *NIPS*, pages 807–813, 2000.

D. F. Shanno. Conditioning of quasi-newton methods for function minimization. *Mathematics of Computing*, 24:647–656, 1970.

V. Shusterman and A. Goldberg. Tracking repolarization dynamics in real-life data. *J Electrocardiol*, 37 Suppl:180–186, 2004.

V. Shusterman, A. Goldberg, and B. London. Upsurge in T-wave alternans and nonalternating repolarization instability precedes spontaneous initiation of ventricular tachyarrhythmias in humans. *Circulation*, 113(25): 2880–2887, Jun 2006.

M. P. Slawnych, T. Nieminen, M. Kähönen, K. M. Kavanagh, T. Lehtimäki, D. Ramadan, J. Viik, S. G. Aggarwal, R. Lehtinen, L. Ellis, K. Nikus, and D. V. Exner. Post-exercise assessment of cardiac repolarization alternans in patients with coronary artery disease using the modified moving average method. *Journal of the American College of Cardiology*, 53(13): 1130 – 1137, 2009.

J. M. Smith, E. A. Clancy, C. R. Valeri, J. N. Ruskin, and R. J. Cohen. Electrical alternans and cardiac electrical instability. *Circulation*, 77(1): 110–121, 1988.

L. Sörnmo and P. Laguna. *Bioelectrical Signal Processing in Cardiac and Neurological Applications*. Elsevier Academic Press, June 2005. ISBN 0124375529.

L. Sörnmo. Time-varying digital filtering of ECG baseline wander. *Med. Biol. Eng. Comput.*, 31(5):503–508, 1993.

P. K. Stein, D. Sanghavi, P. P. Domitrovich, R. Mackey, and P. Deedwania. Ambulatory ECG-based T-wave alternans predicts sudden cardiac

death in high-risk post-MI patients with left ventricular dysfunction in the EPHESUS study. *J Cardiovasc Electrophysiol*, 19(10):1037–1042, 2008.

G. Strang. *Linear Algebra and Its Applications*. Brooks Cole, February 1988. ISBN 0155510053.

G. Turitto, E. B. Caref, G. El-Attar, M. Helal, A. Mohamed, R. P. Pedalino, and N. El-Sherif. Optimal target heart rate for exercise-induced T-wave alternans. *Ann Noninvasive Electrocardiol*, 6(2):123–128, Apr 2001.

R. L. Verrier and B. D. Nearing. Ambulatory ECG monitoring of T-wave alternans for arrhythmia risk assessment. *J Electrocardiol*, 36 Suppl:193–197, 2003.

R. L. Verrier, K. F. Kwaku, B. D. Nearing, and M. E. Josephson. T-wave alternans: Does size matter?. *J Cardiovasc Electrophysiol*, 16(6):625–628, Jun 2005a.

R. L. Verrier, B. D. Nearing, and K. F. Kwaku. Noninvasive sudden death risk stratification by ambulatory ECG-based T-wave alternans analysis: evidence and methodological guidelines. *Ann Noninvasive Electrocardiol*, 10(1):110–120, 2005b.

R. L. Verrier, K. Kumar, and B. D. Nearing. Basis for sudden cardiac death prediction by T-wave alternans from an integrative physiology perspective. *Heart Rhythm*, 6(3):416 – 422, 2009.

R. Vázquez, A. Bayés-Genis, I. Cygankiewicz, D. Pascual-Figal, L. Grigorian-Shamagian, R. Pavon, J. R. Gonzalez-Juanatey, J. M. Cubero, L. Pastor, J. Ordóñez-Llanos, J. Cinca, A. Bayés de Luna, and M. U. S. I. C. Investigators. The MUSIC Risk score: a simple method for predicting mortality in ambulatory patients with chronic heart failure. *Eur Heart J*, 30(9):1088–1096, May 2009.

J. J. Wei, C. J. Chang, N. K. Chou, and G. J. Jan. ECG data compression using truncated singular value decomposition. *IEEE Trans. Tech. Biom.*, 5(4):290–299, 2001.

L. D. Wilson, D. Jeyaraj, X. Wan, G. S. Hoeker, T. H. Said, M. Gittinger, K. R. Laurita, and D. S. Rosenbaum. Heart failure enhances susceptibility to arrhythmogenic cardiac alternans. *Heart Rhythm*, 6(2):251–259, Feb 2009.

B. L. Zaret, M. Moser, and L. S. Cohen. *The Yale University School of Medicine Heart Book*. William Morrow and Company Inc., New York, NY, USA, 1992. ISBN 0688097197.